

See discussions, stats, and author profiles for this publication at: <https://www.researchgate.net/publication/235755222>

Suppression of Tumor Growth by Designed Dimeric Epidithiodiketopiperazine Targeting Hypoxia-Inducible Transcription Factor Complex

ARTICLE in JOURNAL OF THE AMERICAN CHEMICAL SOCIETY · FEBRUARY 2013

Impact Factor: 12.11 · DOI: 10.1021/ja400805b · Source: PubMed

CITATIONS

15

READS

303

9 AUTHORS, INCLUDING:



Swati Kushal

University of Southern California

10 PUBLICATIONS 163 CITATIONS

[SEE PROFILE](#)



Jason Singh

The University of Arizona

1 PUBLICATION 15 CITATIONS

[SEE PROFILE](#)



Jan E Schnitzer

Proteogenomics Research Institute for Syste...

102 PUBLICATIONS 8,350 CITATIONS

[SEE PROFILE](#)



Bogdan Z Olenyuk

Proteogenomics Research Institute for Syste...

53 PUBLICATIONS 6,008 CITATIONS

[SEE PROFILE](#)

Suppression of Tumor Growth by Designed Dimeric Epidithiodiketopiperazine Targeting Hypoxia-Inducible Transcription Factor Complex

Ramin Dubey,[†] Michael D. Levin,[§] Lajos Z. Szabo,[‡] Csaba F. Laszlo,[‡] Swati Kushal,[†] Jason B. Singh,[‡] Philip Oh,[§] Jan E. Schnitzer,[§] and Bogdan Z. Olenyuk^{†}*

Addresses:

[†] Department of Pharmacology and Pharmaceutical Sciences, University of Southern California, 1985 Zonal Ave., PSC B15C, HSC 9121, Los Angeles, CA 90089

[‡] Department of Chemistry and Biochemistry, University of Arizona, 1306 E University Blvd, Tucson, AZ 85721

[§] Proteogenomics Research Institute for Systems Medicine, 11107 Roselle St., San Diego, CA 92121

*Corresponding author, bogdan@usc.edu

Abstract

Hypoxia is a hallmark of solid tumors and is associated with local invasion, metastatic spread, resistance to chemo- and radiotherapy, and is an independent, negative prognostic factor for a diverse range of malignant neoplasms. The cellular response to hypoxia is primarily mediated by a family of transcription factors, among which hypoxia inducible factor 1 (HIF1) plays a major role. Under normoxia, the oxygen-sensitive α subunit of HIF1 is rapidly and constitutively degraded, but is stabilized and accumulates under hypoxia. Upon nuclear translocation HIF1 controls the expression of over 100 genes involved in angiogenesis, altered energy metabolism, anti-apoptotic, and pro-proliferative mechanisms that promote tumor growth. A designed transcriptional antagonist, dimeric epidithiodiketopiperazine (ETP **2**), selectively disrupts the interaction of HIF1 α with p300/CBP coactivators and down-regulates the expression of hypoxia-inducible genes. ETP **2** was synthesized via a novel homo-oxidative coupling of the aliphatic primary carbons of the dithioacetal precursor. It effectively inhibits HIF1-induced activation of *VEGFA*, *LOX*, *Glut1*, and *c-Met* genes in a panel of cell lines representing breast and lung cancers. We observed an outstanding anti-tumor efficacy of both (\pm)-ETP **2** and *meso*-ETP **2** in a fully established breast carcinoma model by intravital microscopy (IVM). Treatment with either form of ETP **2** (1 mg/kg) resulted in a rapid regression of tumor growth that lasted for up to 14 days. These results suggest that inhibition of HIF1 transcriptional activity by designed dimeric ETPs could offer an innovative approach to cancer therapy with the potential to overcome hypoxia-induced tumor growth and resistance.

Introduction

Epidithiodiketopiperazines (ETPs) represent a novel class of designed protein ligands that target hypoxia inducible transcription factor complex. Their design is inspired by the naturally occurring dimeric ETP chetomin (CTM, Figure 1a), which is produced by certain strains of filamentous fungi, such as *Chaetomium coeliodes* and *Chaetomium seminudum*.^{1,2} Chetomin disrupts hypoxia inducible factor 1 (HIF1) activity through direct targeting of the interactions between its α subunit and p300 coactivator or its ortholog, CREB-binding protein (CBP), thereby blocking transactivation of the hypoxia-inducible gene expression (Figure 1b).^{3,4} Intracellular HIF1 α levels are regulated by the oxygen-dependent pathway that involves oxidation of prolines P564 and P402 by prolyl hydroxylase, such as PHD2, polyubiquitination by pVHL, a part of the E3 ubiquitin ligase complex, and subsequent proteasomal degradation (Figure 1c).⁵⁻⁸ Under hypoxic conditions or upon chemical inactivation of PHD2, HIF1 α is stabilized and accumulates, primarily due to the diminished rate of oxygen-dependent hydroxylation. It is then translocated into the nucleus where it binds with its partner HIF1 β /ARNT to the hypoxia response element (HRE, Figure 1c) and transactivates more than 100 hypoxia-inducible genes,^{9,10} including genes involved in tumor angiogenesis, metastasis, proliferation and altered energy metabolism.¹¹⁻¹⁵ For example, *c-Met*, a key proto-oncogene involved in metastasis,¹⁶ has several putative HREs and its expression is up-regulated in tumor cells under hypoxic conditions.¹⁷⁻¹⁹ In solid tumors, where mutations in *RAS*, *SRC* and *HER2/Neu/ErbB2* genes are frequently found, high levels of HIF1 α have been detected even under well-oxygenated conditions.²⁰ Direct targeting of hypoxia-inducible transcription factor-coactivator complex with small molecules that modulate its activity²¹ could become a powerful strategy for the suppression of tumor angiogenesis and simultaneous down-regulation of the

expression of genes involved in invasion, and metastasis. Both angiogenesis and invasion are the two key hallmarks^{22,23} of the malignant phenotype, responsible for aggressiveness, poor prognosis, and the eventual lethality of the neoplastic disease. An effective anti-metastatic strategy can significantly augment conventional anti-angiogenic therapies where direct targeting of vascular endothelial growth factor A (VEGFA), platelet-derived growth factor (PDGF) and their receptors often promotes accelerated metastasis.^{16,24,25}

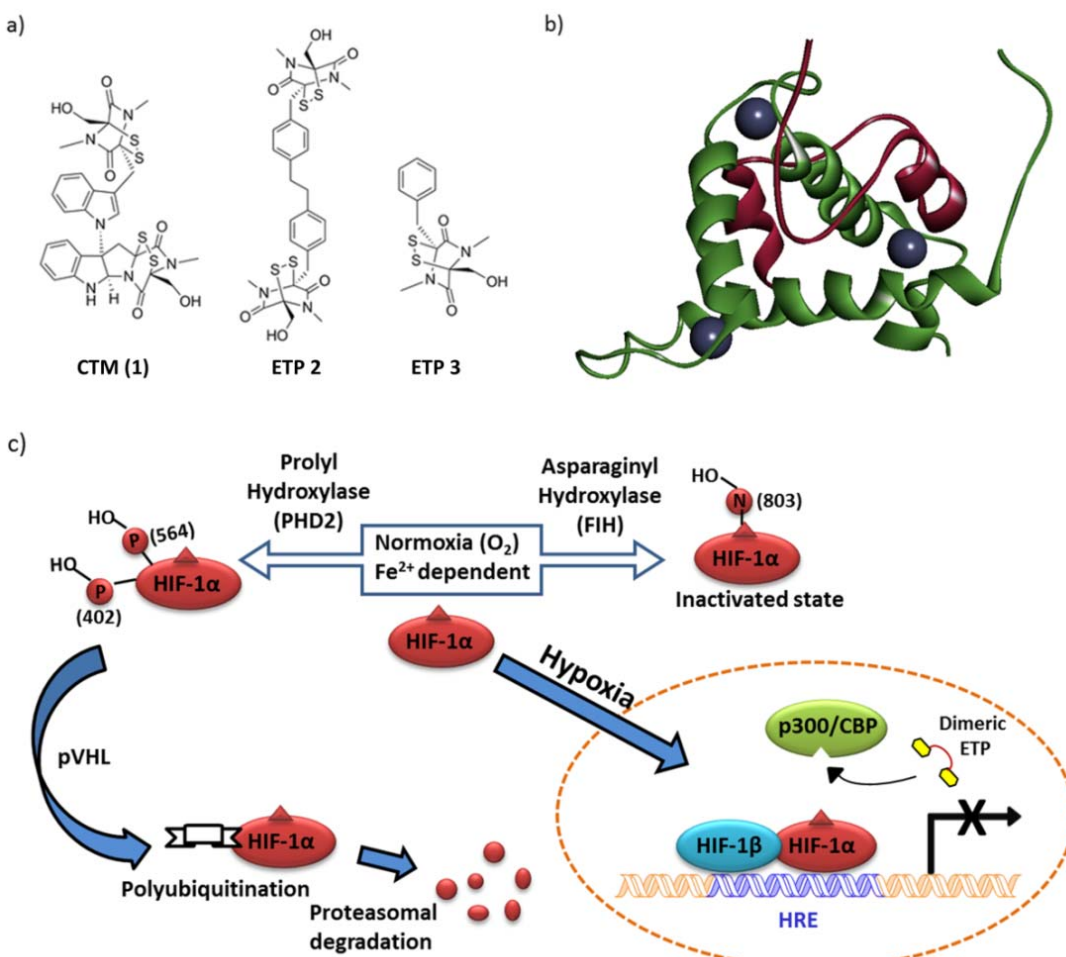


Figure 1. a) Structures of a dimeric ETP natural product chetomin, CTM (1), designed dimeric ETP 2 and monomeric ETP 3. b) Schematic representation of the complex between C-TAD of HIF1 α (red) and CH1 region of the p300/CBP coactivator (green), derived from the high-resolution NMR structure (pdb id: 1L3E).^{26,27} The three Zn²⁺ ions within the CH1 domain of p300 are represented by cyan spheres. c) Dimeric ETP prevents recruitment of the p300/CBP coactivator, thereby blocking overexpression of the hypoxia-inducible genes.

Our previous investigation has established the utility of dimeric ETPs in down-regulation of the activity of hypoxia-inducible transcription factor complex.²⁸ Naturally occurring dimeric ETP chetomin **1** binds the cysteine and histidine-rich 1 (CH1) domain of p300 and disrupts its recruitment by the HIF1 α C-terminal transactivation domain (C-TAD). The main mechanism of the action of ETP is thought to involve zinc ejection from the cysteine-rich sites within the CH1 domain of p300/CBP.^{2,28,29} Despite the promising therapeutic potential of naturally occurring ETPs, their use and structural modification still remain elusive due to the challenges faced in their synthesis. Although a number of monomeric ETPs were prepared by Fukuyama and Kishi³⁰⁻³³ as well as by the others,^{29,34-37} the total synthesis of dimeric ETPs has remained elusive until the recent reports of the synthesis of dideoxyverticillin A,³⁸ and chaetocin.^{39,40}

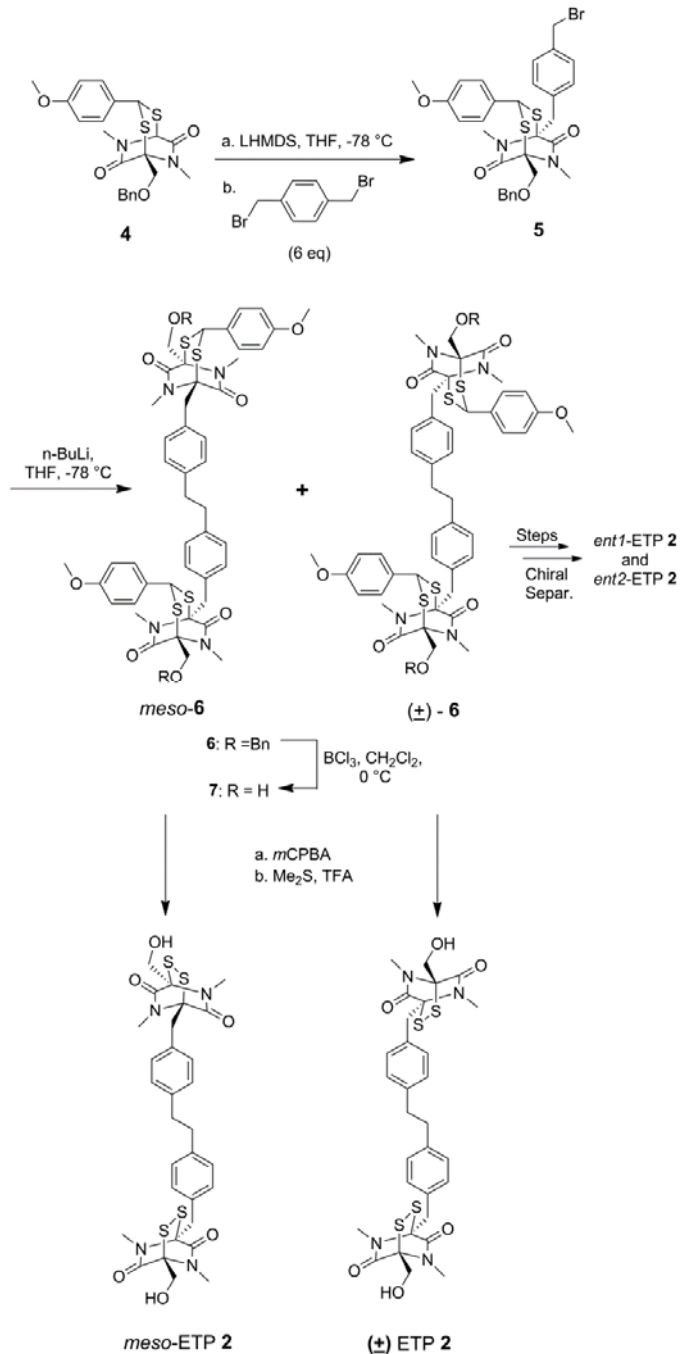
The proposed application of designed dimeric ETPs as transcriptional antagonists prompted us to further evaluate their biophysical properties, genome-wide effects *in vitro* and therapeutic efficacy *in vivo*, especially their ability to suppress growth of solid tumors. The dimerization of the two ETP rings through the aromatic linker creates a high-affinity divalent ligand that can interact with the target protein complex by several mechanisms, such as binding to two Zn²⁺ centers within the p300 CH1 region in a true divalent fashion, increase in the effective molarity of the ETP moiety and the concomitant increase of the efficiency of Zn²⁺ ion ejection, or by the sub-site effect, where the second ETP ring could interact non-covalently with the neighboring residues of the CH1 region. Herein, we present design, synthesis, *in vitro* and *in vivo* studies of a structurally optimized dimeric ETP targeting HIF1-inducible transcription factor complex. We also report a facile synthesis of dimeric ETP via a novel convergent synthetic route that involves homo-oxidative coupling of the primary aliphatic carbon centers, study of its interaction with the CH1 region of p300 protein, disruption of the hypoxia-inducible

transcription factor complex, down-regulation of the levels of the hypoxia-inducible genes, gene expression profiling, and *in vivo* assessment of the efficacy of dimeric ETP in arresting tumor growth and neovascularization.

Results

Preparation of dimeric ETP 2. Our synthetic route involved four key transformations, as shown in Scheme 1: 1) protection of the disulfide bridge in the form of a cyclic dithioacetal, 2) functionalization of the C-3 and C-6 positions of the dithioacetal ring via carbanion chemistry, 3) homo-oxidative coupling of the monomer to form the dimeric precursor, and 4) regeneration of the disulfide bridges of the dimeric precursor to obtain ETP **2**. The starting material in the synthesis of ETP **2** was dithioacetal **4**, which was prepared as previously described.²⁸ Lithium bis(trimethylsilyl)amide was used to deprotonate the C-6 position of dithioacetal **4** and the resulting carbanion readily reacted with α,α' -dibromo-*p*-xylene to yield the intermediate **5**. Our attempts to achieve homo-coupling of **5** using, among others, indium or transition metal-based chemistries, were unsuccessful. However, upon addition of *n*-BuLi in THF at -78 °C compound **5** was readily converted into the dimeric products (\pm)-**6** and *meso*-**6** in a rapid homo-oxidative coupling step. Although mechanistic details of this reaction await further investigation, we hypothesize that the traces of molecular oxygen or *n*-butyl bromide formed in the course of Li-halogen exchange could promote such process. Oxidative homo- and hetero-coupling processes that involve benzyl anions and 1,2-dibromoethane, TEMPO, cerium ammonium nitrate or I₂ as oxidants have been recently described,⁴¹ however to our knowledge, this is a rare example of such homo-oxidative coupling for a relatively complex benzyl halide fragment that requires only added *n*-BuLi as a reactant. Removal of the benzyl protecting groups from *meso*-**6** and (\pm)-**6** was accomplished with boron trichloride to afford *meso*-**7** and (\pm)-**7**, which were separated by

column chromatography. The final step involved removal of dithioacetal groups and closing of the disulfide bridges in both ETP rings by oxidation with *m*-chloroperbenzoic acid followed by the treatment with trifluoroacetic acid. The crude *meso*-ETP **2** and (\pm)-ETP **2** were purified by preparative reverse-phase HPLC (see Supporting Information, Figure S1).



Scheme 1. Synthesis of dimeric ETP **2**.

The individual enantiomers of ETP **2** were obtained through esterification of the racemate (\pm)-**7** with (1*S*)-(–)-camphanic chloride to afford the two diastereomers **8**, which could be separated by column chromatography. Hydrolysis of the separated products *dst1*-**8** and *dst2*-**8** with saturated sodium bicarbonate in methanol yielded enantiomeric diols *ent1*-**7** and *ent2*-**7** and their enantiomeric relationship was confirmed by CD spectra (see Supporting Information). We chose to sidestep the determination of their individual signs of optical rotation and absolute configurations by x-ray crystallography due to the limited quantity of each compound on hand. Each diol was then converted into the corresponding enantiomer *ent1*-ETP **2** and *ent2*-ETP **2**. Both ETP **2** enantiomers were purified by reverse-phase HPLC (see Supporting Information, Figure S2) and their enantiomeric relationship was confirmed by CD spectra.

ETP 2 targets p300 CH1 domain. In order to characterize direct binding of the (\pm)-ETP **2** to its target, CH1 domain of p300, SPR experiments were carried out. We used a chimera of glutathione *S*-transferase (GST) with CH1 domain of human p300 (a.a. residues 323-423) immobilized onto a CM5 chip (carboxymethylated dextran covalently attached to a gold surface), and a buffer with DTT in order to mimic the reducing environment that is found in the hypoxic regions of the tumors. The SPR sensorgrams indicate that dimeric (\pm)-ETP **2** binds directly to the p300 CH1 domain with low micromolar affinity (see Supporting Information, Figure S3b). The measured K_D value for (\pm)-ETP **2** was 3.62×10^{-6} M, the on-rate (K_a) was 4.25×10^3 M⁻¹s⁻¹ and off-rate (K_d) was 1.54×10^{-2} s⁻¹. Based on these data, (\pm)-ETP **2** reversibly binds to p300-CH1-GST protein and exhibits a rapid association and a slow dissociation from the protein immobilized on the chip surface.

ETP 2 disrupts HIF1 α - p300 complex *in vitro*. We used previously described fluorescence polarization (FP) competition assays to measure the extent of disruption of HIF1 α /p300 CH1

complex by each of the stereoisomers and a racemate of ETP **2**.⁴² The assays consisted of the same GST fusion of the p300 CH1 domain and the fluorescein-labeled C-TAD domain of human HIF1 α (a.a. residues 786-826). The racemate (\pm)-ETP **2**, *meso*-ETP **2** and two enantiomers *ent1*-ETP **2** and *ent2*-ETP **2** were tested for their ability to inhibit the association of HIF1 α C-TAD with p300-CH1-GST. Based on saturation binding data between p300-CH1-GST and C-TAD HIF1 α (see Supporting Information, Figure S3a), the appropriate aliquots of p300-CH1-GST and fluorescein-labeled HIF1 α C-TAD were incubated with ETP **2** at different concentrations (see Experimental Section). Analysis of competition binding has shown that the four samples of ETP **2** disrupt complex with HIF1 α peptide and CH1 p300 with similar IC₅₀ values (0.6-0.7 μ M, $P > 0.05$, t-test, see overlay in Figure 2a). This data supports our prior finding that stereoisomers of dimeric ETPs have similar activity toward the p300-HIF1 α complex.

All stereoisomers of ETP **2 show equal efficacy in down-regulation of hypoxia-inducible promoter activity.** A comparative assessment of the activity of each stereoisomer of ETP **2** was carried out using luciferase reporter assays in the MDA-MB-231-HRE-Luc cell line. These cells have five tandem repeats of HRE sequences in the luciferase promoter. For three stereoisomers of ETP **2** and a racemate, a similar inhibitory activity (>95% down-regulation of the promoter activation levels at hypoxia) was observed (Figure 2b). Because all three stereoisomers and (\pm)-ETP **2** showed remarkable similarity in binding affinity and in cell-based activity in luciferase assays, all subsequent cell-based experiments were performed using more synthetically readily accessible racemate, (\pm)-ETP **2**, henceforth referred to as ETP **2**.

Comparison of the efficacies of CTM, ETP **2, and ETP **3** in luciferase-based hypoxia-inducible promoter activity assays.** The HIF1-inducible promoter in the MDA-MB-231-HRE-Luc cell line showed dose-dependent decrease in activity by 90% and 95% at 200 nM and 600

nM concentrations upon treatment with ETP **2**. Treatment with CTM at 200 nM concentration resulted in 95% inhibition of luciferase promoter activity, while treatment with monomeric ETP **3** resulted in a <40% inhibition at 600 nM concentration (Figure 2c), highlighting the higher efficacy of CTM and dimeric ETP **2** in down-regulating the hypoxia-inducible promoter activity.

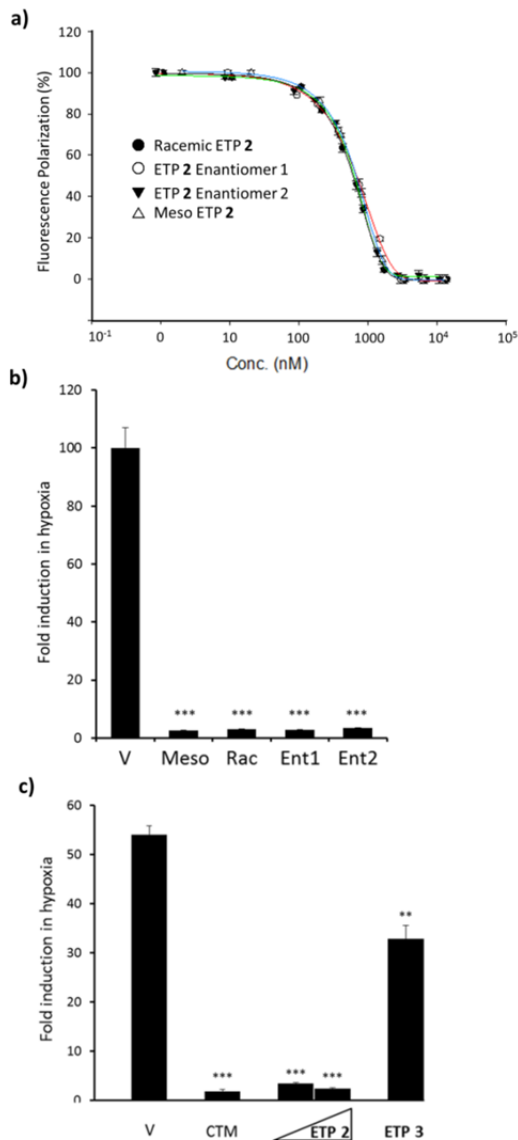


Figure 2. ETP **2** stereoisomers and a racemate show similar activity toward the HIF1 α -p300 complex in fluorescence polarization competition assays and in cell culture. a) Fluorescence polarization competition assays for each of the three stereoisomers of ETP **2** and a racemate show similar IC₅₀ values towards the p300 CH1:HIF1 α C-TAD complex. The IC₅₀s obtained for the isomers are 650 ± 44 nM for *meso*-ETP **2**, 655 ± 46 nM for (\pm)-ETP **2**, 664 ± 48 nM for *ent1*-ETP **2** and 646 ± 47 nM for *ent2*-ETP **2**. b) Results from the luciferase reporter assays in MDA-

MB-231-HRE-Luc cell line, showing comparable activity and effective down-regulation of promoter activity (95%) by *meso*-ETP **2** (Meso), (\pm)-ETP **2** (Rac), enantiomer 1 (*ent1*-ETP **2**) and enantiomer 2 (*ent2*-ETP **2**). c) Results from the luciferase reporter assays showing inhibition of hypoxia-inducible promoter activity by CTM, dimeric ETP **2** and monomeric ETP **3** in MDA-MB-231-HRE-Luc cell line. Error bars are \pm s.e.m. of experiments performed in triplicate. *** $P < 0.001$, ** $P < 0.01$, * $P < 0.05$, *t*-test.

ETP **2 is less toxic than chetomin.** In order to establish the window of viable concentrations for CTM and ETP **2** in MCF7 breast carcinoma and A549 lung adenocarcinoma cells, cytotoxicity assays with ETP **2** and CTM were carried out (Figure 3). In both cell lines ETP **2** was shown to be less cytotoxic as compared to CTM. Interestingly, both CTM and ETP **2** were found to be more cytotoxic in MCF7 cells as compared to A549 cells. For instance, in MCF7 cells an EC₅₀ of 0.2 μ M was determined for CTM, while ETP **2** gave EC₅₀ of 0.55 μ M. In contrast, in A549 cells CTM has an EC₅₀ of 0.9 μ M and ETP **2** has an EC₅₀ of 2.8 μ M.

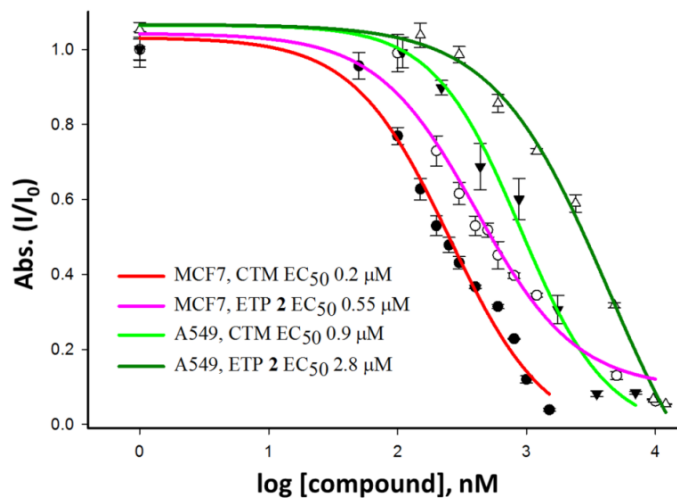


Figure 3. Dimeric ETP **2** shows lower cytotoxicity than CTM in MCF7 and A549 cell lines, as measured by the MTT assay. MCF7 cells were treated with different concentrations CTM and ETP **2** for 24 h. A549 cells were treated with different concentrations of CTM and ETP **2** for 48 h. Error bars are \pm s.e.m. of experiments performed in triplicate.

ETP **2 inhibits transcription of endogenous hypoxia-inducible genes and levels of secreted VEGFA and Met proteins.** To investigate the effect of ETP **2** on transcriptional activity of

VEGFA, an endogenous hypoxia-inducible gene, mRNA levels for that gene were measured in MCF7 cell line. The cells were treated with CTM at 150 nM concentration as well as with ETP **2** and ETP **3** at 200 nM and 400 nM concentrations. Hypoxia was mimicked with CoCl₂ (100 μM). Treatment with ETP **2** resulted in a dose-dependent down-regulation of *VEGFA* mRNA levels by 40% at 200 nM and 50% at 400 nM, respectively (Figure 4a). ETP **3** showed significantly lower activity for *VEGFA*: 25% inhibition at 200 nM and 35% at 400 nM concentrations, respectively. The cells showed higher level of stress upon treatment with ETP **3**, as observed by the change in their morphology, hence we at least in part attribute the observed downregulation in expression by ETP **3** to its non-specific effects on transcriptional machinery. CTM at 150 nM concentration reduced the expression of *VEGFA* mRNA below the basal levels. The results from luciferase promoter activity assays and measurement of *VEGFA* mRNA levels demonstrated significantly reduced efficacy of the monomeric ETP **3** as compared to the dimeric ETP **2**.

The *c-Met* protooncogene is induced and transactivated in metastatic breast tumors under hypoxia conditions. In order to evaluate the efficacy of ETP **2** in the *c-Met* transcription inhibition assays, triple-negative breast cancer cell line MDA-MB-231 was used. ETP **2** showed a dose-dependent down-regulation of *c-Met* levels with 30% inhibition at 50 nM, 35% at 200 nM, and 55% at 400 nM concentrations (Figure 4b). CTM down-regulated *c-Met* levels by 35% at a concentration of 150 nM. In MCF7 cell line the *c-Met* induction under hypoxia was not very pronounced in the media containing 10% serum, therefore serum-free conditions were used and hypoxia was mimicked with desferrioxamine mesylate (DFO, 300 μM). Under these conditions, ETP **2** at 100 nM concentration down-regulated the *c-Met* mRNA levels by 35% (Figure 4c).

The non-small cell lung adenocarcinoma cell line A549 under hypoxia and serum starvation conditions shows robust overexpression of HIF1-inducible genes *VEGFA*, *c-Met*,

Glut1, *LOX*, and *CXCR4* (see Supporting Information, Figure S4). In this assay, hypoxia was mimicked with 300 μ M DFO and serum-free F-12K media was used. Under these conditions, the levels of all five HIF1-inducible genes were significantly down-regulated by ETP **2** at a concentration of 400 nM, as measured by real-time qRT-PCR. For instance, the expression levels of *VEGFA* gene were inhibited by 50%; the levels of *c-Met* were also strongly affected by ETP **2**, with more than 70% observed down-regulation in expression. The *Glut1* gene, which is also overexpressed in hypoxic cells, was down-regulated by 60%. The expression levels of *LOX* and *CXCR4* genes are down-regulated 50% and 40%, respectively (Supporting Information, Figure S4).

To exclude the possibility that the observed down-regulation in the expression of hypoxia-inducible genes was due to a change in the levels of HIF1 α protein itself, Western blot analysis of HIF1 α was performed in hypoxic cells that were treated with ETP **2**. In this assay, A549 cells were treated with ETP **2** in serum-free F-12K media and hypoxia was mimicked with 300 μ M DFO. As expected, HIF1 α protein was not detectable under normoxia but is strongly induced upon treatment with DFO with the levels of induced HIF1 α protein being unaffected by the treatment with ETP **2** (see Supporting Information, Figure S5).

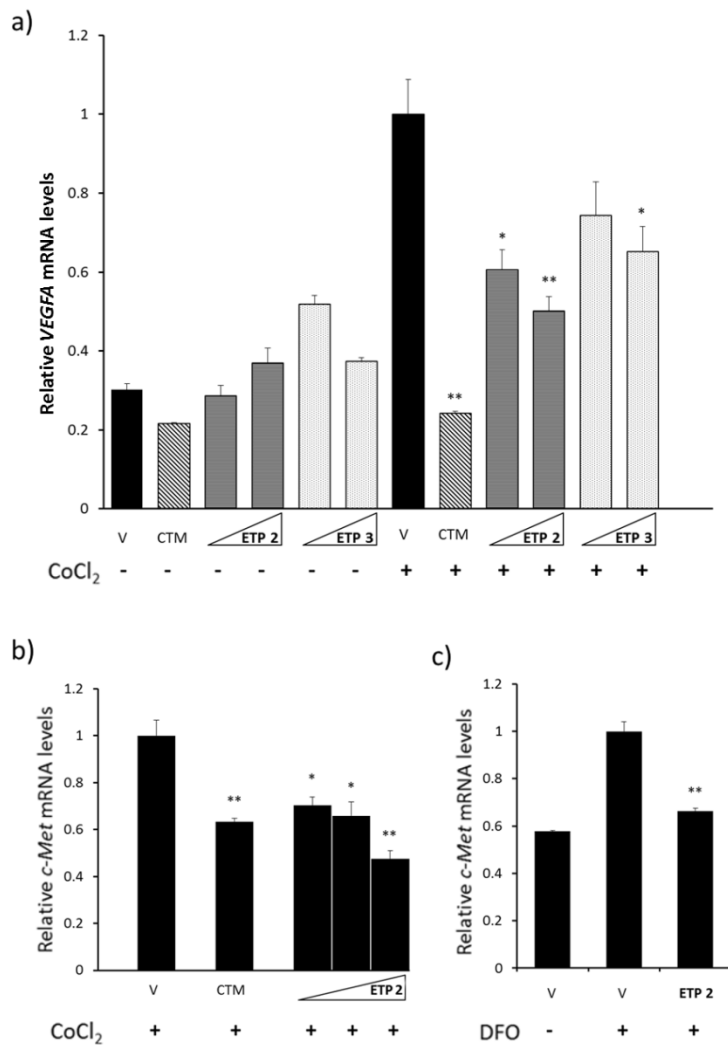


Figure 4. Dimeric ETP **2** down-regulates hypoxia-induced transcription of *VEGFA* and *c-Met* genes in cell culture. a) ETP **2** at 200 nM and 400 nM concentration inhibited *VEGFA* expression in a dose-dependent manner in MCF7 cells under hypoxia conditions as measured by real-time qRT-PCR. Hypoxia was mimicked with CoCl₂ (100 µM). Monomeric ETP **3** has reduced inhibitory activity at the same concentrations (26% at 200 nM and 35% at 400 nM). CTM at a concentration of 150 nM was used as a positive control. b) ETP **2** effectively down-regulates transcription of endogenous *c-Met* gene in MDA-MB-231 cell line. MDA-MB-231 cells were treated with ETP **2** at concentrations of 50 nM, 200 nM and 400 nM in the medium supplemented with 10% serum for 24 h. Hypoxia was mimicked with CoCl₂ (100 µM). A dose-dependent down-regulation of *c-Met* mRNA levels was observed with ETP **2**. c) *c-Met* expression levels in MCF7 cells treated with ETP **2** (100 nM) for 24 h in the serum-free RPMI medium. Hypoxia was mimicked with 300 µM DFO. Error bars are ± s.e.m. of experiments performed in triplicate. *** *P* < 0.001, ** *P* < 0.01, * *P* < 0.05, *t*-test.

In order to investigate dose response, cells were treated with ETP **2** at 100 nM, 400 nM and 1600 nM concentrations. The expression levels of *VEGFA*, *c-Met*, and *Glut1* showed well-defined decrease in mRNA levels upon treatment with ETP **2** at increased concentration. For instance, *VEGFA* gene was down-regulated by 1.4-, 1.6- and 2.0-fold, respectively at these three concentrations (Figure 5a), whereas *c-Met* was down-regulated by 1.2-, 1.7- and 3.0-fold (Figure 5b). The expression levels of *Glut1* gene were reduced by 1.4-, 1.8-, and 2.8-fold, respectively (Figure 5c).

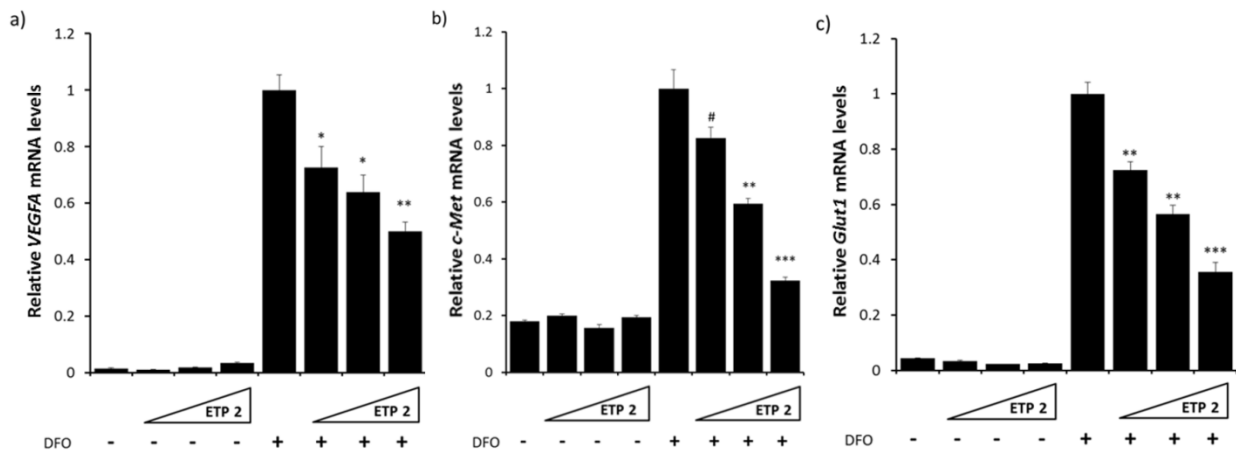


Figure 5. ETP **2** inhibits hypoxia-inducible transcription of (a) *VEGFA*, (b) *c-Met*, and (c) *Glut1* genes in dose-dependent manner in A549 cells as measured by real-time qRT-PCR. Cells were incubated with ETP **2** at three different concentrations (100 nM, 400 nM and 1600 nM) in serum-free F-12K medium for 48 h. Hypoxia was mimicked with DFO (300 μ M). For each concentration of ETP **2** a normoxic control sample was also measured. Error bars are \pm s.e.m. of experiments performed in triplicate. *** $P < 0.001$, ** $P < 0.01$, * $P < 0.05$, # $P < 0.1$, *t*-test.

In order to correlate the observed efficacy in transcriptional blockade of *VEGFA* and *c-Met* genes with decreased levels of its protein products, we performed quantitative Western blot analysis of the levels of these proteins under our conditions of compound treatment. To measure *VEGFA* protein levels, MCF7 cells were treated with CTM, ETP **2**, and ETP **3**. Western blot analysis shows significant down-regulation of *VEGFA* protein levels with ETP **2**, whereas ETP **3**

was having much lower efficacy (Figure 6a). Similarly, in MDA-MB-231 cell line c-Met protein levels were essentially unaffected by ETP **3** but significantly down-regulated by both CTM and ETP **2** (Figure 6b). This suggests that compensatory cellular stress response mechanisms that could affect internal ribosome entry sites or mechanisms enhancing protein translation do not override the observed down-regulation in the mRNA expression.

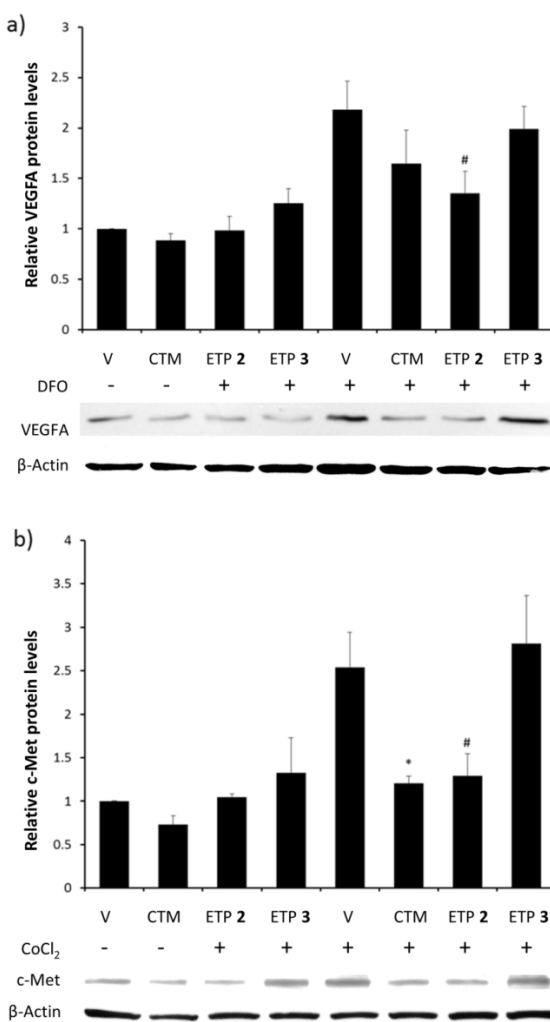


Figure 6. ETP **2** reduces the levels of (a) VEGFA protein in MCF7 cells and (b) c-Met protein in MDA-MB-231 cells under conditions of HIF1 α induction. Western blot analysis under normoxia and hypoxia-mimetic conditions upon treatment with CTM, ETP **2**, and ETP **3**. CTM was at 200 nM, ETP **2** and ETP **3** were at 400 nM, respectively. Hypoxia was mimicked with 300 μ M DFO (a) or 150 μ M CoCl₂ (b). Error bars are \pm s.e.m. of experiments performed in triplicate. * P < 0.05, # P < 0.1, *t*-test.

Gene expression profiling with oligonucleotide microarrays. The target proteins p300 and CBP are pleiotropic coactivators and hence, their CH1 domains are known to interact with multiple transcription factors. One potential limitation of the use of ETPs for gene regulation is specificity, because inhibiting the interaction between p300/CBP and transcription factors other than HIF1 could disrupt multiple signaling pathways, leading to a large number of affected genes. To probe the genome-wide specificity of ETPs, the global effects of ETP treatment on hypoxia-induced gene expression were evaluated with Affymetrix Human Gene ST 1.0 arrays containing oligonucleotide sequences representing 28,869 transcripts. Gene expression levels were normalized to hypoxic cells as controls.

In order to interrogate the genome for global effects, MCF7 cells treated with ETP **2** at 400 nM and DFO at 300 μ M concentrations were used. Clustering analysis was performed to identify similarities in the expression profiles between the different treatments (Figure 7a). The gene expression profile of cells treated with ETP **2** and DFO (+ETP **2**/+DFO) is significantly different from the profile of cells treated with DFO alone (-ETP **2**/+DFO), but shows clear regions of similarity with the profile of cells under normoxia conditions (-ETP **2**/-DFO). The profile of normoxic control cells (-ETP **2**/-DFO) and normoxic cells treated with ETP **2** (+ETP **2**/-DFO) also show greater similarities, as expected for ETP having diminished effect due to the absence of its direct target, HIF1 α under normoxia. Treatment of cells with ETP **2** at a concentration of 400 nM under hypoxia (300 μ M DFO) affected the expression of only 178 genes by ≥ 2.0 -fold (Figure 7b). By comparison, treatment with DFO alone changed expression levels of 329 genes over 2.0-fold. Of these, 88 genes were down-regulated by over 2.0-fold and 90 were up-regulated by over 2.0-fold.

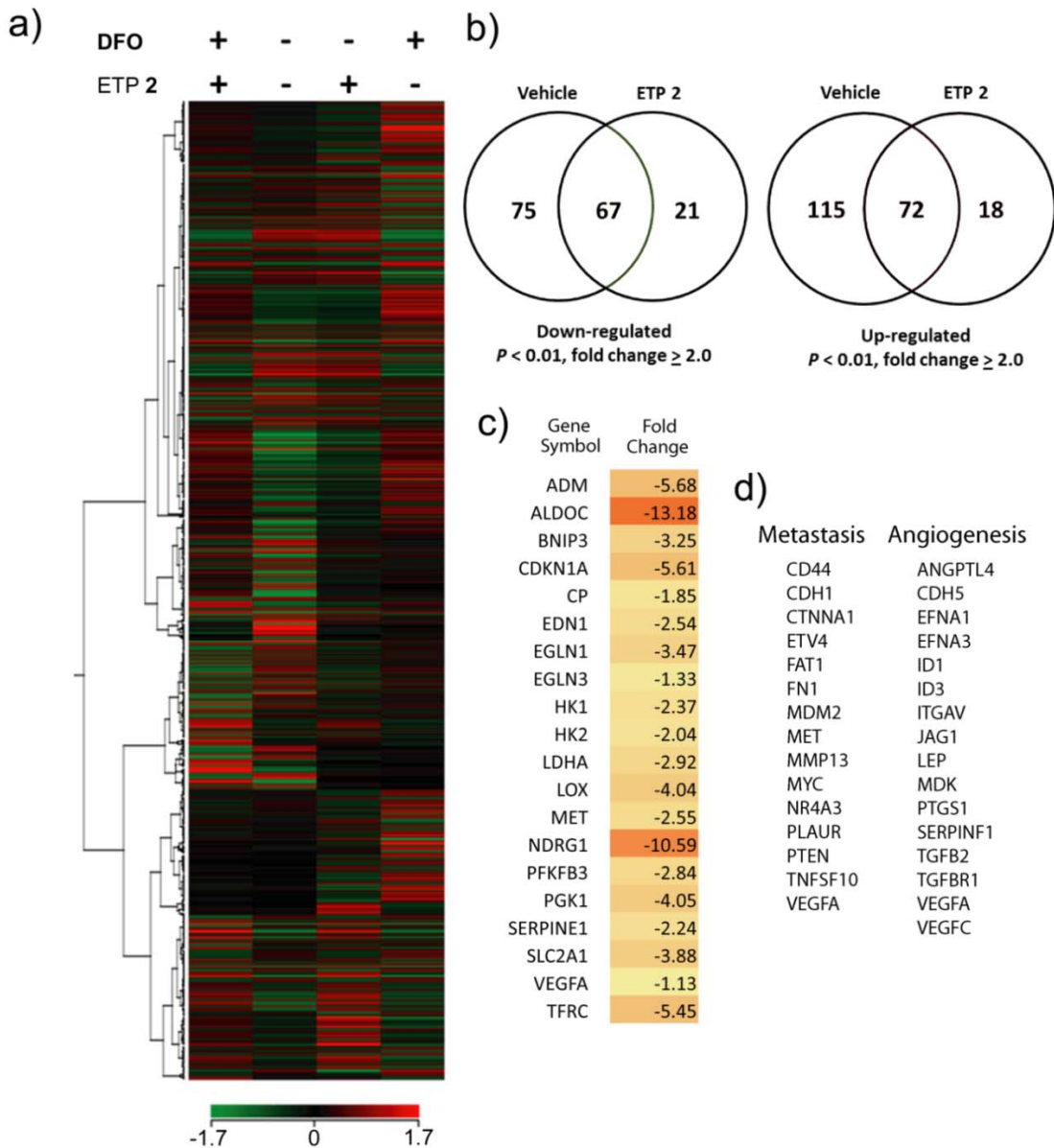


Figure 7. Results from gene expression profiling experiments in MCF7 cells treated with **ETP 2**. Global effects on gene expression in MCF7 cell line treated with **ETP 2** at 400 nM concentration interrogated with Affymetrix Human Gene ST 1.0 arrays. a) Hierarchical agglomerative clustering of all measured transcripts (ANOVA, $P < 0.01$) under the four indicated conditions (*left to right*: ETP 2 + DFO, vehicle at normoxia, ETP 2 at normoxia, and vehicle + DFO). Colors indicate relative transcription levels. b) Venn diagrams indicating the overlap of the transcripts affected more than 2-fold under hypoxia conditions and two specified treatments: vehicle (+DFO vs. -DFO) and ETP 2 (ETP 2 + DFO vs. ETP 2 at normoxia). c) Effect of the treatment with **ETP 2** on the panel of genes, previously characterized as direct targets of hypoxia-inducible gene expression that were also induced by at least 1.5-fold with DFO. d) Select group of genes associated with tumor metastasis and angiogenesis that are affected by the treatment with **ETP 2**.

The results suggest that treatment with ETP **2** reduces the hypoxia mimetic effect of DFO on certain group of genes, as expected for the transcriptional inhibitor that affects hypoxia-inducible pathway. The results also demonstrate high specificity of ETP **2** in its blockage of hypoxia-inducible signaling pathway. To more closely examine the effects of ETP **2** on genes induced directly by HIF1, a limited set of 20 transcripts was selected (Figure 7c), consisting of previously identified direct targets of hypoxia-inducible factor complex that were up-regulated by at least 1.5-fold ($P<0.01$) under conditions of DFO treatment. In all cases, ETP **2** reduced expression of these transcripts and in most cases the expression levels were approaching the levels observed in normoxic cells. We also examined the effect of ETP **2** on the two limited sets of genes implicated in promoting tumor angiogenesis and metastasis (Figure 7d). These interrogated genes also showed reduction in the expression levels, despite that only a subset of them (*VEGFA*, *VEGFC*, *Met*) is known to be direct targets of HIF1-inducible transcription. Since oncogenic signaling pathways are tightly interconnected, it is not entirely surprising that blockade of the hypoxia-induced transcription results in a concurrent down-regulation of the levels of other tumor-promoting genes, as the levels of secreted cytokines that are *direct* targets of HIF1 induced transcription and drive overexpression of these tumor-promoting genes are also being reduced.

***In vivo* efficacy of ETP **2** in arresting tumor growth: intravital microscopy (IVM) imaging of mouse tumor xenografts.** We chose intravital microscopy (IVM) imaging in order to evaluate the effect on ETP **2** on tumor growth *in vivo*, because it offers an unparalleled view into tumor development, allowing rapid, high-resolution *in vivo* imaging of molecular and cellular events.⁴³⁻⁴⁵ IVM is especially powerful for imaging dynamic changes in growing tumors, such as extent and patterns of neovascularization, tumor endocytosis, changes in blood

flow, and tumor responses to therapeutic agents.^{44,46-50} As described previously,⁴⁸ nude mice were fitted with dorsal skinfold window chambers with subcutaneously implanted tumor spheroids that consisted of N202 cells (murine mammary carcinoma) stably expressing recombinant green fluorescent protein fused to histone H2B. Tumors were allowed to vascularize for 10-14 days after which mice were injected with 1 mg/kg of *meso*-ETP **2** via tail vein on days 0, 8, 10, and 12. The representative images clearly show that the tumor vasculature and tumor growth are significantly suppressed in the mice injected with *meso*-ETP **2** as compared to the mice injected with the vehicle (Figure 8a). High-resolution images show significant decrease in the density of tumor vasculature after 14 days (Figure 8b). Quantification of the fluorescent signals from tumor cells obtained from the IVM images of six mice indicates tumor growth arrest in all animals (Figure 8c). Similar results were obtained in mice treated with (\pm)-ETP **2** (see Supporting Information, Figure S6). In the course of these experiments, both racemic and *meso*-ETP **2** showed very low toxicity to mice, as confirmed by observation of the behavior of the animals and monitoring of their body weights. In our study, all mice treated with ETP **2** survived the 14-day treatment and did not show any signs of local necrosis at the site of intravenous injection or acute toxicity. This establishes the *in vivo* efficacy of ETP **2** in suppressing tumor growth in a mouse xenograft model.

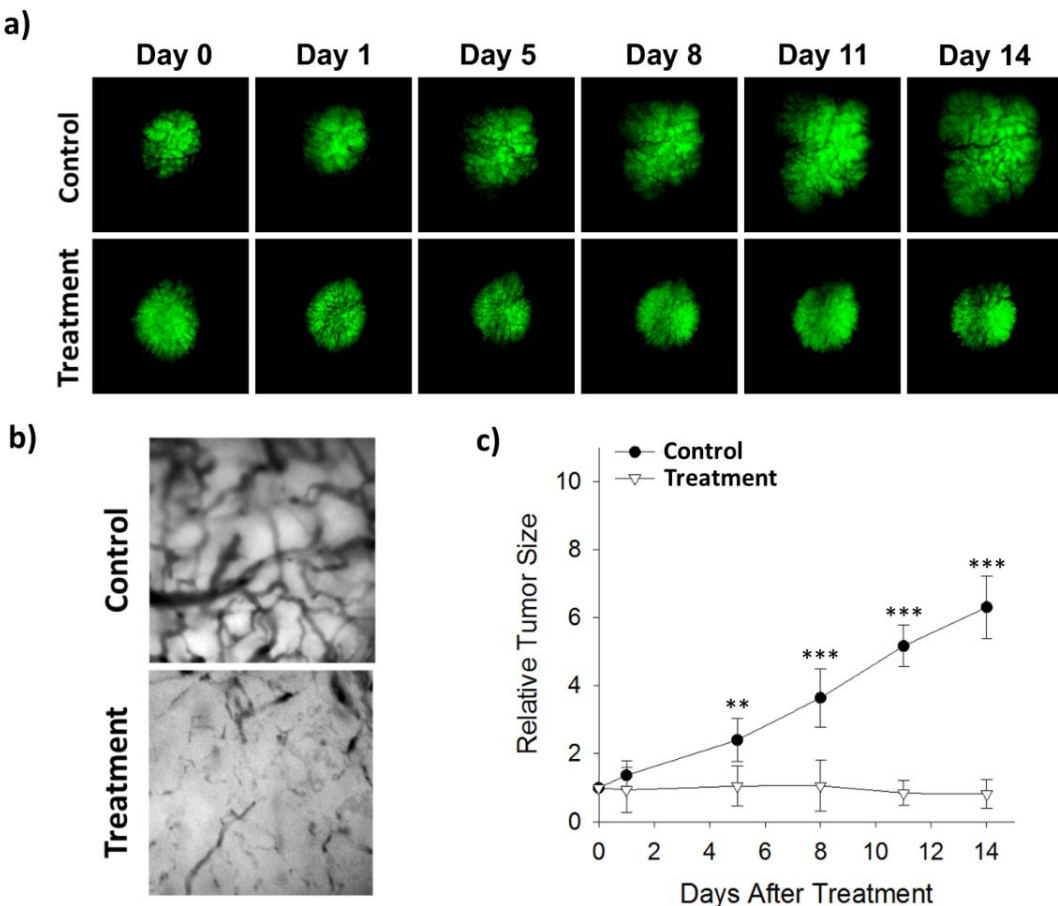


Figure 8. Effect of ETP 2 on tumor growth. Intravital microscopy images illustrating the effect of a HIF1 α inhibitor ETP 2 on the rate of tumor growth. a) Fluorescence IVM images of tumors taken on days indicated post-treatment. b) Effect of treatment on tumor vasculature after 14 days. c) Comparison of the relative tumor sizes for treated and control groups obtained by the quantification of the tumor fluorescence. *** $P < 0.001$, ** $P < 0.01$, t -test.

Discussion

Oncogenic transcription factors are the points of convergence of multiple signaling pathways leading to tumor proliferation and metastasis.⁵¹ Activated by primary genetic events (translocation, amplification) or upstream signaling pathways, they mediate and maintain the aggressiveness and neoplastic phenotype in cancer. Due to the fact that much smaller set of oncogenic transcription factors are overactive in cancers than signaling proteins,⁵¹ the ability to

directly modulate activity of oncogenic transcription factors with synthetic small molecules in diseases that are characterized by multiple activations of signaling networks *upstream* of these factors opens an intriguing possibility for therapeutic intervention. In addition, small molecules can serve as precise molecular-level tools for dissection of the fundamental mechanisms of transcription,^{52,53} such as decoding the delicate balance between interactions of a common coactivator protein and several transcription factors and modulating the ability of two distinct classes of activators to form a complex with the coactivator without affecting other related complexes.⁵⁴

Designed ligands that target DNA, transcription factors, or coactivators with high affinity and specificity could lead to promoter-selective destabilization of the multi-protein assembly responsible for the recruitment of RNA polymerase II, resulting in down-regulation of gene expression.^{51,52,55,56} To that end, small molecules often circumvent the need for delivery strategies, and a number of natural and synthetic compounds have been explored for their ability to regulate gene expression *in vitro* and *in cell culture*.⁵⁷ Such molecules, capable of allosterically targeting activator-coactivator interactions, represent a molecular-level toolkit that is complementary to programmable DNA minor groove binding oligomers,²⁴ such as pyrrole-imidazole polyamides,⁵⁸ in their ability to allosterically target DNA.⁵⁹ The success of the design and application of small molecule DNA ligands targeting predetermined sequence in regulating gene expression,⁶⁰⁻⁶⁸ and the recent advances in achieving efficient cell uptake,⁶⁹⁻⁷³ studies of pharmacokinetics,^{74,75} as well as specificity in the genome-sized sequence space⁷⁶ suggest that direct targeting of transcription factor complexes could become a powerful strategy in regulation of cancer cell signaling and gene expression.

Our dimeric ETP **2** disrupts function of the hypoxia-inducible factor complex and modulates the transcriptional activity caused by elevated levels of HIF1 α under conditions of chronic hypoxia found in solid tumors. This approach offers numerous advantages over targeting of proangiogenic cytokines and their receptors, as HIF1-inducible transcription system provides a unique opportunity for direct blockade of genes involved in angiogenesis and other accompanying processes, such as extracellular matrix remodeling and cell invasion. The endpoint of such a targeting could not only diminish blood supply to growing tumors, but also block the escape of tumorigenic cells leading to metastasis. The design of ETP **2** was inspired by natural product chetomin (CTM, **1**). It targets CH1 domain of p300 in complex with HIF1 α C-TAD with sub-micromolar affinity and down-regulates hypoxia-inducible gene expression, while being significantly less toxic to cells and synthetically accessible. In contrast to our previously reported first-generation dimeric ETP **9** that mimics distance between the bridging disulfides in CTM,²⁸ ETP **2** was designed to maintain the conformationally-averaged distance between the bridging disulfides of ~20 Å, matching the distance between the two neighboring Zn²⁺ ions within the structures of p300/CBP CH1 domain. As in the case of ETP **9**, we found that all stereoisomers and the racemic mixture of ETP **2** disrupt binding between HIF1 α CTAD and p300 CH1 region with similar IC₅₀s (0.6 μM), as measured by fluorescence polarization competition assays. This 2.5-fold increase in IC₅₀ of ETP **2** as compared to our first-generation ETP **9** (1.5 μM)²⁸ suggests that structural optimization has favorable impact on its affinity despite the dynamic, ductile nature of the CH1 region of the target protein. Furthermore, a comparative study of ETP **2** and ETP **9** in luciferase-based, hypoxia-inducible promoter activity assays and analysis of the levels of secreted VEGF protein in cells treated with these compounds also clearly show superior efficacy of the second-generation dimeric ETP **2** in these cell-based

assays ($P < 0.01$, *t*-test, Figure S7). A detailed investigation of the structure-activity relationship of the dimeric ETPs is currently ongoing.

Prior to undertaking rigorous cell-based studies, we first compared the cytotoxicities of ETP **2** and CTM in breast cancer MCF7 and metastatic non-small cell lung carcinoma A549 cell lines. ETP **2** showed lower cytotoxicity as compared to CTM (Figure 3) which has been known for its off-target effects *in vivo*.² The sub-micromolar affinity of ETP **2** towards its target, CH1 region of human p300 coactivator, was demonstrated in our binding assays and its ability to down-regulate hypoxia-inducible gene expression was confirmed in assays that included MDA-MB-231-HRE-Luc, MCF7, and A549 cell lines. In cell culture, the five HIF1-inducible genes that were interrogated (*VEGFA*, *c-Met*, *Glut1*, *LOX*, and *CXCR4*) showed significant down-regulation in the expression levels upon treatment with ETP **2** at sub-micromolar concentrations. These five genes are involved in angiogenesis, metastasis, glucose metabolism, extracellular matrix (ECM) remodeling, and chemotaxis, suggesting that ETP **2** could suppress tumor growth by several different mechanisms. In comparison, control monomeric ETP **3** has significantly lower reported affinity (>100 μ M) toward the HIF1 α CTAD - p300 CH1 complex⁷⁷ and it consistently showed significantly lower efficacy in cell culture assays, such as luciferase (Figure 2c), and in its ability to down-regulate VEGF and Met protein levels (Figure 6 a-b).

Analysis of genome-wide effects in MCF7 cells treated with ETP **2** under HIF1 α induction shows down-regulation of the expression levels of multiple hypoxia-inducible genes linked to tumor angiogenesis and metastasis. Aside from the hypoxia-inducible group, transcription levels of only 39 additional genes have been affected more than 2-fold. These results underscore high efficacy of ETP **2** in achieving a blockade of hypoxia-inducible gene

expression and indicate a high degree of specificity of ETP **2** in a context of the entire transcriptome.

The tumors developed in nude mice showed complete growth arrest for at least 14 days after treatment with ETP **2**, as monitored by intravital microscopy. This makes ETP **2** comparable in efficacy to such therapeutic agents as doxorubicin, docetaxel and cisplatin in the comparable animal models.⁷⁸ All mice showed no side effects after treatment with ETP **2** for the entire duration of the study. Intravital microscopy images revealed significant, steady decrease in the vascularization of tumors upon treatment with ETP **2**, which is consistent with the suggested mechanism for transcriptional blockade of hypoxia-inducible proangiogenic cytokines. The success of intravenously injected ETP **2** in arresting tumor growth also suggests its ability to rapidly gain entry into the tumor tissue and its sufficient retention within tumors and systemic stability.

Conclusion

We designed and synthesized a novel dimeric epidithiodiketopiperazine, ETP **2**, that targets pleiotropic coactivators p300/CBP, disrupts HIF1 α -p300/CBP complex *in vitro*, and effectively down-regulates hypoxia-inducible signaling and gene expression. In our *in vivo* IVM models of breast cancer, four intravenous injections of *meso*-ETP **2** at a dose of 1 mg/kg at days 0, 8, 10, and 12 arrested tumor growth for at least 14 days (the entire duration of the study). Designed dimeric ETP **2** was shown to be an efficacious and non-toxic transcription-based antagonist as compared to the natural product CTM. These results suggest that dimeric epidithiodiketopiperazines could be promising leads for future development as therapeutic agents for treatment of solid tumors. The aim of the future work will be to elucidate the mechanism of tumor growth arrest by ETP **2** *in vivo*, and to study its effect on chemotaxis of tumorigenic cells.

The high efficacy in suppression of tumor growth in our experiments suggests that ETP **2** might have an additional effect on differentiation of cancer stem cells and progenitor cells. Further investigation of the efficacy of ETP **2** in a variety of preclinical tumor models and its pharmacokinetic and pharmacodynamic profiling are currently underway.

Experimental Section

Plasmids. The DNA sequence of human p300 CH1 domain (amino acid residues 323-423) was designed as an insert and subcloned into a pUC57 plasmid (Genscript, Inc.). After transformation of the plasmid in JM109 bacteria (Promega), the DNA sequence was directionally subcloned into a pGEX 4T-2 expression vector (Amersham) with BamHI and EcoRI (New England Biolabs).

Protein Expression. The pGEX 4T-2-p300 fusion vector was transformed into BL21 DE3 pLys competent E. coli (Novagen). Production of the desired p300-CH1-GST fusion product was carried out in LB media supplemented with 0.1 mM ZnCl₂ and verified by SDS-PAGE and by sequencing. Bacteria were harvested and resuspended in a lysis buffer that consisted of 50 mM Tris (Sigma), 150 mM NaCl (Fisher), 100 µM ZnCl₂ (Sigma), 1 mM EDTA (Fisher), 10 mM MgCl₂ (Fisher), 1 mM DTT (RPI corporation), and 0.1% NP-40 (Tergitol, 70% solution, Sigma) at pH 8.0. Protease inhibitor cocktail (Sigma) at 10 µL per 1 mL of resuspended pellet was added, and bacteria samples were frozen. Thawed pellets were then lysed by sonication and centrifuged at 4 °C and 15,000 × g for 45 min. Fusion protein was collected from the bacterial supernatant and purified by affinity chromatography using glutathione Sepharose 4B beads (Amersham) prepared according to the manufacturer's directions. The packed column was washed two times with PBS followed by three washes with protein buffer containing 50 mM Tris (RPI Corporation) and 150 mM NaCl (RPI Corporation), 0.1% NP-40 (Tergitol, 70% solution,

Sigma), 1 mM DTT (RPI corporation), and 100 μ M ZnCl₂ (Sigma) at pH 8.0. Two washes with 10 mM 1,10-phenanthroline (Sigma) in protein buffer was given to the beads to remove any heavy metal ions. Next, the protein buffer mentioned above was augmented with zinc chloride (100 μ M) and was used to wash the beads four times to reconstitute zinc in the protein. An elution gradient was run using increasing concentrations of glutathione (Sigma) ranging from 2.5 mM to 10 mM in the protein buffer mentioned above. Collected fractions were pooled and dialyzed against the protein buffer mentioned above supplemented with 10% glycerol. Dialysis was done in dialysis tubing (7 kDa cut-off, Spectrum) with three buffer changes to remove glutathione from the protein buffer solution. Purity was confirmed by SDS-PAGE and concentration was determined by Bradford assay.

Fluorescence Polarization Competition Experiments. The relative binding affinity of each compound for p300-CH1-GST was determined using fluorescence polarization-based competitive binding assay with fluorescein-labeled C-terminal fragment of HIF1 α (C-TAD, a.a. 786-826). Anisotropy experiments were performed with a Synergy 2 Multi-Mode Microplate Reader (BioTek) at 25 °C, with excitation and emission wavelengths of 485 and 525 nm, respectively. All samples were prepared in opaque 96-well plates (Greiner BioOne) in FP buffer of 50 mM Tris, 150 mM NaCl, 10% glycerol (v/v), 1 mM DTT, 100 μ M ZnCl₂, pH 8.0 with 0.1% pluronic F-68 (Sigma) and 2% DMSO.

Determination of the Binding Affinity of HIF1 α C-TAD Toward the p300 CH1 Region. Prior to the competition experiments, the affinity of fluorescein-labeled HIF1 α C-TAD for p300 CH1 was determined by monitoring polarization of the fluorescent probe upon addition of p300-CH1-GST. Saturation binding curves were obtained by addition of an increasing amount of p300-CH1-GST (0-1600 nM final concentration) to a 15 nM solution of fluorescein-labeled

HIF1 α CTAD in FP buffer (mentioned above) at 25 °C. The dissociation constant (K_D) value for the fluorescein-labeled HIF1 α CTAD and p300-CH1-GST complex was determined as the concentration of p300-CH1-GST where 50% of HIF1 α CTAD is bound to it (see Supporting Information).

Determination of ETP 2 Binding Affinity in Competition Assays. A solution of 75 nM p300-CH1-GST and 15 nM fluorescein-labeled HIF1 α peptide, corresponding to more than 50% saturation of protein with fluorescent probe, was incubated at 25 °C. After 1 h, ETP 2 was added with final concentrations ranging from 1 nM to 12 μ M; the total volume of the solution was 120 μ L. After 1 h, the amount of dissociated fluorescent probe was determined by the Synergy 2 Multi-Mode Microplate Reader (BioTek). The IC₅₀ values were determined for the compound ETP 2 by fitting the averages of three individual measurements to a sigmoidal 4-parameter curve using nonlinear regression model with SigmaPlot version 11.0 software (Systat Software, Inc.).

Cell Lines. Human breast carcinoma (MCF7 and MDA-MB-231) and human epithelial lung carcinoma (A549) cell lines were obtained from ATCC (accession numbers CCL-2 and HTB-22). An aggressive human breast carcinoma stably transfected with an HRE luciferase construct (MDA-MB-231-HRE-Luc) was a gift of Dr. Robert Gillies.

Cell Culture. MCF7 cells were maintained in RPMI 1640 media (Sigma) supplemented with 10% fetal bovine serum, penicillin (50 U/mL), and streptomycin (50 μ g/mL). MDA-MB-231-HRE-Luc cells were grown in high glucose DMEM (Sigma) supplemented with 10% fetal bovine serum (Irvine Scientific) and 0.4 g/L geneticin (RPI). A549 cells were grown in F-12K medium (ATCC) supplemented with 10% fetal bovine serum, penicillin (50 U/mL), and streptomycin (50 μ g/mL). All cells were incubated at 37 °C in a humidified atmosphere with 5% CO₂. Cell growth and morphology were monitored by phase-contrast microscopy.

Luciferase Assays. MDA-MB-231-HRE-Luc cells were plated in 24-well dishes (BD Falcon) at a density of 6.5×10^4 cells/mL. After attachment, cells were treated with 1 mL of fresh media containing CTM (150 nM, EMD Biosciences), ETP **2**, and ETP **3** at 200 and 600 nM concentrations, or with the four stereoisomers of ETP **2** (meso, racemate, ent1 and ent2) at 200 nM concentrations. All samples contained a final concentration of 0.1% DMSO; vehicle samples were treated with cell culture media containing 0.1% DMSO. Cells were incubated for 6 h, hypoxia was mimicked with desferrioxamine mesylate (DFO, 300 μ M, Sigma), and cells were incubated for another 18 h. The whole cell lysate was isolated by washing the cells twice with ice-cold PBS and then adding 150 μ L of CCLR reagent from the Luciferase Assay Kit (Promega). Further steps were carried out according to the manufacturer's instructions. Relative light intensity was measured using a Turner TD-20e luminometer and the results were normalized to total protein content determined by BCA assay (Thermo Scientific).

Cell Viability Assays. MCF7 cells were plated in 96-well plates (Greiner BioOne) at a density of 10,000 cells/well in 200 μ L RPMI medium supplemented with 10% fetal bovine serum. A549 cells were transferred into an 96-well plates at a density of 5,000 cells/well in 200 μ L serum-free F-12K. Both MCF7 and A549 cell lines were grown to 70% confluence and were treated with 100 μ L of fresh media containing CTM or ETP **2** at concentrations ranging from 0 to 1.5 μ M and 0 to 7 μ M for CTM in MCF7 and A549 cells, respectively, and for ETP **2** from 0 to 10 μ M and 0 to 12 μ M in MCF7 and A549 cells, respectively. All samples contained a final concentration of 0.1% to 0.5% DMSO. Vehicle samples were treated with cell culture media containing 0.1% DMSO. MCF7 cells were incubated with compounds for a total of 24 h. Once the incubation was complete, 11 μ L of MTT (Promega) stock solution (5 mg/mL in PBS) was added to each well, and plates were incubated at 37 °C and 5% CO₂ for 3.5 h. The 110 μ L of media was removed

and 100 μ L of DMSO was added to each well. Plates were incubated at 37 °C for 5 minutes to dissolve the formazan crystals. Absorbance for the plate was measured at 570 nm and reference absorbance was at 690 nm. Synergy 2 Multi-Mode Microplate reader (BioTek) was used to read the plate. The GI₅₀ curves were plotted using SigmaPlot version 11.0 from Systat Software, Inc.

Isolation of mRNA. MCF7 cells were plated in 6-well plates (BD Falcon) in 2 mL of media at a density of 0.75×10^5 cells/mL. After 48 h the attached cells were at 80% confluency. Cells were treated with fresh media containing CTM, ETP **2**, or ETP **3** at desired concentrations. All samples contained a final concentration of 0.1% DMSO; vehicle samples were treated with cell culture media containing 0.1% DMSO. After 6 h, hypoxia was mimicked with cobalt chloride to a final concentration of 100 μ M and cells were incubated for another 18 hours. Cells were washed with ice-cold PBS. Total RNA was isolated with an RNeasy kit (Qiagen) according to the manufacturer's instructions and quantified by UV absorbance. The RNA was further treated with DNase I (Ambion, DNAfree kit) to remove any remaining genomic DNA. Reverse transcription was performed with SuperScript III Reverse Transcriptase (Invitrogen) as recommended by the manufacturer.

MDA-MB-231 cells were plated in 6-well plates in 2 mL of DMEM media supplemented with 10% fetal bovine serum at a density of 1.25×10^5 cells/mL. Cells were treated with fresh media containing CTM or ETP **2** at desired concentrations. Further steps were carried out as described for MCF7 cells.

A549 cells were grown in low serum F-12K containing 2% fetal bovine serum, penicillin (50 U/mL), and streptomycin (50 μ g/mL) for 1 week. A549 cells were plated in 6-well plates in 2 mL of serum-free media (0.2% fetal bovine serum) at a density of 1.25×10^5 cells/mL. Cells were treated with fresh serum-free media containing ETP **2** at desired concentrations. After 6 h

hypoxia was mimicked by adding DFO to a final concentration of 300 μ M. Further steps were carried out as described for MCF7 cells.

Analysis of Gene Expression Levels. Real-time qRT-PCR was used to determine the effect of ETPs on *VEGFA*, *c-Met*, *Glut1*, *LOX*, and *CXCR4* genes in the MCF7, MDA-MB-231, and A549 cell lines. Primers were synthesized by Integrated DNA Technologies (IDT, Coralville, IA). Compounds were examined under both normoxic and hypoxic conditions. For *VEGFA*, the forward primer 5'-AGG CCA GCA CAT AGG AGA GA-3' and reverse primer 5'-TTT CCC TTT CCT CGA ACT GA-3' were used to amplify a 104-bp fragment from the 3'-translated region of the gene. For *c-Met* gene the following primer pair was used: forward 5'-GGA AGA GGG CAT TTT GGT TG-3', reverse 5'-TTG GGA AAC TTC TCC TAT GTC A-3' to yield a product of 117 bp. For the *Glut1* gene the following primers were used: forward 5'-AGT ATG TGG AGC AAC TGT GTG G-3', reverse 5'-CGG CCT TTA GTC TCA GGA AC-3' to yield a product of 106 bp. For *LOX*, we employed the following primer pair: forward 5'-ATG AGT TTA GCC ACT ATG ACC TGC TT-3' and reverse 5'-AAA CTT GCT TTG TGG CCT TCA- 3' to amplify a 73 bp product. For *CXCR4*, following primer pair were used: forward 5'- GAA GCT GTT GGC TGA AAA GG-3', reverse 5'-CTC ACT GAC GTT GGC AAA GA-3' to yield a product of 94 bp. RNA levels were standardized by quantification of the β -glucuronidase as the housekeeping gene with forward primer 5'-CTC ATT TGG AAT TTT GCC GAT T-3' and reverse primer 5'- CCG AGT GAA GAT CCC CTT TTT A-3'. The experiments were performed with Applied Biosystems SYBR Green RT-PCR master mix. Temperature cycling and detection of the SYBR green emission were performed with an ABI 7900HT Fast Real-Time PCR System. Data were analyzed with Applied Biosystems Sequence Detection System, version 2.4.

Western Blot Analysis of VEGFA and c-Met Protein Levels. MCF7 and MDA-MB-231 cells were plated in 60 mm diameter cell culture dishes (BD Falcon) to a density of 1.0×10^6 cells/mL. After attachment, they were treated with media containing CTM (200 nM), ETP **2**, and ETP **3** (400 nM). All samples contained a final concentration 0.1-0.2% v/v of DMSO. After a 6 hour incubation period, hypoxia was induced with 300 μ M DFO in MCF7 or with 150 μ M CoCl₂ in MDA-MB-231 cells. Samples were incubated for an additional 18 hours. Total cellular proteins were extracted from the cells using cell lysis buffer according to manufacturer's protocol (Cell Signaling). Protein concentrations were measured with BCA Protein assay kit (Pierce/Thermo Scientific). Equal amounts of protein samples were subjected to SDS-PAGE and electroblotted to PVDF membrane (Bio-Rad). These were probed first with an anti-VEGFA mouse monoclonal (sc-57496, Santa Cruz Biotechnology) or anti-c-Met rabbit polyclonal antibody (sc-10, Santa Cruz Biotechnology), stripped with Restore Western Blot Stripping Buffer (Pierce/Thermo Scientific) and re-probed with a rabbit polyclonal anti- β -actin antibody (4867, Cell Signaling).

After washing with tris-buffered saline – Tween 20 (TBST) solution, the membranes were incubated with horseradish peroxidase (HRP)-conjugated secondary antibodies (Santa Cruz Biotechnology). Signals were detected by using SuperSignal chemiluminescent kit (Pierce/Thermo Scientific).

Western Blot Analysis of HIF1 α Levels. A549 cells were plated in T75 cell culture flasks (BD Falcon) to a density of 2.0×10^5 cells/mL. After the cells were 80% confluent, they were treated with media containing ETP **2** (1600 nM). All samples contained a final concentration 0.1% v/v of DMSO. After a 6 hour incubation period, hypoxia was induced with 300 μ M DFO. Samples were incubated for an additional 42 hours. Cells were washed twice with ice cold PBS buffer.

Total cellular proteins were extracted from the cells using 0.5 mL RIPA cell lysis buffer (Promega) per T75 flask. Protein concentrations were measured with BCA Protein assay kit (Pierce/Thermo Scientific). Equal amounts of protein samples were subjected to SDS-PAGE and electroblotted to PVDF membrane. These were probed first with a monoclonal mouse anti-human HIF1 α antibody (BD Biosciences), stripped with Restore Western Blot Stripping Buffer and probed with a goat polyclonal anti-Lamin A/C antibody (sc-6215, Santa Cruz Biotechnology). After washing with tris-buffered saline – Tween 20 (TBST) solution, the membrane was incubated with horseradish peroxidase (HRP)-conjugated secondary antibody. Signals were detected by using SuperSignal chemiluminescent kit (Pierce/Thermo Scientific).

Animal Use. Animal experiments were done in accordance with federal guidelines following review and approval by the Proteogenomics Research Institute for Systems Medicine Institutional Animal Care and Use Committee (PRISM IACUC). Athymic nude mice were 8–9 weeks old and purchased from Harlan, Inc.

Fluorescent Tumor Cell Lines. N202 (a gift from Joseph Lustgarten, Mayo Clinic, Scottsdale, AZ) were maintained in DMEM high glucose supplemented with L-glutamine (2 mM), penicillin (100 U/ml), streptomycin (100 U/ml), sodium pyruvate (1 mM) (Invitrogen, Carlsbad, CA) and 10% heat inactivated FBS (Omega Scientific, Tarzana, CA) at 37 °C in 5% CO₂ in air. The histone H2B-GFP was subcloned into the SalI/HpaI sites in the LXRN vector (Clontech, Inc., Palo Alto, CA) using SalI and blunted NotI sites from the BOSH2BGFPN1 vector. N202 were transduced with the viable virus to stably incorporate the H2B-GFP gene. The transduced cells were sorted twice using fluorescence-activated cell sorter (FACS) to ensure that 100% of the cells stably expressed the H2B-GFP protein.

Tumor Models. We used the classic IVM tumor model⁷⁹ with minor modifications. The athymic nude mice (25-30 g body weight) were anesthetized (7.3 mg ketamine hydrochloride and 2.3 mg xylazine per 100 g body weight, intraperitoneal injection) and placed on a heating pad. A titanium frame was placed onto the dorsal skinfold of mice to sandwich the extended double layer of skin. A 15 mm diameter full-thickness circular layer of skin was then excised. The superficial fascia on top of the remaining skin is carefully removed to expose the underlying muscle and subcutaneous tissue which is then covered with another titanium frame with a glass cover slip to form the window chamber. After a recovery period of 1-2 days, the animals were prepared for the procedure of implanting of tumor spheroids.

Tumor spheroids were formed by plating 50,000 N202 cells onto 1% agar-coated 96-well non-tissue culture treated flat bottom dishes (20 µL cells in 100 µL medium) and centrifuging 4 times at 2000 rpm for 15 min, rotating the dish after every centrifugation. The cells were incubated an additional 3-7 days (depending on cell type) at 37 °C in 5% CO₂ in air to form tight tumor spheroids.

The spheroids were implanted directly onto the dorsal skin in the window chamber alone. Tumors were allowed to vascularize over 10-14 days before the injection of 1 mg/kg of either *meso*-ETP **2** or (\pm)-ETP **2** on Day 0, followed by the injections on Day 8, 10, and 12.

Tumor Growth. Tumors were imaged via intravital fluorescence microscopy, as described in the literature.⁴⁸ Tumor growth was analyzed from the recorded grayscale 0-to-256 levels of gray images using Image-Pro Plus (Media Cybernetics, Bethesda, MD). Tumor growth was determined by quantifying the cumulative fluorescence signal for the tumor over time. The cumulative fluorescence signal from each tumor was measured by signal summation of all pixels.

Acknowledgments. We thank Dr. Hui Wang for his assistance in preparation of (\pm)-ETP **2** and Dr. Zuohe Song and Dr. Emmanuelle MeUILLET for their help in obtaining preliminary SPR data. Financial support by the US National Science Foundation (CHE-0748838) and the National Institute of Health (R21 HL094969) to BZO are gratefully acknowledged.

Supporting Information Available. Synthesis and characterization of ETP **2**, supplemental figures for LCMS of ETP **2**, CD spectra of *ent1-7*, *ent2-7*, *ent1*-ETP **2** and *ent2*-ETP **2**, SPR sensorgrams for binding of (\pm)-ETP **2** to p300 CH1 region, saturation binding curve of HIF-1 α C-TAD fluorescent probe to p300-CH1-GST fusion protein, relative mRNA expression levels in A549 cells, comparison of the levels of hypoxia-inducible promoter activity and VEGF ELISA for MCF7 cells treated with (\pm)-ETP **2** and ETP **9**, and intravital microscopy images of murine subcutaneous tumor models treated with (\pm)-ETP **2**. This material is available free of charge via the Internet at <http://pubs.acs.org/>.

References:

- (1) Waksman, S. A.; Bugie, E. *J. Bacteriol.* **1944**, *48*, 527.
- (2) Kung, A. L.; Zabludoff, S. D.; France, D. S.; Freedman, S. J.; Tanner, E. A.; Vieira, A.; Cornell-Kennon, S.; Lee, J.; Wang, B. Q.; Wang, J. M.; Memmert, K.; Naegeli, H. U.; Petersen, F.; Eck, M. J.; Bair, K. W.; Wood, A. W.; Livingston, D. M. *Cancer Cell* **2004**, *6*, 33.
- (3) Wang, G. L.; Jiang, B. H.; Rue, E. A.; Semenza, G. L. *Proc. Natl. Acad. Sci. U. S. A.* **1995**, *92*, 5510.
- (4) Brown, J. M.; Wilson, W. R. *Nat. Rev. Cancer* **2004**, *4*, 437.
- (5) Ivan, M.; Kondo, K.; Yang, H. F.; Kim, W.; Valiando, J.; Ohh, M.; Salic, A.; Asara, J. M.; Lane, W. S.; Kaelin, W. G. *Science* **2001**, *292*, 464.
- (6) Jaakkola, P.; Mole, D. R.; Tian, Y. M.; Wilson, M. I.; Gielbert, J.; Gaskell, S. J.; von Kriegsheim, A.; Hebestreit, H. F.; Mukherji, M.; Schofield, C. J.; Maxwell, P. H.; Pugh, C. W.; Ratcliffe, P. J. *Science* **2001**, *292*, 468.

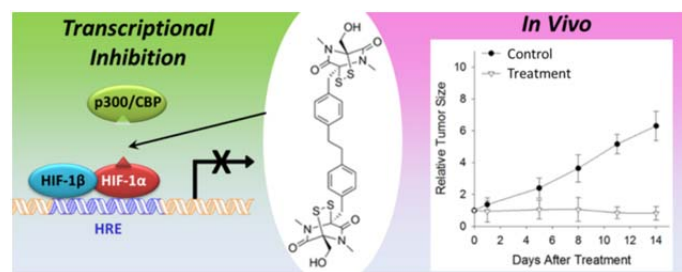
- (7) Masson, N.; Willam, C.; Maxwell, P. H.; Pugh, C. W.; Ratcliffe, P. J. *EMBO J.* **2001**, *20*, 5197.
- (8) Lando, D.; Peet, D. J.; Gorman, J. J.; Whelan, D. A.; Whitelaw, M. L.; Bruick, R. K. *Genes Dev.* **2002**, *16*, 1466.
- (9) Huang, L. E.; Bunn, H. F. *J. Biol. Chem.* **2003**, *278*, 19575.
- (10) Pugh, C. W.; Ratcliffe, P. J. *Nat. Med.* **2003**, *9*, 677.
- (11) Olsson, A. K.; Dimberg, A.; Kreuger, J.; Claesson-Welsh, L. *Nat. Rev. Mol. Cell Biol.* **2006**, *7*, 359.
- (12) Carmeliet, P.; Ferreira, V.; Breier, G.; Pollefeyt, S.; Kieckens, L.; Gertsenstein, M.; Fahrig, M.; Vandenhoeck, A.; Harpal, K.; Eberhardt, C.; Declercq, C.; Pawling, J.; Moons, L.; Collen, D.; Risau, W.; Nagy, A. *Nature* **1996**, *380*, 435.
- (13) Ferrara, N.; CarverMoore, K.; Chen, H.; Dowd, M.; Lu, L.; Oshea, K. S.; PowellBraxton, L.; Hillan, K. J.; Moore, M. W. *Nature* **1996**, *380*, 439.
- (14) Kubo, H.; Alitalo, K. *Genes Dev.* **2003**, *17*, 322.
- (15) Schatteman, G. C.; Awad, O. *Anat. Rec. Part A* **2004**, *276A*, 13.
- (16) Shojaei, F.; Simmons, B. H.; Lee, J. H.; Lappin, P. B.; Christensen, J. G. *Cancer Lett.* **2012**, *320*, 48.
- (17) Boccaccio, C.; Comoglio, P. M. *Nat. Rev. Cancer* **2006**, *6*, 637.
- (18) Pennacchietti, S.; Michieli, P.; Galluzzo, M.; Mazzone, M.; Giordano, S.; Comoglio, P. M. *Cancer Cell* **2003**, *3*, 347.
- (19) Trusolino, L.; Comoglio, P. M. *Nat. Rev. Cancer* **2002**, *2*, 289.
- (20) Giaccia, A.; Siim, B. G.; Johnson, R. S. *Nat. Rev. Drug Discov.* **2003**, *2*, 803.
- (21) Lee, L. W.; Mapp, A. K. *J. Biol. Chem.* **2010**, *285*, 11033.
- (22) Hanahan, D.; Weinberg, R. A. *Cell* **2000**, *100*, 57.
- (23) Hanahan, D.; Weinberg, R. A. *Cell* **2011**, *144*, 646.
- (24) Ribatti, D. *Leuk. Res.* **2011**, *35*, 24.
- (25) Xu, Y.; Li, Q.; Li, X. Y.; Yang, Q. Y.; Xu, W. W.; Liu, G. L. *J. Exp. Clin. Cancer Res.* **2012**, *31*.
- (26) Freedman, S. J.; Sun, Z. Y.; Poy, F.; Kung, A. L.; Livingston, D. M.; Wagner, G.; Eck, M. J. *Proc. Natl. Acad. Sci. U. S. A.* **2002**, *99*, 5367.

- (27) Dames, S. A.; Martinez-Yamout, M.; De Guzman, R. N.; Dyson, H. J.; Wright, P. E. *Proc. Natl. Acad. Sci. U. S. A.* **2002**, *99*, 5271.
- (28) Block, K. M.; Wang, H.; Szabo, L. Z.; Polaske, N. W.; Henchey, L. K.; Dubey, R.; Kushal, S.; Laszlo, C. F.; Makhoul, J.; Song, Z. H.; Meuillet, E. J.; Olenyuk, B. Z. *J. Am. Chem. Soc.* **2009**, *131*, 18078.
- (29) Cook, K. M.; Hilton, S. T.; Mecinovic, J.; Motherwell, W. B.; Figg, W. D.; Schofield, C. *J. J. Biol. Chem.* **2009**, *284*, 26831.
- (30) Kishi, Y.; Nakatsuka, S.; Fukuyama, T.; Havel, M. *J. Am. Chem. Soc.* **1973**, *95*, 6493.
- (31) Fukuyama, T.; Nakatsuka, S.; Kishi, Y. *Tetrahedron* **1981**, *37*, 2045.
- (32) Fukuyama, T.; Kishi, Y. *J. Am. Chem. Soc.* **1976**, *98*, 6723.
- (33) Nakatsuka, S.; Fukuyama, T.; Kishi, Y. *Tetrahedron Lett.* **1974**, *1549*.
- (34) Nicolaou, K. C.; Lu, M.; Totokotsopoulos, S.; Heretsch, P.; Giguere, D.; Sun, Y. P.; Sarlah, D.; Nguyen, T. H.; Wolf, I. C.; Smee, D. F.; Day, C. W.; Bopp, S.; Winzeler, E. A. *J. Am. Chem. Soc.* **2012**, *134*, 17320.
- (35) Codelli, J. A.; Puchlopek, A. L. A.; Reisman, S. E. *J. Am. Chem. Soc.* **2012**, *134*, 1930.
- (36) Overman, L. E.; Sato, T. *Org Lett* **2007**, *9*, 5267.
- (37) DeLorbe, J. E.; Jabri, S. Y.; Mennen, S. M.; Overman, L. E.; Zhang, F. L. *J. Am. Chem. Soc.* **2011**, *133*, 6549.
- (38) Kim, J.; Ashenhurst, J. A.; Movassaghi, M. *Science* **2009**, *324*, 238.
- (39) Iwasa, E.; Hamashima, Y.; Fujishiro, S.; Higuchi, E.; Ito, A.; Yoshida, M.; Sodeoka, M. *J. Am. Chem. Soc.* **2010**, *132*, 4078.
- (40) Sodeoka, M.; Dodo, K.; Teng, Y. O.; Iuchi, K.; Hamashima, Y.; Iwasa, E.; Fujishiro, S. *Pure Appl. Chem.* **2012**, *84*, 1369.
- (41) Blangetti, M.; Fleming, P.; O'Shea, D. F. *J. Org. Chem.* **2012**, *77*, 2870.
- (42) Roehrl, M. H. A.; Wang, J. Y.; Wagner, G. *Biochemistry* **2004**, *43*, 16056.
- (43) Lohela, M.; Werb, Z. *Curr. Opin. Genet. Dev.* **2010**, *20*, 72.
- (44) Lunt, S. J.; Gray, C.; Reyes-Aldasoro, C. C.; Matcher, S. J.; Tozer, G. M. *J. Biomed. Opt.* **2010**, *15*, 011113.
- (45) Vajkoczy, P.; Ullrich, A.; Menger, M. D. *Neoplasia* **2000**, *2*, 53.
- (46) Hak, S.; Reitan, N. K.; Haraldseth, O.; de Lange Davies, C. *Angiogenesis* **2010**, *13*, 113.
- (47) Koehl, G. E.; Gaumann, A.; Geissler, E. K. *Clin. Exp. Metastasis* **2009**, *26*, 329.

- (48) Oh, P.; Borgstrom, P.; Witkiewicz, H.; Li, Y.; Borgstrom, B. J.; Chrastina, A.; Iwata, K.; Zinn, K. R.; Baldwin, R.; Testa, J. E.; Schnitzer, J. E. *Nat. Biotechnol.* **2007**, *25*, 327.
- (49) Reitan, N. K.; Thuen, M.; Goa, P. E.; de Lange Davies, C. *J. Biomed. Opt.* **2010**, *15*, 036004.
- (50) Testa, J. E.; Chrastina, A.; Oh, P.; Li, Y.; Witkiewicz, H.; Czarny, M.; Buss, T.; Schnitzer, J. E. *Am. J. Physiol.* **2009**, *297*, L251.
- (51) Darnell, J. E., Jr. *Nat Rev Cancer* **2002**, *2*, 740.
- (52) Mapp, A. K.; Ansari, A. Z. *ACS Chem. Biol.* **2007**, *2*, 62.
- (53) Koehler, A. N. *Curr. Opin. Chem. Biol.* **2010**, *14*, 331.
- (54) Majmudar, C. Y.; Hojfeldt, J. W.; Arevang, C. J.; Pomerantz, W. C.; Gagnon, J. K.; Schultz, P. J.; Cesa, L. C.; Doss, C. H.; Rowe, S. P.; Vasquez, V.; Tamayo-Castillo, G.; Cierpicki, T.; Brooks, C. L.; Sherman, D. H.; Mapp, A. K. *Angew. Chem. -Int. Edit.* **2012**, *51*, 11258.
- (55) Arndt, H. D. *Angew. Chem. -Int. Edit.* **2006**, *45*, 4552.
- (56) Mapp, A. K. *Org. Biomol. Chem.* **2003**, *1*, 2217.
- (57) Denison, C.; Kodadek, T. *Chem. Biol.* **1998**, *5*, R129.
- (58) Dervan, P. B. *Bioorg. Med. Chem.* **2001**, *9*, 2215.
- (59) Chenoweth, D. M.; Dervan, P. B. *Proc. Natl. Acad. Sci. U. S. A.* **2009**, *106*, 13175.
- (60) Rai, M.; Gottesfeld, J.; Dervan, P.; Pandolfo, M. *Neuromusc. Disord.* **2006**, *16*, 705.
- (61) Olenyuk, B. Z.; Zhang, G. J.; Klco, J. M.; Nickols, N. G.; Kaelin, W. G.; Dervan, P. B. *Proc. Natl. Acad. Sci. U. S. A.* **2004**, *101*, 16768.
- (62) Dervan, P. B.; Poulin-Kerstien, A. T.; Fechter, E. J.; Edelson, B. S. In *DNA Binders and Related Subjects*; Springer-Verlag: Berlin, 2005; Vol. 253, p 1.
- (63) Alvarez, D.; Chou, C. J.; Latella, L.; Zeitlin, S. G.; Ku, S.; Puri, P. L.; Dervan, P. B.; Gottesfeld, J. M. *Cell Cycle* **2006**, *5*, 1537.
- (64) Dickinson, L. A.; Burnett, R.; Melander, C.; Edelson, B. S.; Arora, P. S.; Dervan, P. B.; Gottesfeld, J. M. *Chem. Biol.* **2004**, *11*, 1583.
- (65) Muzikar, K. A.; Nickols, N. G.; Dervan, P. B. *Proc. Natl. Acad. Sci. U. S. A.* **2009**, *106*, 16598.
- (66) Nickols, N. G.; Dervan, P. B. *Proc. Natl. Acad. Sci. U. S. A.* **2007**, *104*, 10418.

- (67) Nickols, N. G.; Jacobs, C. S.; Farkas, M. E.; Dervan, P. B. *Acs Chemical Biology* **2007**, *2*, 561.
- (68) Raskatov, J. A.; Meier, J. L.; Puckett, J. W.; Yang, F.; Ramakrishnan, P.; Dervan, P. B. *Proc. Natl. Acad. Sci. U. S. A.* **2012**, *109*, 1023.
- (69) Belitsky, J. M.; Leslie, S. J.; Arora, P. S.; Beerman, T. A.; Dervan, P. B. *Bioorg. Med. Chem.* **2002**, *10*, 3313.
- (70) Best, T. P.; Edelson, B. S.; Nickols, N. G.; Dervan, P. B. *Proc. Natl. Acad. Sci. U. S. A.* **2003**, *100*, 12063.
- (71) Edelson, B. S.; Best, T. P.; Olenyuk, B.; Nickols, N. G.; Doss, R. M.; Foister, S.; Heckel, A.; Dervan, P. B. *Nucl. Acids Res.* **2004**, *32*, 2802.
- (72) Jacobs, C. S.; Dervan, P. B. *J. Med. Chem.* **2009**, *52*, 7380.
- (73) Meier, J. L.; Montgomery, D. C.; Dervan, P. B. *Nucl. Acids Res.* **2012**, *40*, 2345.
- (74) Raskatov, J. A.; Hargrove, A. E.; So, A. Y.; Dervan, P. B. *J. Am. Chem. Soc.* **2012**, *134*, 7995.
- (75) Synold, T. W.; Xi, B. X.; Wu, J.; Yen, Y.; Li, B. C.; Yang, F.; Phillips, J. W.; Nickols, N. G.; Dervan, P. B. *Cancer. Chemoth. Pharm.* **2012**, *70*, 617.
- (76) Meier, J. L.; Yu, A. S.; Korf, I.; Segal, D. J.; Dervan, P. B. *J. Am. Chem. Soc.* **2012**, *134*, 17814.
- (77) Kushal, S.; Wang, H.; Laszlo, C. F.; Szabo, L. Z.; Olenyuk, B. Z. *Biopolymers* **2011**, *95*, 8.
- (78) PaineMurrieta, G. D.; Taylor, C. W.; Curtis, R. A.; Lopez, M. H. A.; Dorr, R. T.; Johnson, C. S.; Funk, C. Y.; Thompson, F.; Hersh, E. M. *Cancer. Chemoth. Pharm.* **1997**, *40*, 209.
- (79) Frost, G. I.; Lustgarten, J.; Dudouet, B.; Nyberg, L.; Hartley-Asp, B.; Borgstrom, P. *Microvasc. Res.* **2005**, *69*, 1.

TOC Graphic



Supporting Information of

Suppression of Tumor Growth by Designed Dimeric Epidithiodiketopiperazine Targeting Hypoxia- Inducible Transcription Factor Complex

Ramin Dubey,[†] Michael D. Levin,[§] Lajos Z. Szabo,[‡] Csaba F. Laszlo,[‡] Swati Kushal,[†] Jason B. Singh,[‡] Philip Oh,[§] Jan E. Schnitzer,[§] and Bogdan Z. Olenyuk[†]*

Addresses:

[†] Department of Pharmacology and Pharmaceutical Sciences, University of Southern California, 1985 Zonal Ave., PSC B15C, HSC 9121, Los Angeles, CA 90089

[‡] Department of Chemistry and Biochemistry, University of Arizona, 1306 E University Blvd, Tucson, AZ 85721

[§] Proteogenomics Research Institute for Systems Medicine, 11107 Roselle St., San Diego, CA 92121

*Corresponding author, bogdan@usc.edu

Contents:

Figure S1.....	S2
Figure S2.....	S3
Figure S3.....	S4
Figure S4.....	S5
Figure S5.....	S5
Figure S6.....	S6
Figure S7.....	S6
Surface Plasmon Resonance Experiments	S7
Measuring VEGF Protein Levels with ELISA	S8
General Synthetic Methods.....	S8
Figure S8.....	S17
Figure S9.....	S18
NMR Spectra	S19

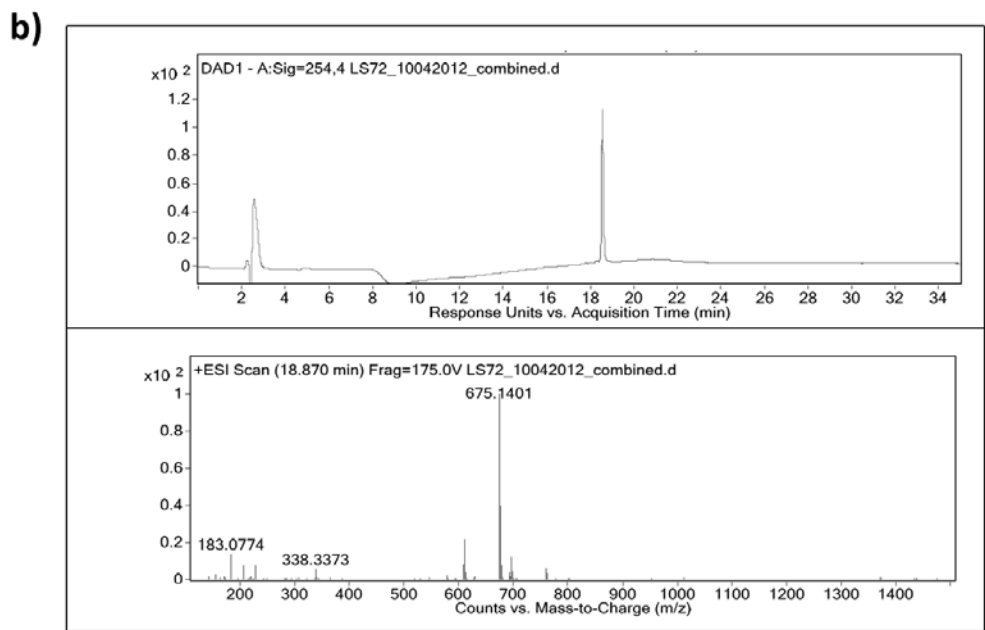
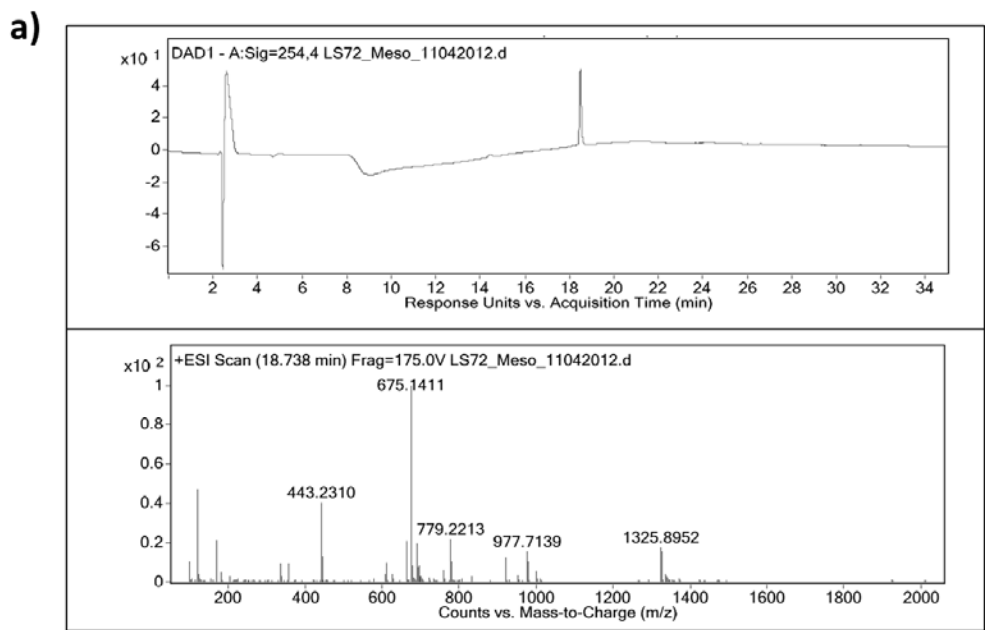


Figure S1. UV traces (254 nm) of chromatograms (top), and mass spectra (bottom) for (a) *meso*-ETP **2** and (b) (\pm)-ETP **2**.

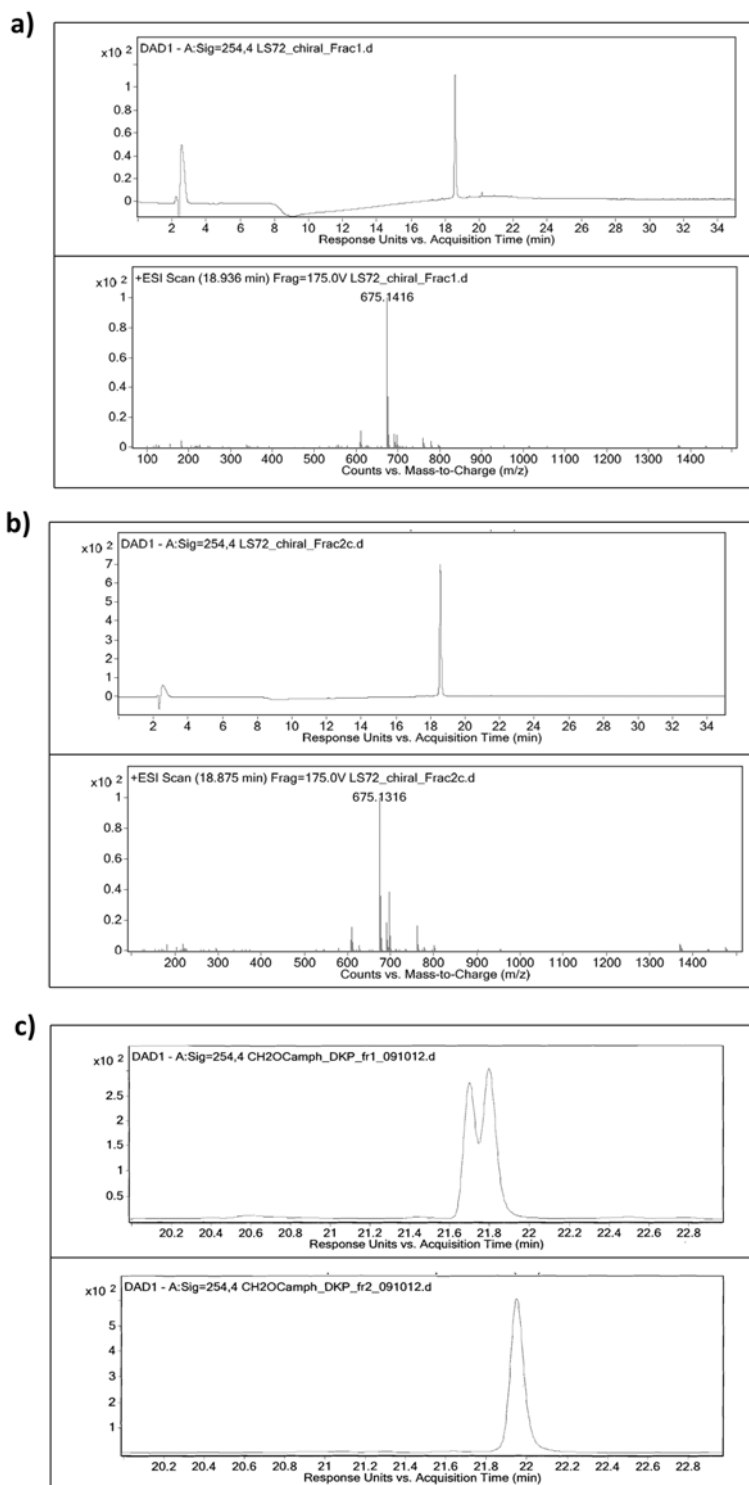


Figure S2. UV traces (254 nm) of chromatograms (top) and mass spectra (bottom) of the two enantiomers (a) *ent1*-ETP **2** and (b) *ent2*-ETP **2**. (c) UV traces (254 nm) of chromatograms of camphanic esters *dst1*-**8** and *dst2*-**8** derived from (\pm)-**7** (top) and *meso*-**7** (bottom).

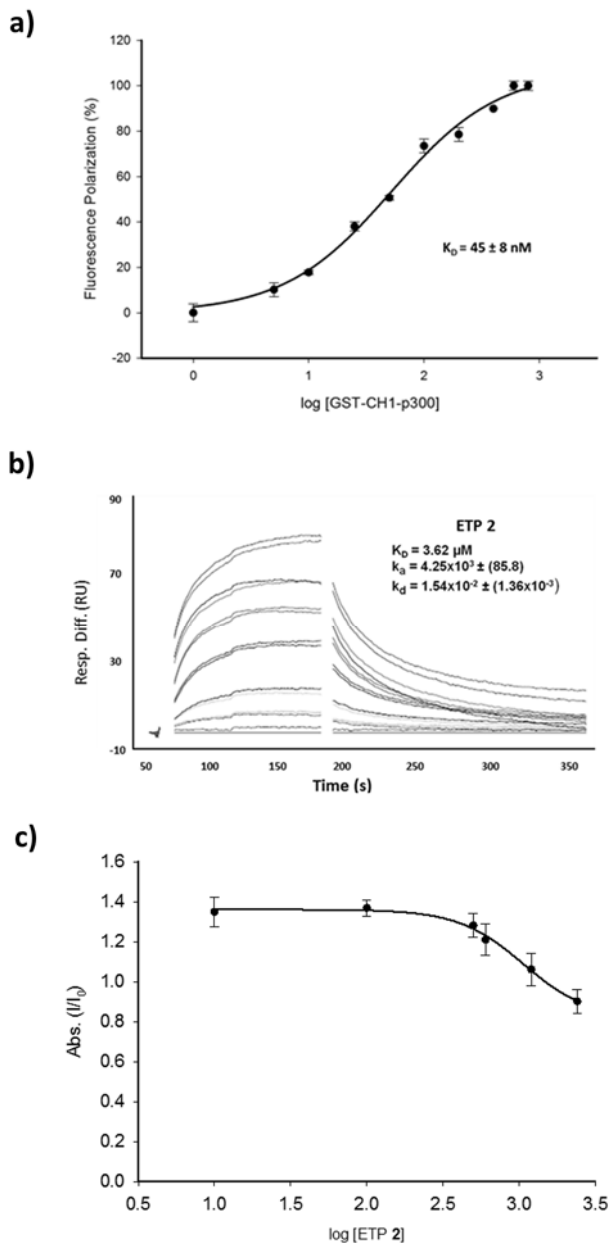


Figure S3. a) Saturation binding curve of fluorescein-labeled HIF1 α C-TAD peptide (15 μ M) to p300-CH1-GST protein. b) SPR sensorgrams showing high affinity direct binding of ETP 2 to CH1-GST fusion protein immobilized on the SPR CM5 chip. c) Cytotoxicity of dimeric ETP 2 in MDA-MB-231 cell line as measured by the MTT assay. Cells were treated with ETP 2 for 24 h at a range of concentrations from 100 nM to 2.4 μ M.

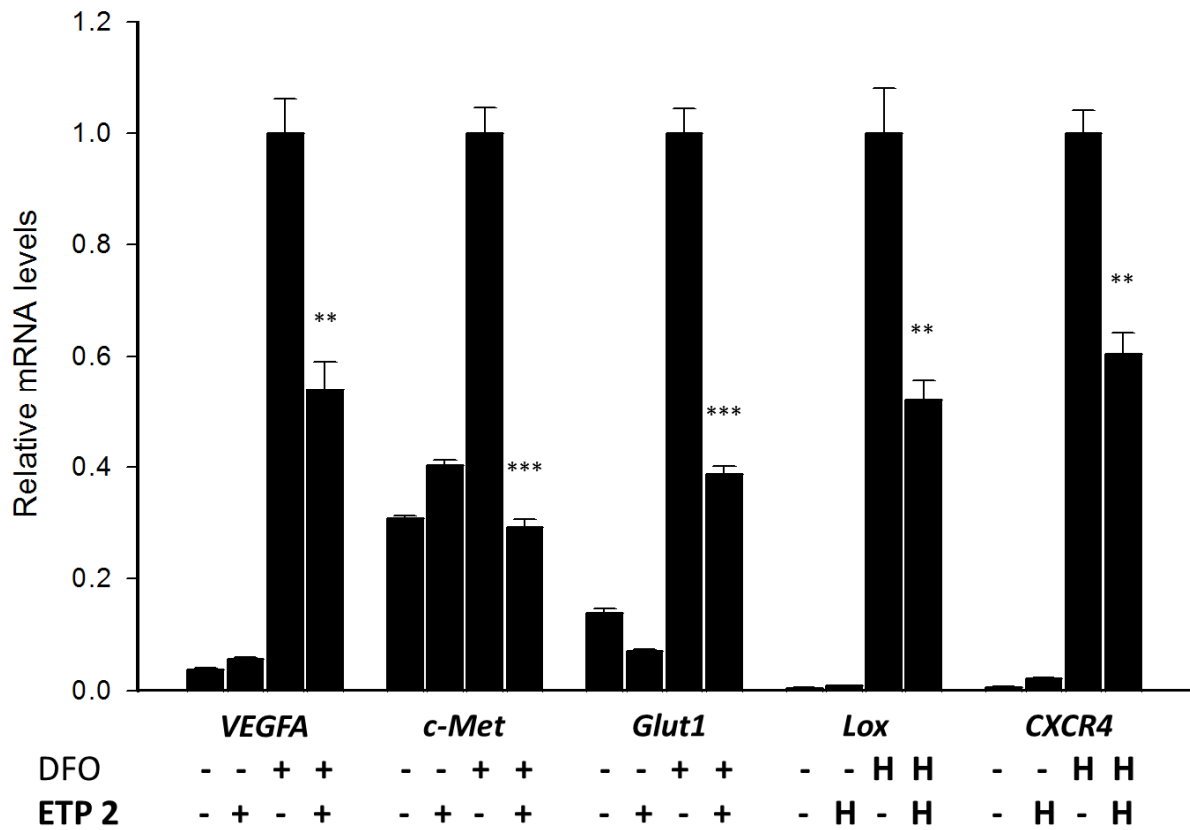


Figure S4. Results from real-time qRT-PCR assay with A549 cells treated with ETP 2 (400 nM) in serum-free F-12K medium. Hypoxia was chemically mimicked with DFO (300 μ M) or hypoxic environment, H (BD GasPak EZ pouch). All five genes (*VEGFA*, *c-Met*, *Glut1*, *LOX*, and *CXCR4*) are upregulated at hypoxia and show significant reduction of the mRNA levels upon treatment with ETP 2. *** $P < 0.001$, ** $P < 0.01$, *t*-test.



Figure S5. HIF1 α protein levels are unaffected by ETP 2. A549 cells were treated with ETP 2 (1.6 μ M) in presence or absence of DFO (300 μ M) to mimic hypoxia. Lamin-A/C protein was used as a control.

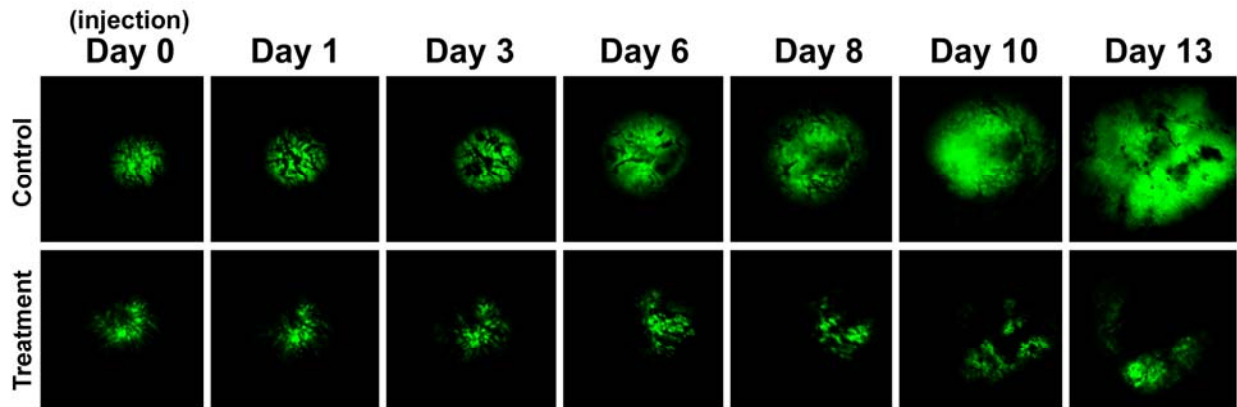


Figure S6. Intravital microscopy images of murine subcutaneous tumor model of N202 cells stably transfected with a H2B-GFP construct. Mice with N202 H2B-GFP tumors were injected intravenously on day 0 with 1 mg/kg of (\pm)-ETP **2** followed by daily injections of the same compound after day 8. Fluorescence IVM images of tumors were taken on the days indicated.

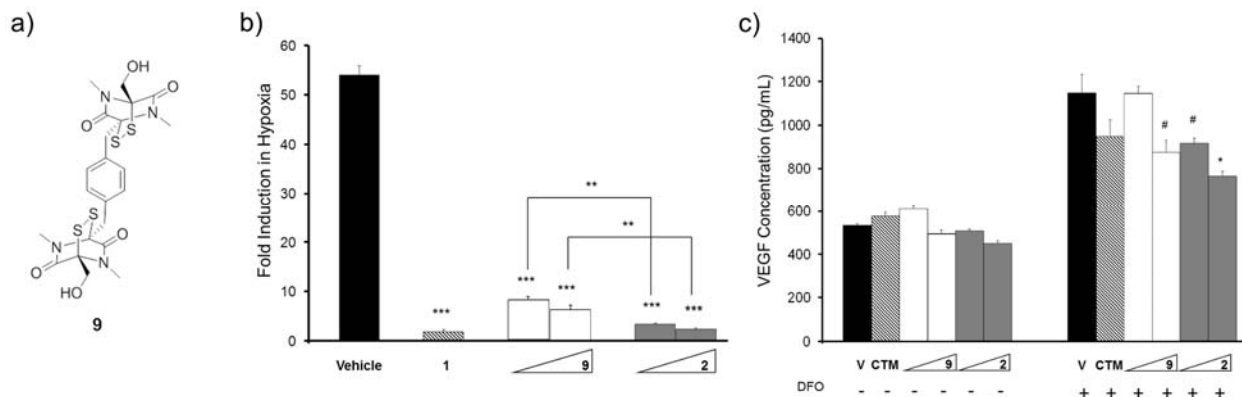


Figure S7. a) Structure of the first-generation dimeric ETP **9**. b) ETP **2** is more effective than ETP **9** in reducing the hypoxia-inducible promoter activity in MDA-MB-231-HRE-Luc cell line ($P < 0.01$, *t*-test). c) ETP **2** shows greater efficacy than ETP **9** in downregulating the VEGF protein levels in MCF7 cell line as determined by the ELISA assay. CTM was a positive control and was at a final concentration of 200 nM; synthetic ETPs **2** and **9** were at final concentrations 200 nM and 600 nM. Hypoxia was mimicked with 300 μ M DFO. Error bars are \pm s.e.m of experiments performed in triplicate. *** $P < 0.001$, ** $P < 0.01$, * $P < 0.05$, # $P < 0.1$, *t*-test.

Surface Plasmon Resonance Experiments

Measurements were made using a Biacore T100 instrument (GE Healthcare). A Biacore CM5 Sensor Chip and an amine coupling kit were purchased directly from Biacore. The CM5 chip contains a carboxymethylated dextran polymer covalently attached to a gold surface; molecules are covalently coupled to the sensor chip via linkage to these carboxyl groups.

Activation of chip surface and immobilization of anti-GST capture antibody. The CM5 sensor chip was activated with 0.4 M 1-ethyl-3-(3-dimethylpropyl)-carbodiimide mixed with 0.1 M N-hydroxysuccinimide in a 1:1 (v/v) ratio. This was followed with an injection of 1 M ethanolamine-HCl at pH 8.5. Flow rate was 5 μ L/min with an injection time of 10 min. Goat anti-GST antibody (50 μ g/mL, Pharmacia) was coupled to the chip surface utilizing a flow rate of 15 μ L/min with 10 min injections.

Immobilization of p300-CH1-GST fusion protein. A 1 mg/mL solution of p300-CH1-GST was allowed to flow over the surface of the sensor chip with anti-GST previously immobilized. Injections (10 min at a rate of 10 μ L/min) were repeated until the desired level of immobilization was achieved.

Binding experiments. ETP **2** was assayed at each of the following concentrations: 50 μ M, 10 μ M, 1 μ M, 500 nM, 200 nM, and 50 nM. Samples were prepared from 100% DMSO stock solutions in a buffer containing 10 mM Tris, 100 mM NaH₂PO₄, 100 μ M DTT, and 100 μ M ZnCl₂ at pH 8.0. This buffer was used for all SPR assays and was filtered through a 0.2 μ m filter and thoroughly degassed prior to use or during sample preparation. All samples contained a final concentration of 5% DMSO.

A sample containing 5% DMSO in buffer was run to establish a baseline for the blank. All runs were also double-referenced against a flow cell containing only immobilized anti-GST

antibody but not p300-CH1-GST to account for any nonspecific binding. A run consisted of 3.3 min with a 100 μ L sample injection (flow rate was 30 μ L/min) followed by 3.3 min buffer flow as a wash. After each injection, the chip surface was regenerated (1 min injection at a flow rate of 30 μ L/min) of 10 mM H₃PO₄ following the buffer wash. All experiments were performed in triplicate.

Measuring VEGF Protein Levels with ELISA

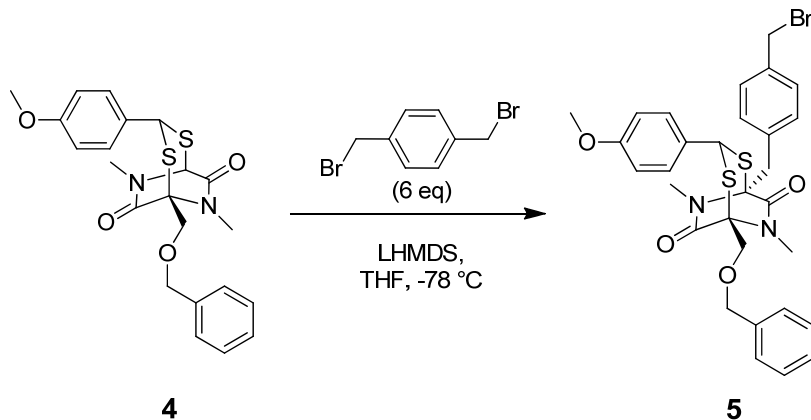
MCF7 cells were plated in 24-well culture dishes (BD Falcon) in 1 mL of media to a density of 1.1×10^5 cells/mL. After attachment, wells were treated with 1 mL media containing CTM, ETPs **2** and **6** at concentrations of 200 nM and 600 nM. All samples contained a final concentration of 0.1% DMSO; vehicle samples were treated with cell culture media containing 0.1% DMSO. After a 6 hour incubation period, hypoxia was induced and samples were incubated for an additional 18 hours. Cell culture supernatants (200 μ L) were collected. The ELISA assays (R&D Systems) were performed in accordance with the manufacturer's protocol. Absorbance measurements were taken at 450 nM using a BioTek Synergy 2 microplate reader. The amounts of protein were normalized to the total protein content determined by the Bradford assay.

General Synthetic Methods

All reagents and solvents were obtained from commercial sources and were used as received unless otherwise stated. Chetomin was purchased from EMD Biosciences. Dry THF was obtained by distillation with sodium and benzophenone. Dry CH₂Cl₂ was freshly distilled with calcium hydride. All reactions involving moisture-sensitive reagents were conducted under argon

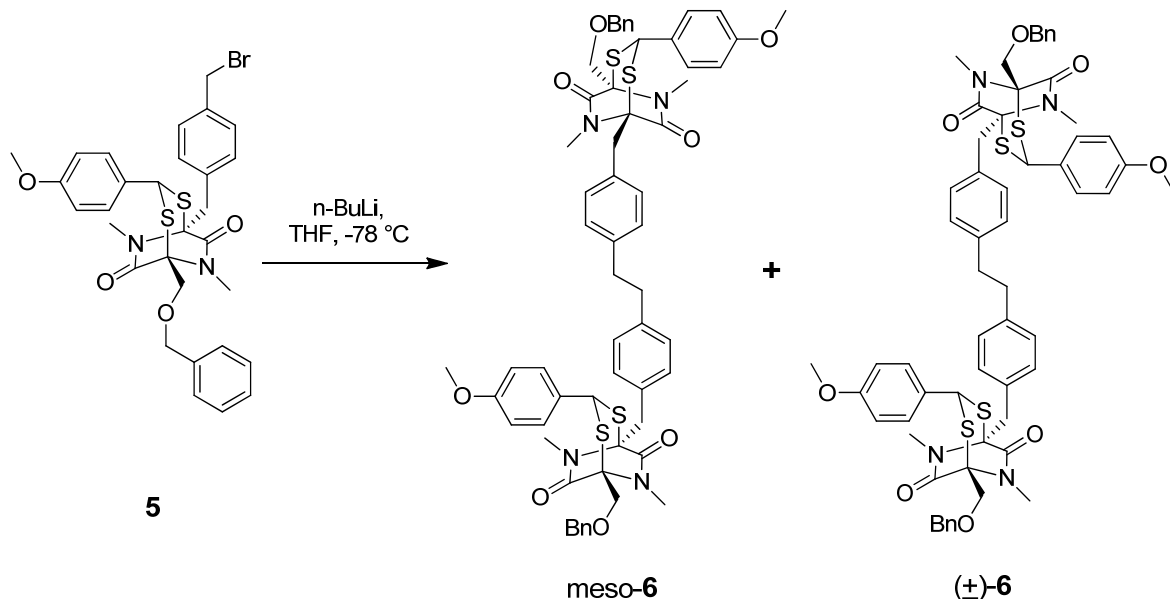
atmosphere with anhydrous solvents and flame-dried glassware. Hygroscopic liquids were transferred via a syringe and were introduced into reaction vessels through rubber septa. Reaction product solutions were concentrated using a rotary evaporator at 30-150 mm Hg. Column chromatography was performed on silica gel (230-400 mesh) using reagent grade solvents. Analytical thin-layer chromatography (TLC) was performed on glass-backed, pre-coated plates (0.25 mm, silica gel 60, F-254, EM Science). Preparatory HPLC purifications were carried out with C₈ reverse phase preparative column (Alltech/Grace Davison). The flow rate was 4 or 5 mL/min. In all cases, gradients of acetonitrile in 0.1% aqueous trifluoroacetic acid (TFA) were used as eluents. Water (18 MΩ) was obtained from a Millipore MilliQ water purification system, and all buffers were filtered through 0.2 μm nylon filter. Nuclear magnetic resonance (NMR) spectra were collected on Varian 400 and Bruker 500 MHz instruments in the indicated solvents. The peak positions are reported with chemical shifts (δ) in parts per million (ppm) downfield from the signal for tetramethylsilane (0 ppm) and referenced to the signal resulting from the incomplete deuteration of a solvent used in the experiment (CDCl₃: 7.26 ppm, or the center line of the multiplet of DMSO-*d*₆: 2.50 ppm). Carbon-13 chemical shifts are reported as δ values in ppm and referenced to the carbon-13 signal of a solvent used in the experiment (CDCl₃: 77.0 ppm, or the center line of the multiplet DMSO-*d*₆: 39.51 ppm). The following abbreviations are used: singlet (s), doublet (d), triplet (t), doublet of doublets (dd), multiplet (m). Mass spectra were obtained at Thermo Finnigan LCQ and Agilent 6200 Series Accurate-Mass Time-of-Flight (TOF) LCMS instruments, School of Pharmacy, University of Southern California.

1-((Benzyl)oxy)methyl-5-(4-(bromomethyl)benzyl)-3-(4-methoxyphenyl)-6,8-dimethyl-2,4-dithia-6,8-diazabicyclo[3.2.2]nonane-7,9-dione (5).



The protected dithioacetal **4** (444 mg, 1 mmol, 1.0 eq.) and α,α' -dibromo-*p*-xylene (1.58 g, 6 mmol, 6 eq.) were dissolved in anhydrous THF (80 mL) and cooled to -78 °C. Next, a 1 M solution of LHMDS in THF (1.3 mL, 1.3 mmol, 1.3 eq.) was added dropwise over a period of 3 min with stirring. The stirring was continued at -78 °C for an additional 5 min. The cooling bath was then removed, and the mixture was allowed to warm to room temperature and stirring continued for an additional 3 h. Saturated NaCl solution was added to the reaction mixture next and the red solution was extracted with dichloromethane (3 × 50 mL). The combined organic extracts were dried over anhydrous MgSO₄, filtered and concentrated under reduced pressure. The solid residue was separated by column chromatography on silica gel using dichloromethane as an eluent to give product **5**, 388 mg (77 % yield). ¹H NMR (CDCl₃, TMS, ppm) δ: 7.33 (m, 9H), 7.13 (d, *J* = 8.4 Hz, 2H), 6.85 (d, *J* = 8.8 Hz, 2H), 5.08 (s, 1H), 4.78 (d, *J* = 12.0 Hz, 1H), 4.56 (d, *J* = 12.0 Hz, 1H), 4.46 (s, 2H), 4.37 (d, *J* = 16.8 Hz, 1H), 4.32 (d, *J* = 10.5 Hz, 1H), 3.85 (d, *J* = 10.5 Hz, 1H), 3.80 (s, 3H), 3.35 (s, 3H), 3.15 (d, *J* = 16.8 Hz, 1H), 2.97 (s, 3H). ¹³C NMR (CDCl₃, ppm) δ: 165.72, 165.46, 160.55, 137.39, 136.30, 135.50, 130.46, 129.38, 128.75, 128.45, 127.93, 127.78, 126.52, 114.39, 74.02, 73.39, 71.07, 68.68, 55.37, 51.24, 40.21, 33.07, 29.80, 28.08. FABMS: Calcd. for C₃₀H₃₁BrN₂O₄S₂: 626.1, Found [M+H]⁺: 627.0.

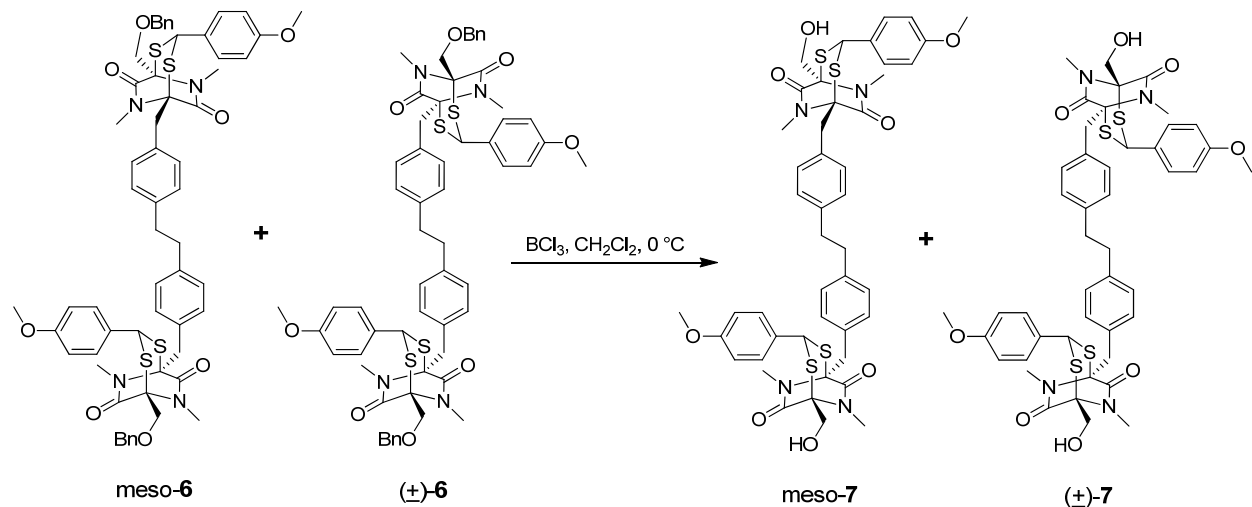
5,5'-((Ethane-1,2-diylbis(4,1-phenylene))bis(methylene))bis(1-((benzyloxy)methyl)-3-(4-methoxyphenyl)-6,8-dimethyl-2,4-dithia-6,8-diazabicyclo[3.2.2]nonane-7,9-dione) (6**)**



A solution of **5** (2.14 g, 3.40 mmol, 1.0 eq.) was cooled to -78 °C and 1.6 M *n*-butyllithium in hexane (2.77 mL, 4.43 mmol, 1.3 eq.) was added dropwise upon stirring over a period of 2 min. Following the addition, the stirring was continued at -78 °C for an additional 5 min. The cooling bath was then removed and the mixture was allowed to gradually warm up to room temperature over the period of 3 h. The reaction mixture was then poured into ice-cold water and extracted with dichloromethane (3 × 50 mL). The combined organic extracts were dried over anhydrous MgSO₄, filtered and concentrated under reduced pressure to yield product as a mixture of *meso*-**6** and (\pm) -**6**. The products were purified from reactants by column chromatography on silica gel using CH₂Cl₂ : Hexane : EtOAc = 5 : 4 : 1 as an eluent and were used as a mixture in the next step. Total yield: 638 mg (34%). A sample of the obtained product was subjected to a second column chromatography on silica gel using the same eluent system, where a portion of racemic (\pm) -**6** was separated from the mixture of (\pm) -**6** and *meso*-**6** and used for analysis. Analysis data for (\pm) -**6**: ¹H NMR (CDCl₃, ppm) δ: 7.34 (m, 14H), 7.08 (q, 8H), 6.85 (d, *J* = 8.8 Hz, 4H), 5.07 (s, 2H), 4.78 (d, *J* = 12.2 Hz, 2H), 4.56 (d, *J* = 12.2 Hz, 2H), 4.36 (d, *J* = 16.8 Hz, 2H), 4.31 (d, *J* = 10.7 Hz, 2H), 3.84 (d, *J* = 10.7 Hz, 2H), 3.80 (s, 6H), 3.34 (s, 6H), 3.10 (d, *J* = 16.8 Hz, 2H), 2.97 (d, 6H), 2.86 (s, 4H). ¹³C NMR (CDCl₃, ppm) δ: 165.76, 165.63, 160.51, 140.26, 137.44, 132.66, 130.46, 128.69, 128.42, 127.89, 127.76, 126.67, 114.36, 74.00, 73.56, 71.08, 68.71,

55.36, 51.23, 40.24, 37.27, 29.78, 28.07. HRFABMS: Calcd. for $C_{60}H_{62}N_4O_8S_4$ 1094.345, Found $[M+H]^+$ 1095.356.

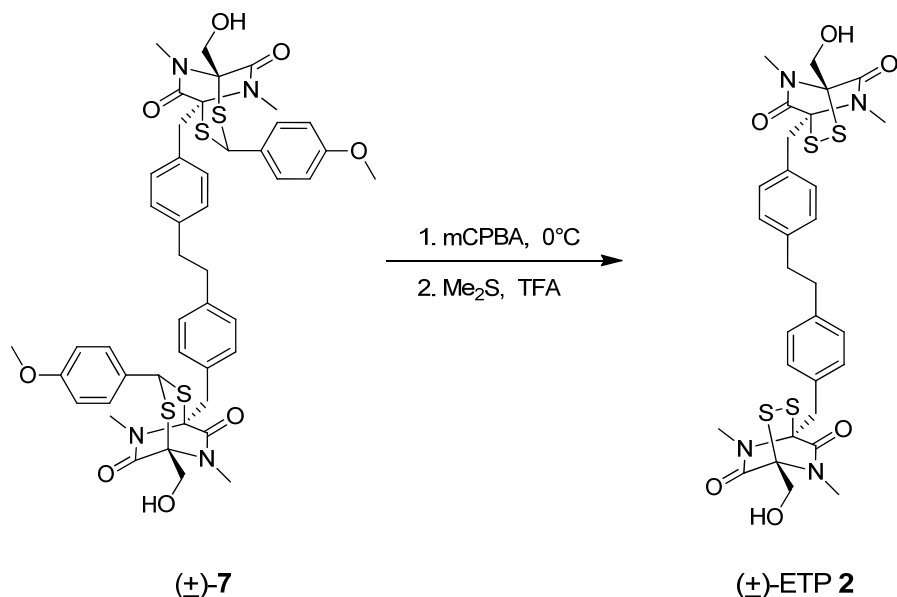
5,5'-(*(Ethane-1,2-diylbis(4,1-phenylene))bis(methylene)*)bis(1-(hydroxymethyl)-3-(4-methoxyphenyl)-6,8-dimethyl-2,4-dithia-6,8-diazabicyclo[3.2.2]nonane-7,9-dione) (7)



To an ice-cooled solution of **6** (125 mg, 0.126 mmol, 1 eq.) in dichloromethane, a 1 M solution of boron trichloride in dichloromethane (320 μ L, 0.32 mmol, 2.5 eq) was added dropwise while stirring. The mixture was allowed to stand at $0^\circ C$ for 15 min and then was poured into the ice-cold water. The aqueous layer was extracted with dichloromethane (3×50 mL). The combined organic extracts were dried over anhydrous magnesium sulfate, filtered and evaporated under reduced pressure. The crude reaction mixture was purified by flash column chromatography to give 78 mg of product mixture of *meso*-**7** and *(±)*-**7** as a white solid (75% combined yield). The mixture of *meso*-**7** and *(±)*-**7** was further purified on silica gel column using gradient of EtOAC in dichloromethane from 10% to 50% in order to separate *meso*-**7** and *(±)*-**7**. Analytical data for *(±)*-**7**: 1H NMR ($CDCl_3$, ppm) δ : 7.32 (d, 4H), 6.93 (d, 4H) 6.89 (d, 4H), 6.86 (d, 4H), 5.08 (s, 2H), 4.47 (dd, $J = 6$ Hz, 13 Hz, 2H), 4.37 (d, 2H), 4.26 (m, 2H), 3.98 (dd, $J = 10$ Hz, 13 Hz, 2H), 3.80 (s, 6H), 3.41 (s, 6H), 2.98 (d, 2H), 2.84 (s, 6H), 2.69 (d, 2H). ^{13}C NMR ($DMSO-d_6$, ppm) δ : 165.42, 165.19, 160.06, 140.00, 132.93, 130.52, 128.53, 128.42, 126.82, 114.38, 73.47, 71.51, 60.79, 55.29, 49.91, 40.14, 36.36, 29.60, 27.96. FABMS: Calcd. for $C_{46}H_{50}N_4O_8S_4$: 914.3 Found $[M+Na]^+$: 936.9. Analytical data for *meso*-**7**: 1H NMR ($CDCl_3$, ppm) δ : 7.33 (d, 4H), 7.02 (d, 4H) 6.99 (d, 4H), 6.86 (d, 4H), 5.09 (s, 2H), 4.35 (dd, $J = 10$ Hz, 13 Hz, 2H), 4.37 (d, 2H), 3.11

(m, 2H), 4.04 (dd, J = 10 Hz, 13 Hz, 2H), 3.81 (s, 6H), 3.41 (s, 6H), 2.91 (s, 6H), 2.85 (s, 4H). ^{13}C NMR (DMSO-d₆, ppm) δ : 165.47, 165.24, 160.10, 140.04, 132.96, 130.56, 128.55, 128.48, 126.85, 114.42, 73.50, 71.55, 60.83, 55.34, 49.96, 40.14, 36.42, 29.63, 28.00. FABMS: Calcd. for C₄₆H₅₀N₄O₈S₄: 914.3 Found [M+Na]⁺: 936.9.

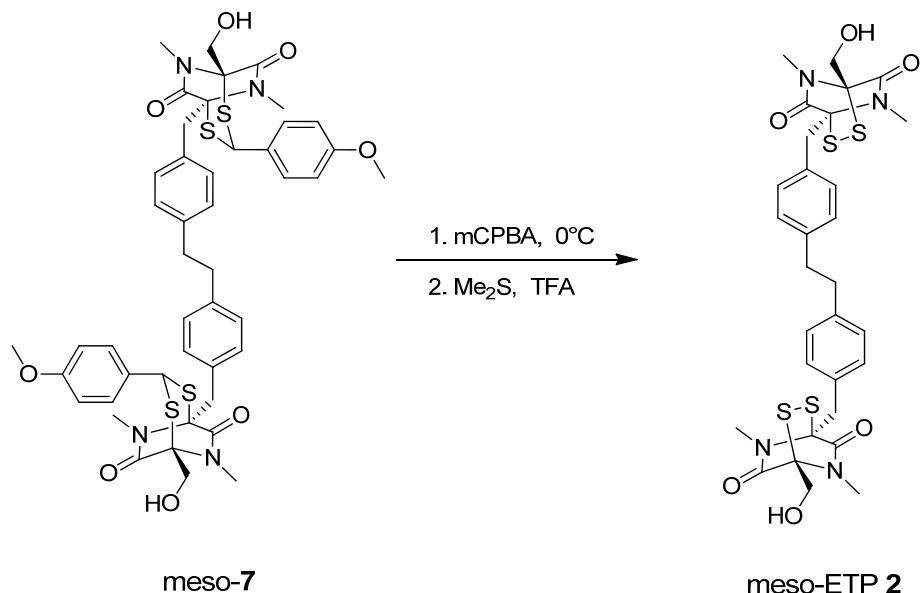
(\pm)-4,4'-(ethane-1,2-diylbis(4,1-phenylene))bis(methylene))bis(1-(hydroxymethyl)-5,7-dimethyl-2,3-dithia-5,7-diazabicyclo[2.2.2]octane-6,8-dione) ((\pm)-ETP 2)



A 50 mL round-bottom flask was charged with the dithioacetal (\pm)-7 (20 mg, 0.022 mmol) which was dissolved in 35 mL of CH₂Cl₂. The flask was cooled to 0 °C and excess of *m*-chloroperbenzoic acid (15 mg, 77% content, 0.07 mmol) was added. After 30 min of stirring at 0 °C the ice bath was removed and dimethyl sulfide (6.4 μ L, 0.09 mmol) was added, followed by the addition of trifluoroacetic acid (126 μ L). The reaction mixture was stirred at room temperature for 3 h. An aqueous saturated sodium bicarbonate (15 mL) was added to the reaction mixture and the organic layer was separated. The aqueous layer was further extracted with dichloromethane (20 mL). The combined organic layers were dried over anhydrous Mg₂SO₄, filtered and concentrated under reduced pressure. The glassy residue was dissolved in 50% DMSO in acetonitrile and purified by reverse-phase HPLC to obtain (\pm)-ETP 2 in 61% yield. Alternatively, to purify the larger amount of (\pm)-ETP 2, a post work-up crystallization of the reaction mixture was performed. Briefly, to the residue (25 mg) acetonitrile was added (2 mL) and the mixture was briefly sonicated at room temperature to dissolve the residue. The

mixture was cooled to 4 °C and maintained at that temperature for 2 h, after which it was stored overnight at -20 °C. The supernatant was removed by filtration and the white crystals were washed with acetonitrile cooled to -20 °C. The supernatant was recrystallized again by employing the above procedure. The purity of the final product was verified by analytical HPLC using gradient of acetonitrile (40% – 95% over 20 min) in an aqueous phase that contained 0.05% v/v of trifluoroacetic acid. ¹H NMR (CDCl₃, ppm) δ: 7.19 (d, 4H), 7.07 (d, 4H), 4.39 (d, 2H), 4.30 (d, 2H), 4.04 (d, 2H), 3.59 (d, 2H), 3.21 (s, 6H), 2.96 (s, 6H), 2.86 (m, 4H). ¹³C NMR (CDCl₃, ppm) δ: 166.85, 165.57, 140.65, 131.58, 129.07, 128.81, 75.80, 75.18, 61.21, 37.22, 36.51, 28.59, 27.53. HR-ESIMS: Calcd. for C₃₀H₃₄N₄O₆S₄+H⁺: 675.14, Found [M+H]⁺: 675.1401.

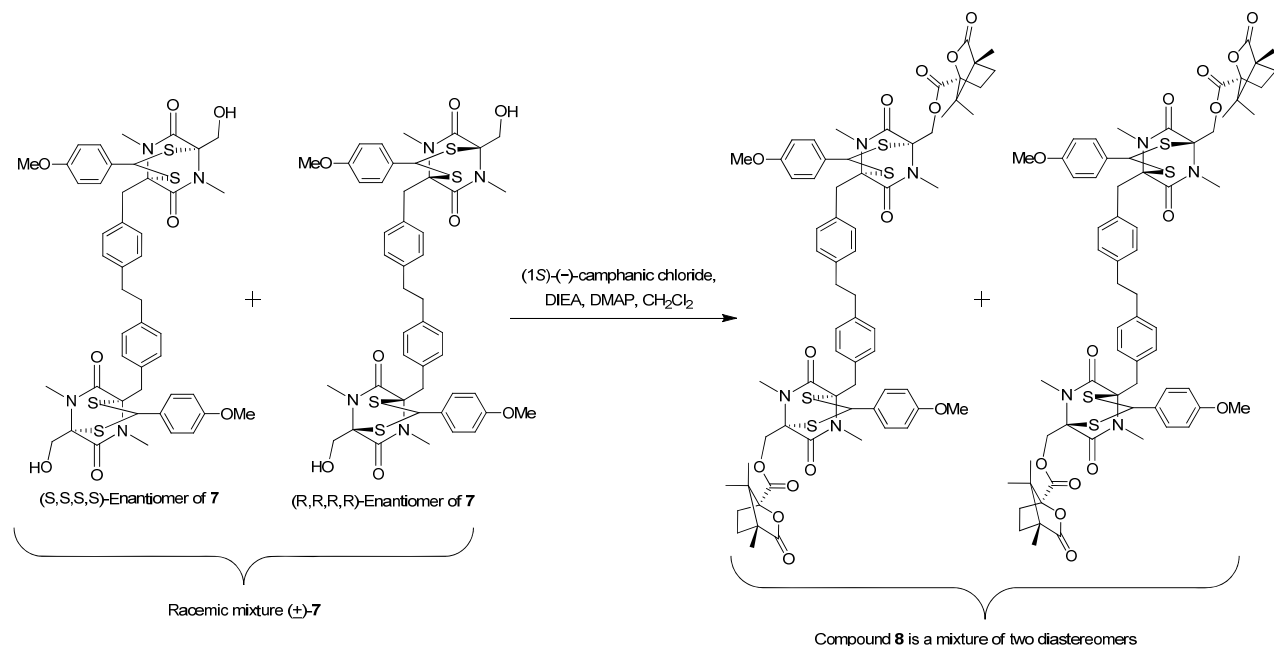
Meso-4,4'-(ethane-1,2-diylbis(4,1-phenylene))bis(methylene)bis(1-(hydroxymethyl)-5,7-dimethyl-2,3-dithia-5,7-diazabicyclo[2.2.2]octane-6,8-dione) (*meso*-ETP 2)



Meso-ETP 2 was prepared from dithioacetal *meso*-7 by following the procedure analogous to that of (±)-7. Yield 60%, ¹H NMR (CDCl₃, ppm) δ: 7.21 (d, 4H), 7.09 (d, 4H), 4.39 (d, 2H), 4.31 (d, 2H), 4.04 (d, 2H), 3.59 (d, 2H), 3.21 (s, 6H), 2.97 (s, 6H), 2.87 (m, 4H). ¹³C NMR (CDCl₃, ppm) δ: 166.92, 165.58, 140.73, 131.59, 129.16, 128.77, 75.81, 75.15, 61.26, 37.15,

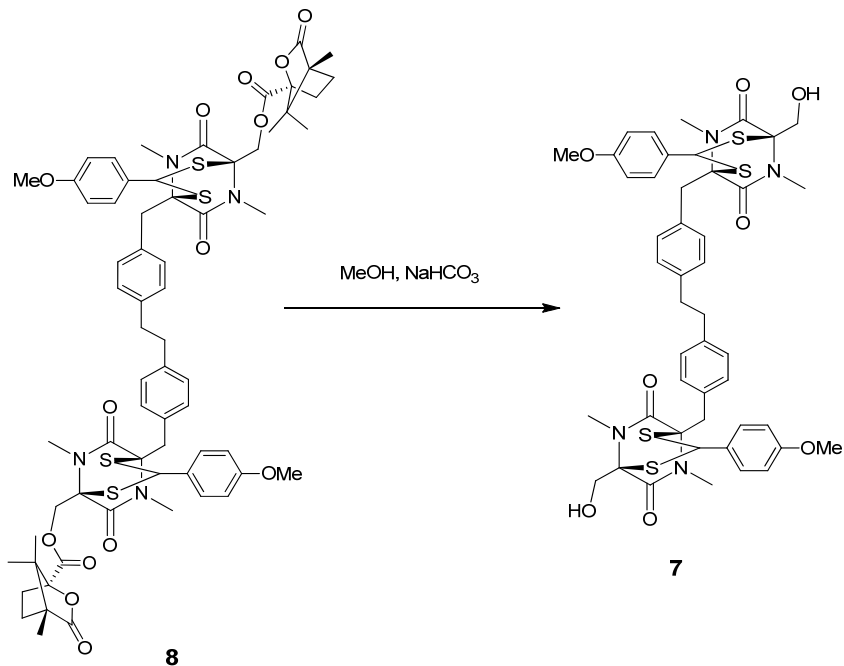
36.53, 28.61, 27.52. HR-ESIMS: Calcd. for $C_{30}H_{34}N_4O_6S_4 + H^+$: 675.14, Found [M+H]⁺: 675.1411.

Chiral Separation of (\pm)-7.



A round-bottom flask was charged with (\pm)-7 (20 mg, 0.22 mmol) and 5 mL of dichloromethane. To this mixture, (1S)-(-)-camphanic chloride (71 mg, 0.3 mmol, 1.4 eq.), 4-dimethylaminopyridine (0.8 mg, 0.007 mmol, 0.03 eq.) and *N,N*-diisopropylethylamine (150 μ L, 0.86 mmol, 3.9 eq.) were added sequentially with stirring. The stirring was maintained for 1 h at room temperature. The reaction mixture was washed with 0.1 M HCl (5 mL) and dried over anhydrous $MgSO_4$. The solvent was removed under reduced pressure to obtain crude 8 (23 mg, 83% total yield). The two diastereomers of 8 were separated by column chromatography using initial solvent system of 10% CH_2Cl_2 in hexanes and gradually increasing the amounts of CH_2Cl_2 and EtOAc to final solvent system of hexanes : EtOAc : CH_2Cl_2 = 4 : 3 : 3. The two fractions obtained were named *dst1*-8 (13 mg recovered) and *dst2*-8 (10 mg recovered), respectively. Data from analysis of *dst1*-8: 1H NMR ($CDCl_3$, ppm) δ : 7.33 (d, 2H), 7.09 (d, 2H), 7.00 (d, 2H), 6.87 (d, 2H), 5.31 (d, 1H), 5.11 (s, 1H), 4.42 (d, 1H), 4.36 (d, 1H), 3.81 (s, 3H), 3.40 (s, 3H), 3.08 (d, 1H), 2.88 (s, 3H), 2.83 (br, 2), 2.40 (m, 1H), 2.02 (m, 1H), 1.89 (m, 1H), 1.68 (m, 1H), 1.09 (s, 3H), 0.97 (s, 3H), 0.81 (s, 3H). ^{13}C NMR ($CDCl_3$, ppm) δ : 177.78, 166.42, 165.86, 164.81, 160.94, 140.68, 132.58, 130.79, 129.03, 128.42, 126.10, 114.69, 91.01, 73.54, 70.13, 63.05,

55.62, 55.10, 54.62, 51.83, 40.28, 37.53, 30.90, 29.87, 28.92, 28.47, 16.77, 16.67, 10.05. Data from analysis of *dst2-8*: ^1H NMR (CDCl_3 , ppm) δ : 7.33 (d, 2H), 7.09 (d, 2H), 7.02 (d, 2H), 6.87 (d, 2H), 5.28 (d, 1H), 5.10 (s, 1H), 4.43 (d, 1H), 4.35 (d, 1H), 3.81 (s, 3H), 3.36 (s, 3H), 3.12 (d, 1H), 2.93 (s, 3H), 2.84 (br, 2), 2.33 (m, 1H), 2.05 (m, 1H), 1.90 (m, 1H), 1.71 (m, 1H), 1.10 (s, 3H), 0.94 (s, 3H), 0.91 (s, 3H). ^{13}C NMR (CDCl_3 , ppm) δ : 178.12, 166.16, 165.89, 164.74, 160.96, 140.57, 132.73, 130.78, 128.90, 128.42, 126.21, 114.70, 90.87, 73.46, 70.03, 63.16, 55.61, 54.95, 54.47, 51.76, 40.19, 37.44, 30.97, 29.92, 29.19, 28.39, 16.74, 16.64, 9.96.



To 10 mg of each diastereomer of **8**, 1 mL of saturated solution of sodium bicarbonate in methanol was added. The reaction was stirred for 24 h at room temperature. Reaction was initially purified by short silica gel column followed by purification on reverse phase HPLC. Each of the reaction of the two diastereomers yielded two enantiomers *en1-7* or *ent2-7* (6 mg each enantiomer recovered, 74%). CD spectra confirmed the enantiomeric relationship of the two products.

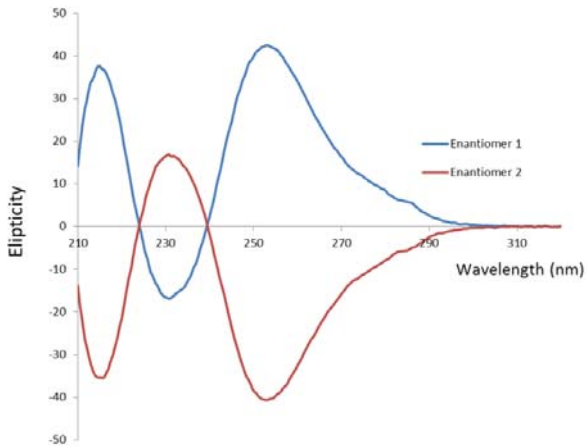
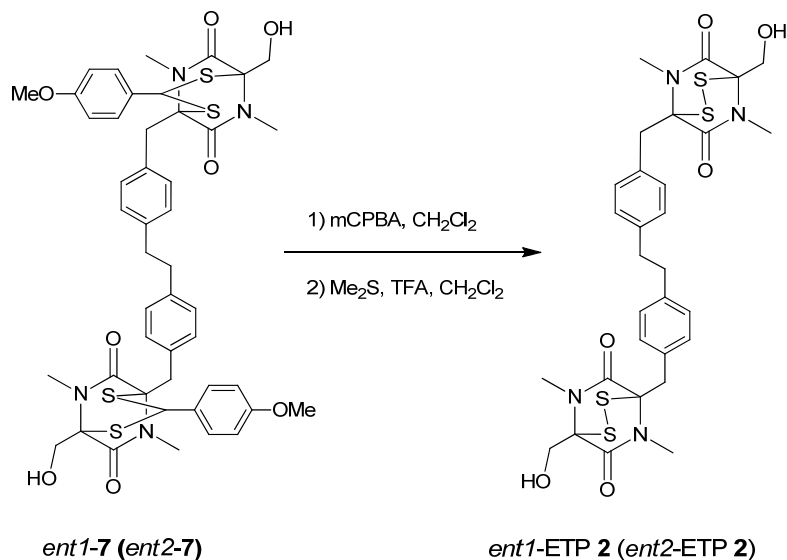


Figure S8. CD spectra of *ent1-7* (blue) and *ent2-7* (red).



Each *ent1*-ETP **2** and *ent2*-ETP **2** were obtained in 61% yield from the dithioacetals *ent1-7* and *ent2-7* by following the procedure analogous to that of (\pm) -7. As expected, the NMR data for *ent1*-ETP **2**, *ent2*-ETP **2** and racemic mixture were identical. *Ent1*-ETP **2**: ^1H NMR (CDCl_3 , ppm) δ : 7.19 (d, 4H), 7.07 (d, 4H), 4.39 (d, 2H), 4.30 (d, 2H), 4.04 (d, 2H), 3.59 (d, 2H), 3.21 (s, 6H), 2.96 (s, 6H), 2.86 (m, 4H). *Ent1*-ETP **2**: Calcd. for $\text{C}_{30}\text{H}_{34}\text{N}_4\text{O}_6\text{S}_4 + \text{H}^+$: 675.14, Found $[\text{M}+\text{H}]^+$: 675.1416. *ent2*-ETP **2**: Calcd. for $\text{C}_{30}\text{H}_{34}\text{N}_4\text{O}_6\text{S}_4 + \text{H}^+$: 675.14, Found $[\text{M}+\text{H}]^+$: 675.1316. CD spectra for *ent1*-ETP **2** and *ent2*-ETP **2** confirmed the enantiomeric relationship.

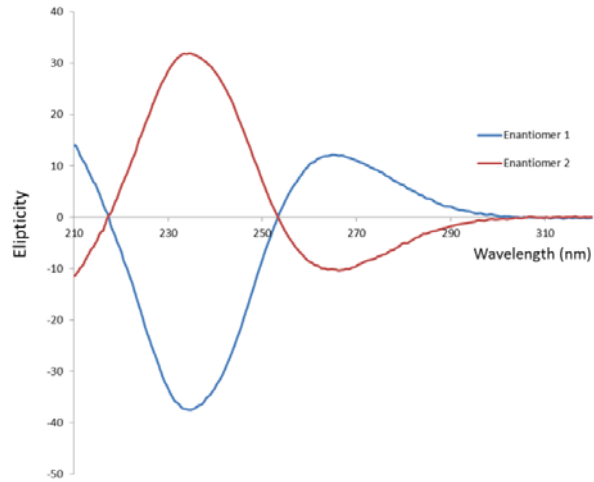


Figure S9. CD spectra of *ent*1-ETP **2** (blue) and *ent*2-ETP **2** (red).

NMR Spectra

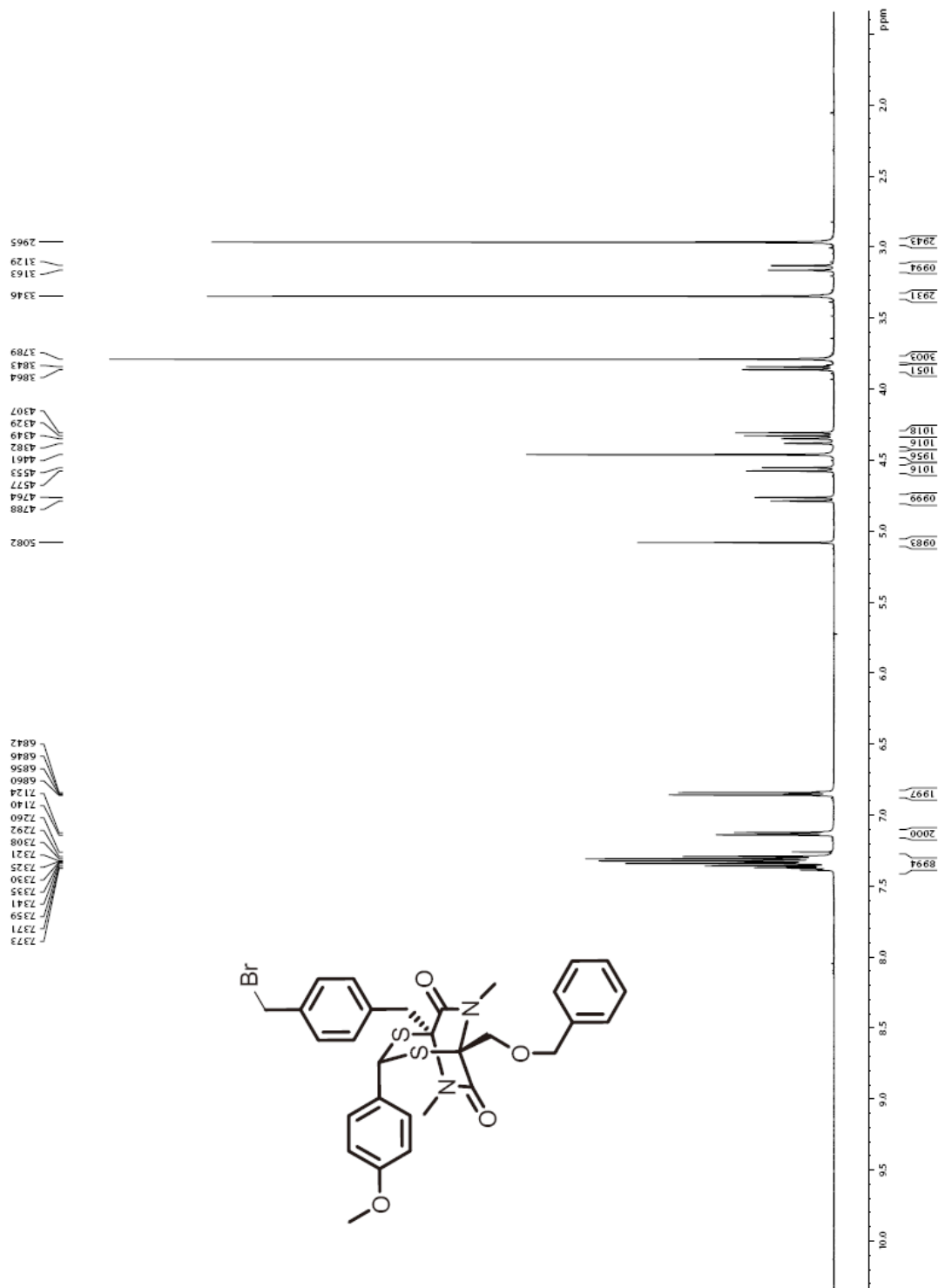


Figure S10. ¹H NMR spectrum of (\pm)-5 (500 MHz, CDCl₃).

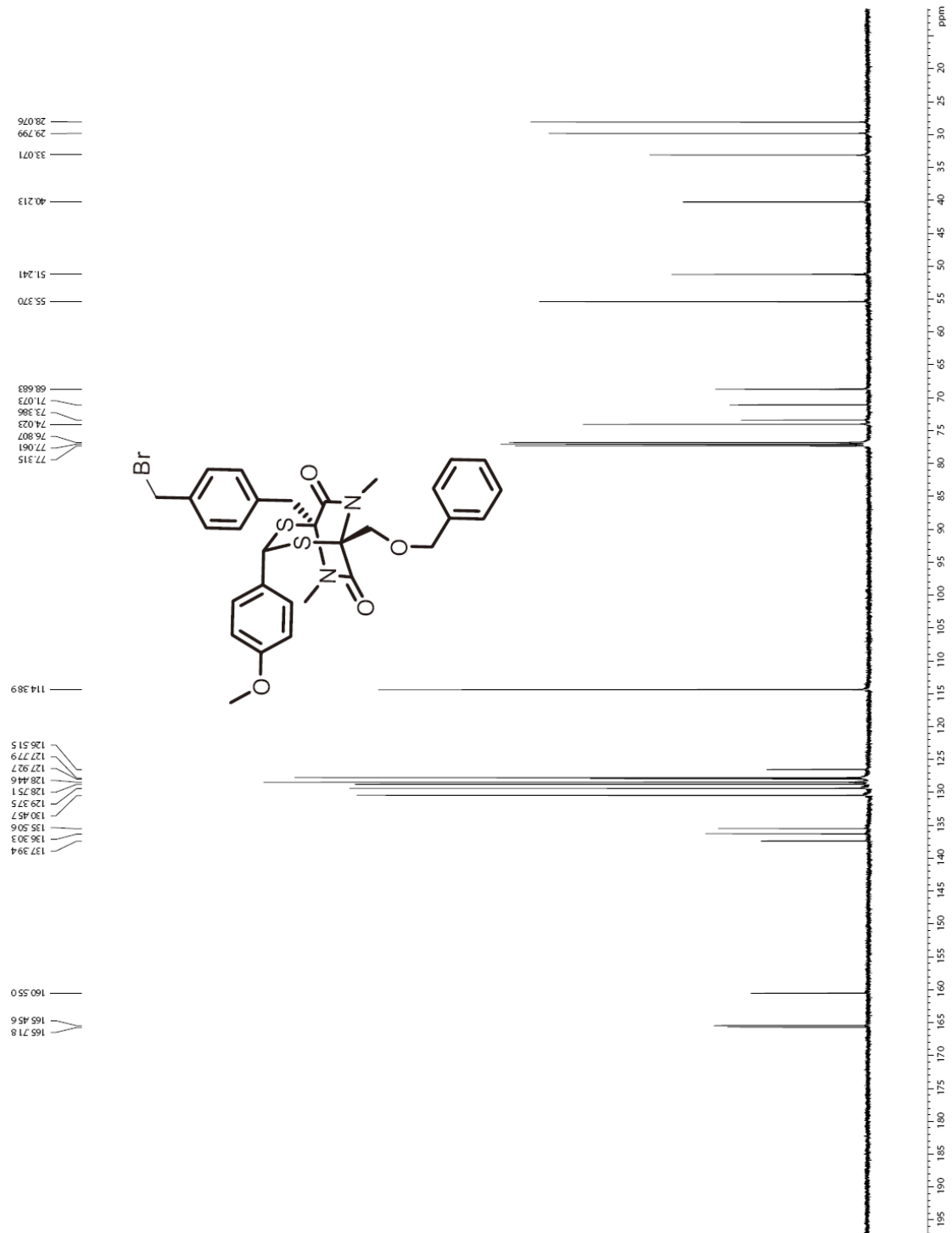


Figure S11. ^{13}C NMR spectrum of $(\pm)\text{-5}$ (125 MHz, CDCl_3).

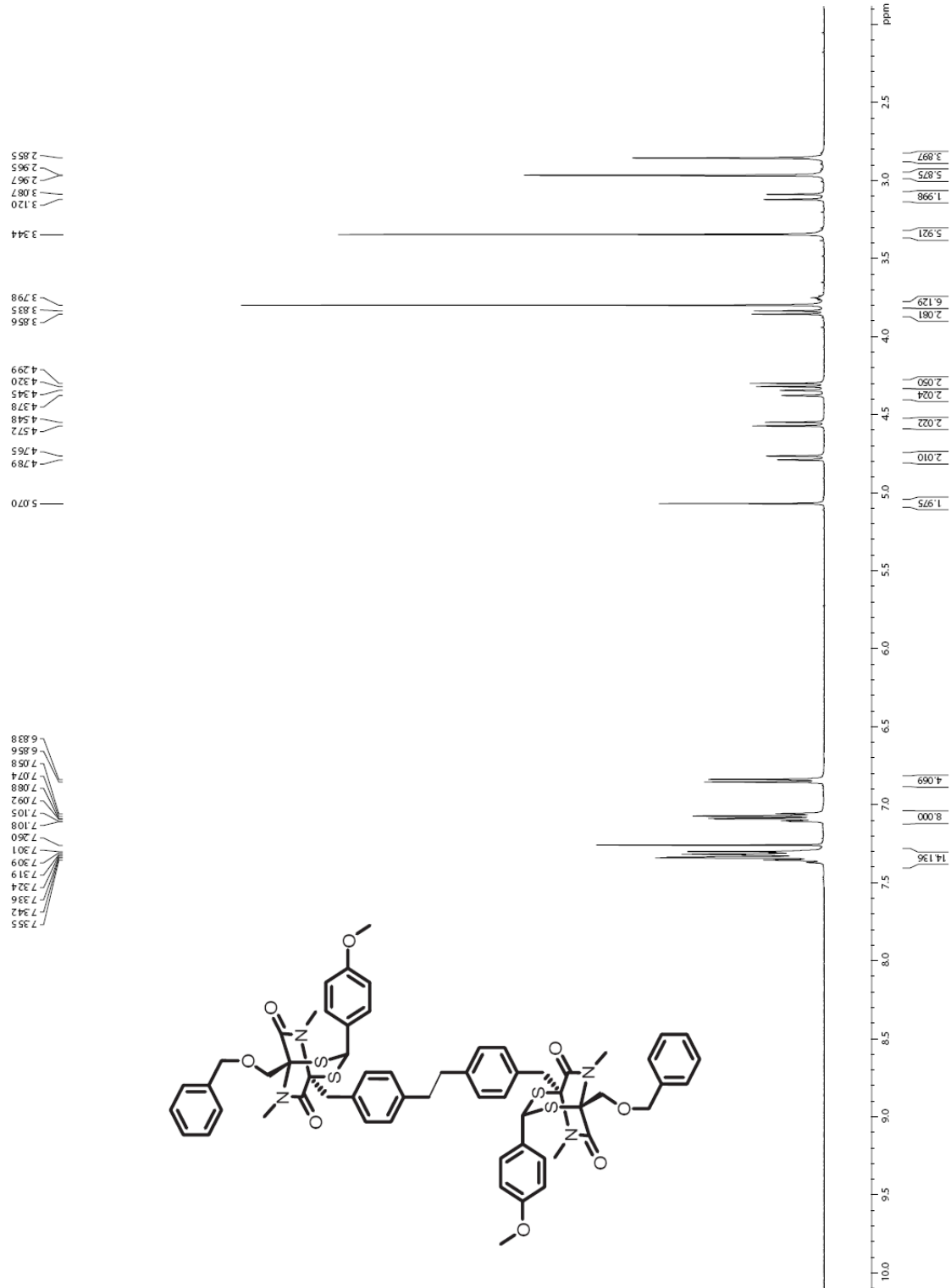


Figure S12. ^1H NMR spectrum of (\pm) -6 (500 MHz, CDCl_3).

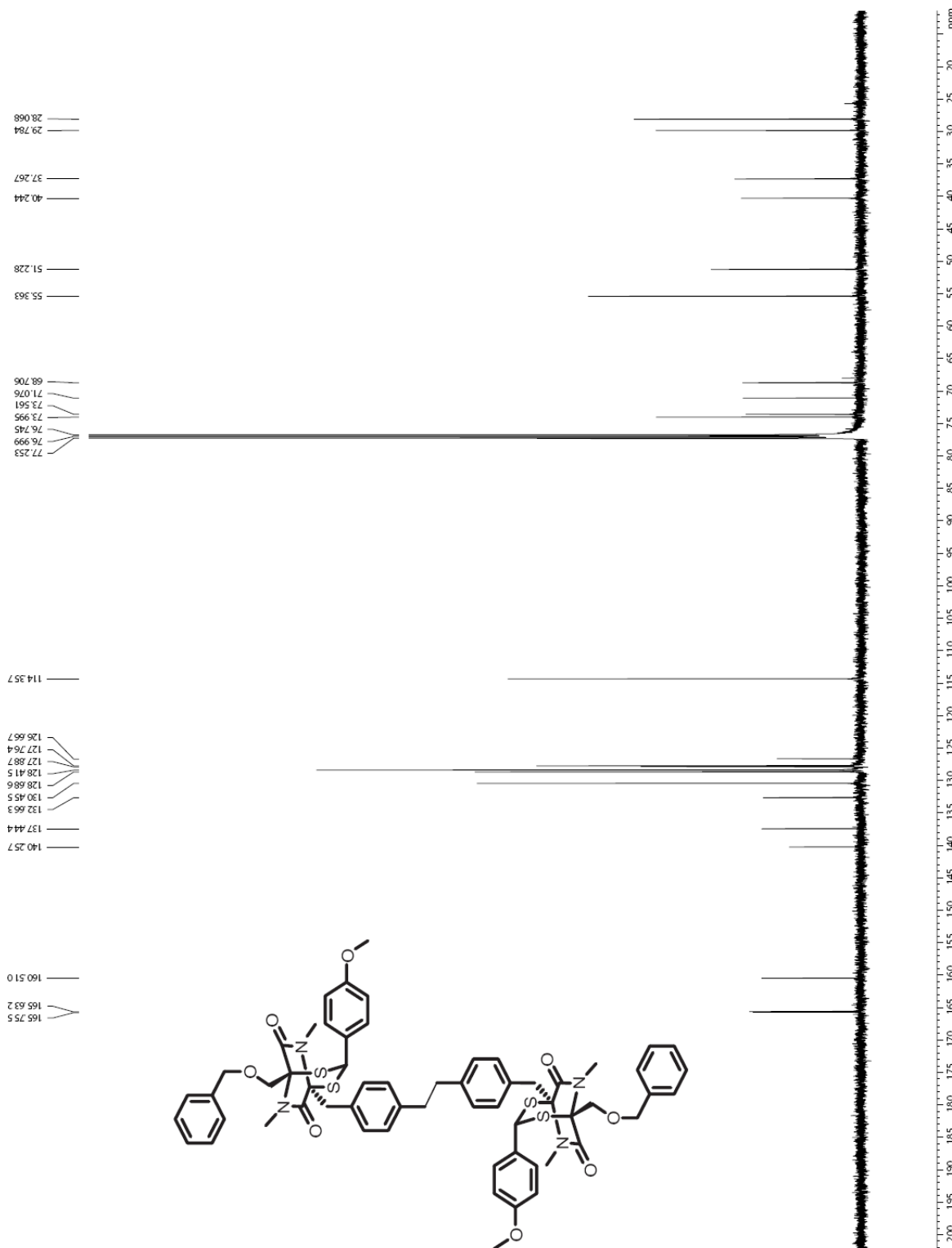


Figure S13. ^{13}C NMR spectrum of (\pm) -6 (125 MHz, CDCl_3).

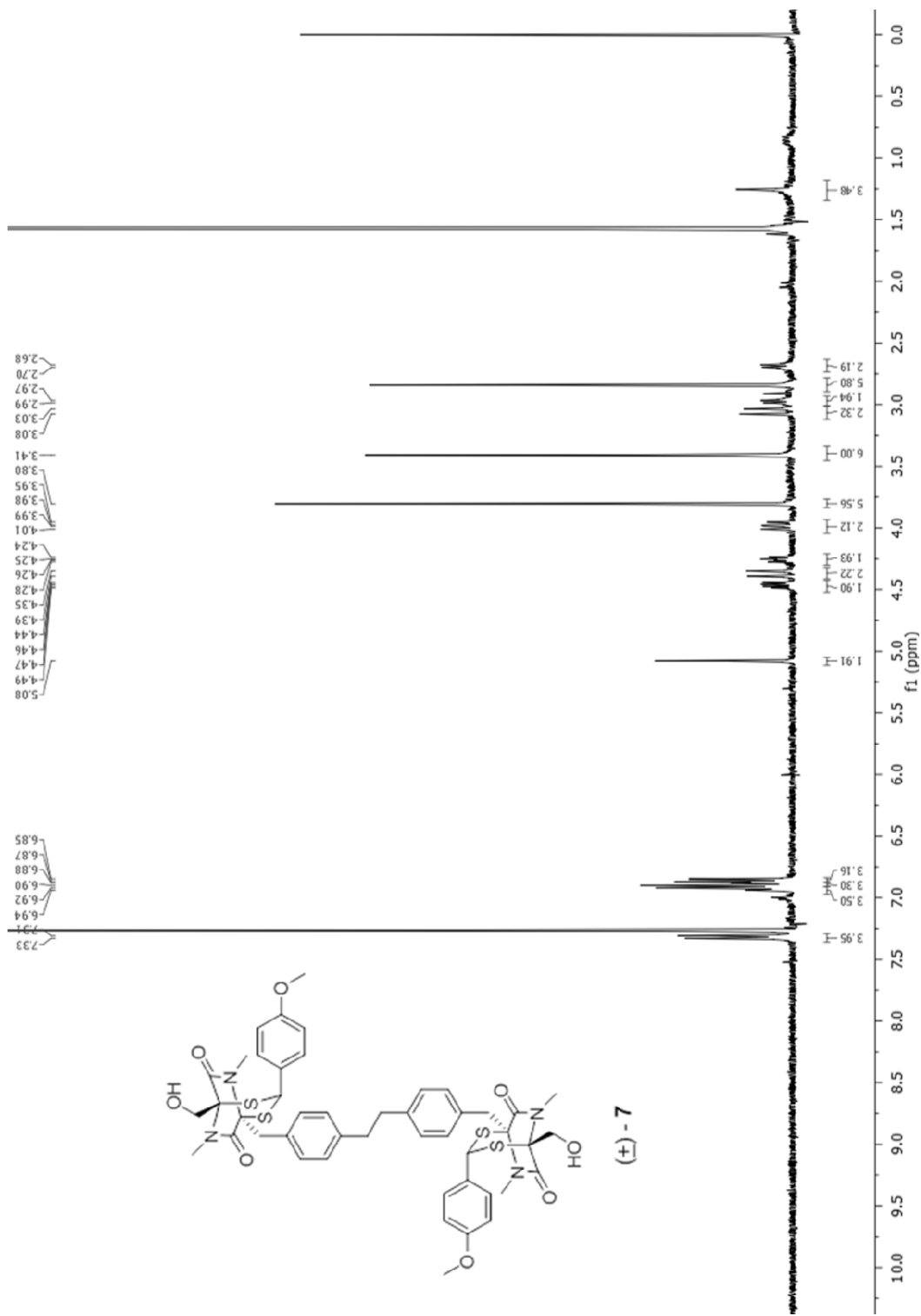


Figure S14. ^1H NMR spectrum of (\pm) -7 (400 MHz, CDCl_3).

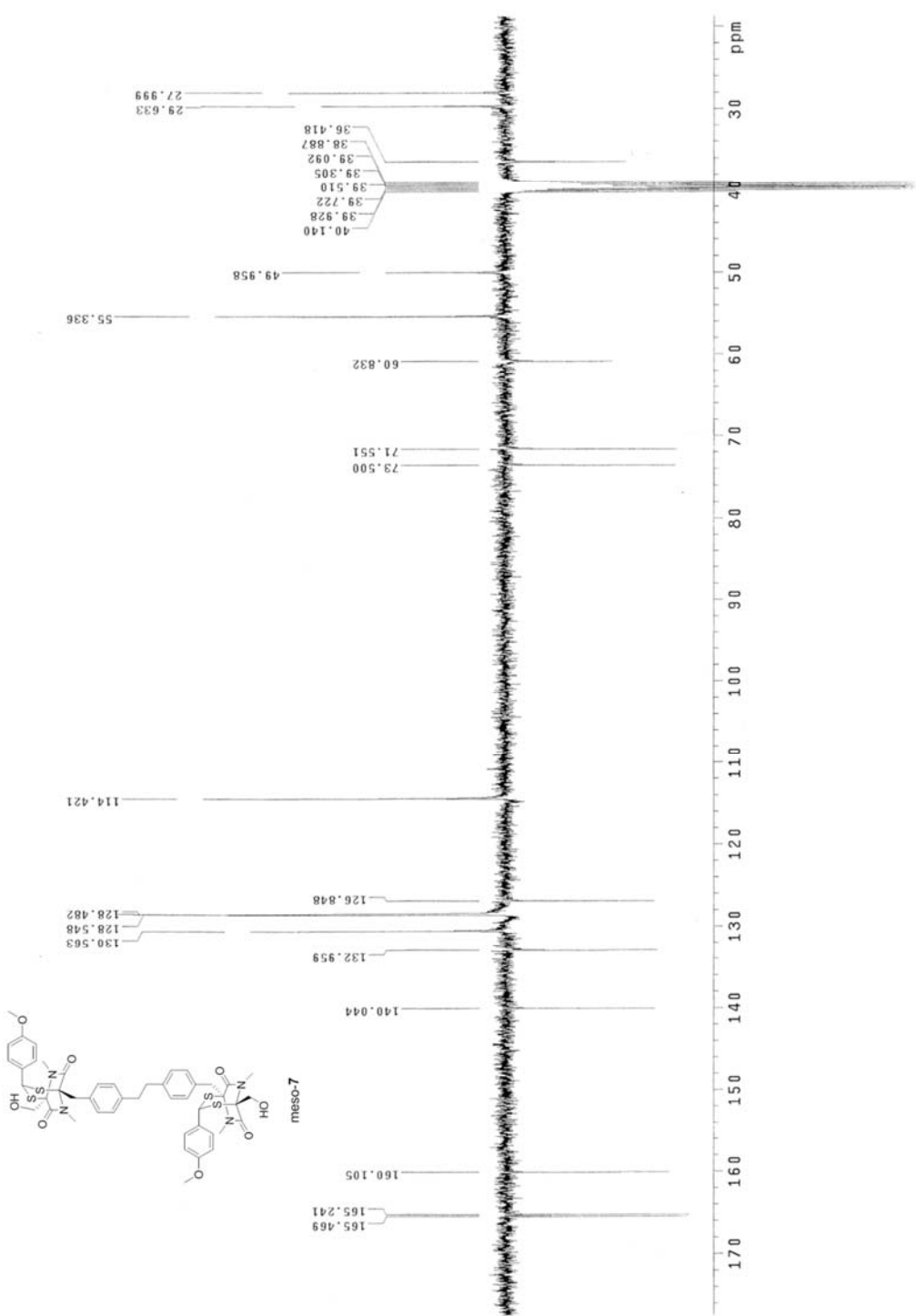


Figure S15. ^{13}C NMR APT spectrum of $(\pm)\text{-7}$ (100 MHz, CDCl_3).

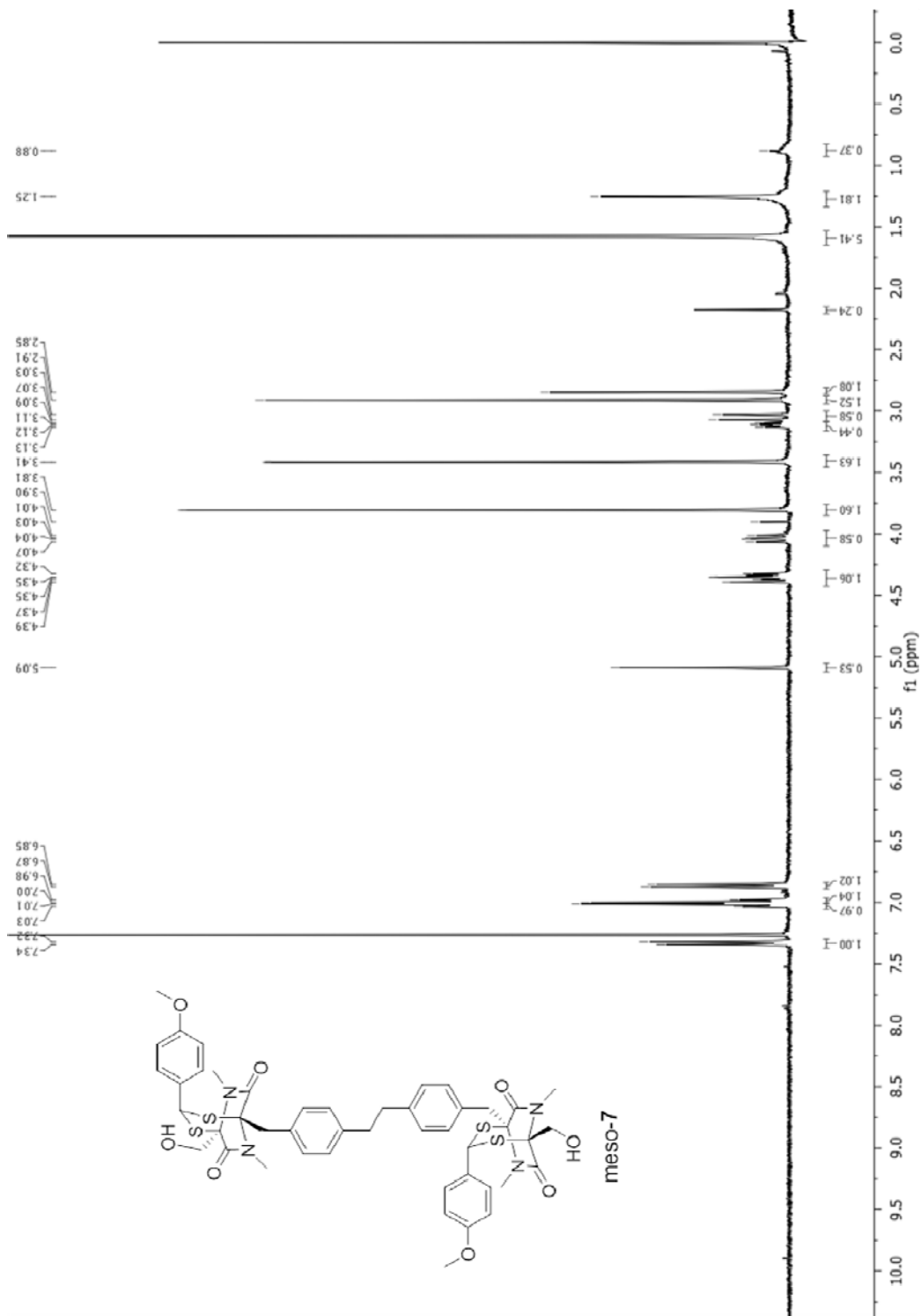


Figure S16. ^1H NMR spectrum of *meso*-7 (400 MHz, CDCl_3).

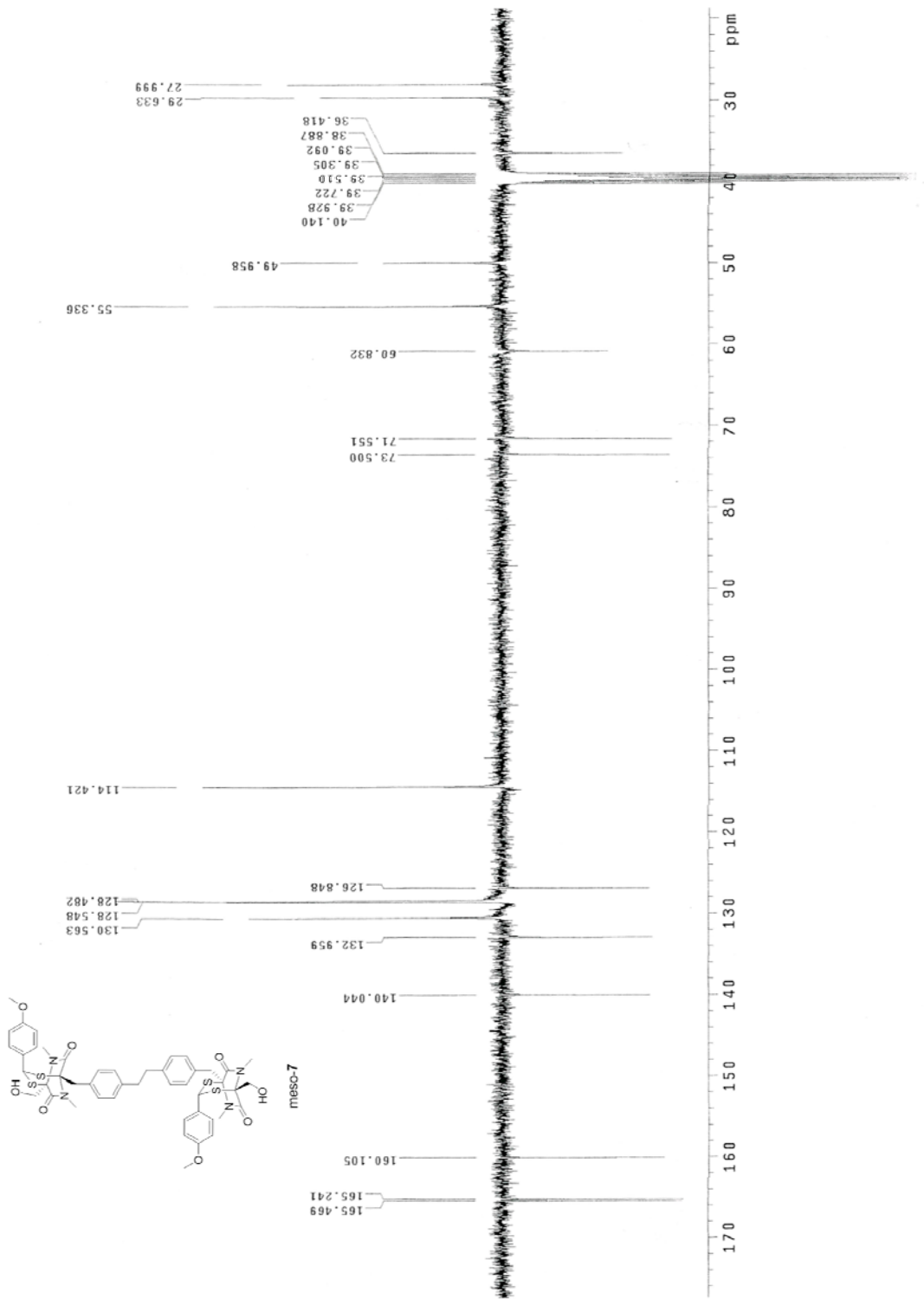


Figure S17. ^{13}C APT NMR spectrum of *meso*-7 (100 MHz, CDCl_3).

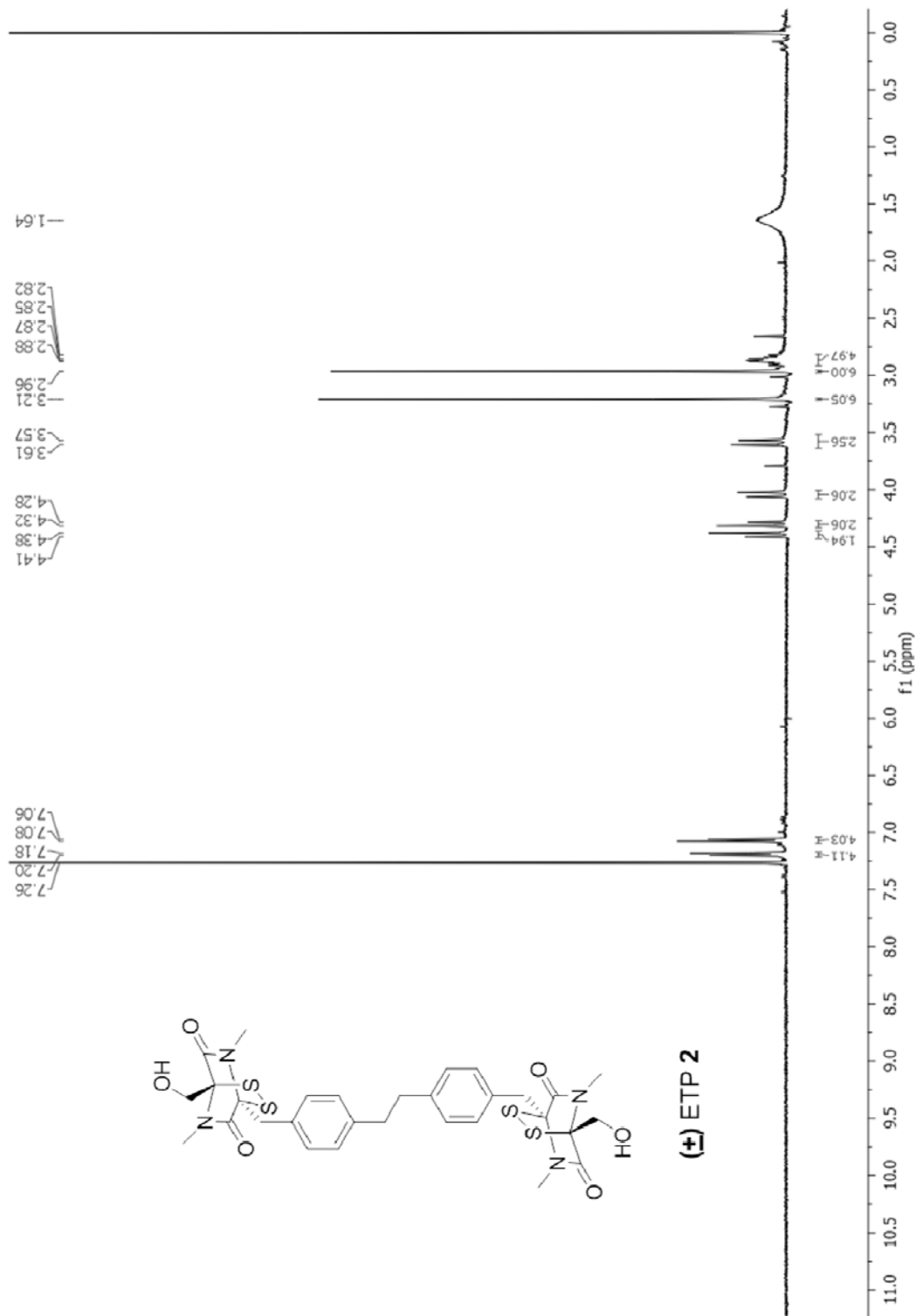


Figure S18. ¹H NMR spectrum of (±)-ETP 2 (400 MHz, CDCl₃).

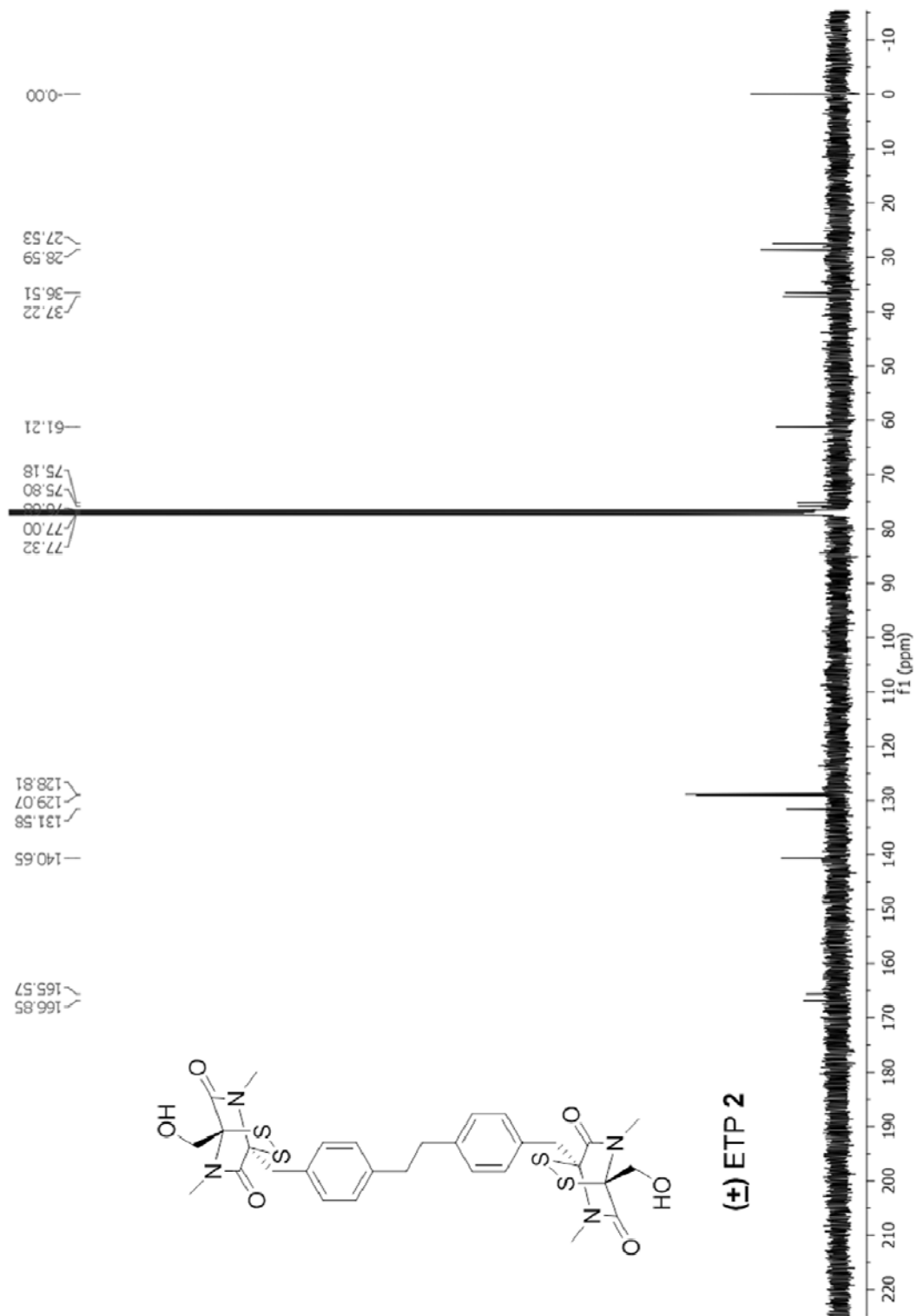


Figure S19. ^{13}C NMR spectrum of (\pm) -ETP 2 (100 MHz, CDCl_3).

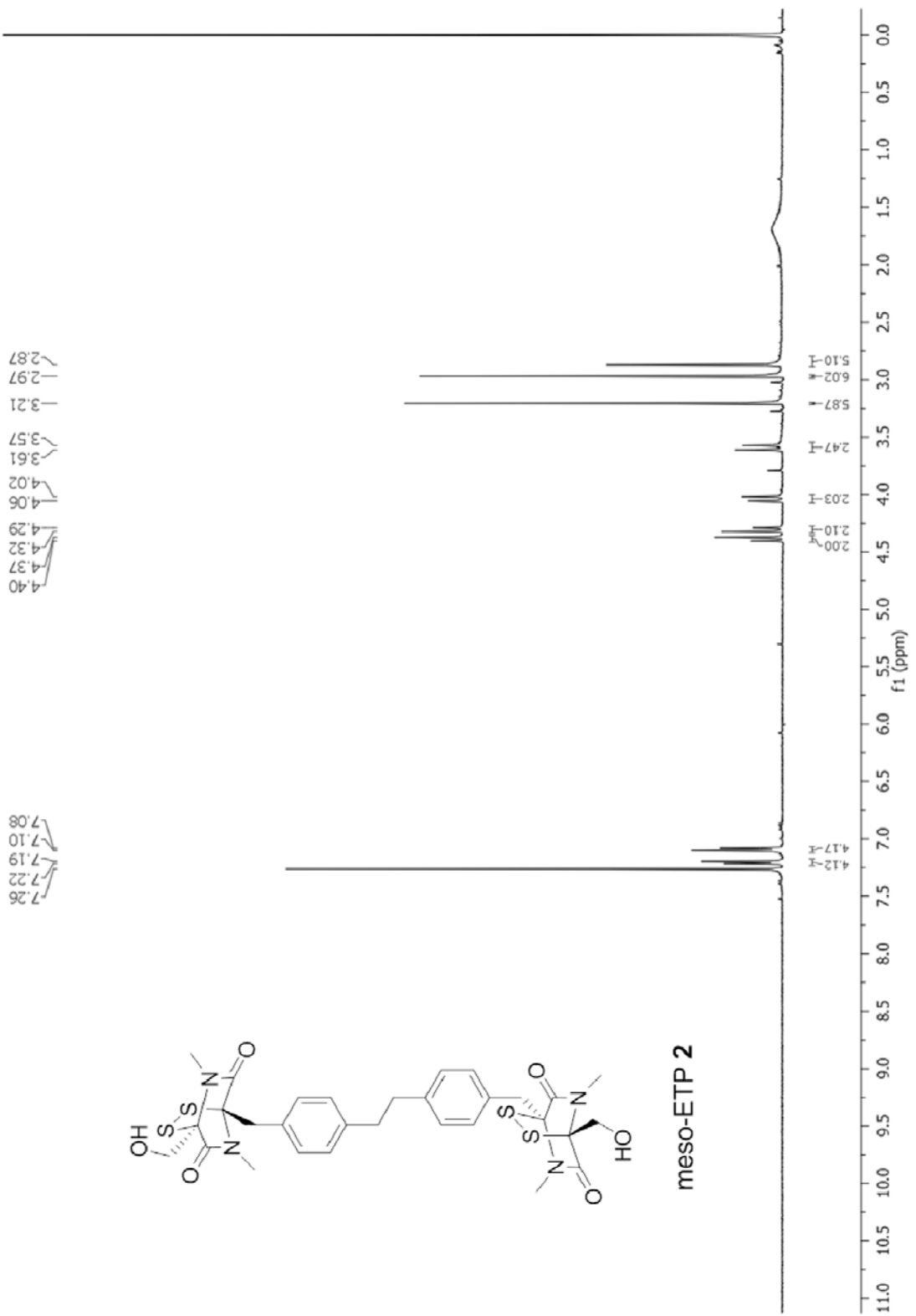


Figure S20. ^1H NMR spectrum of *meso*-ETP **2** (400 MHz, CDCl_3).

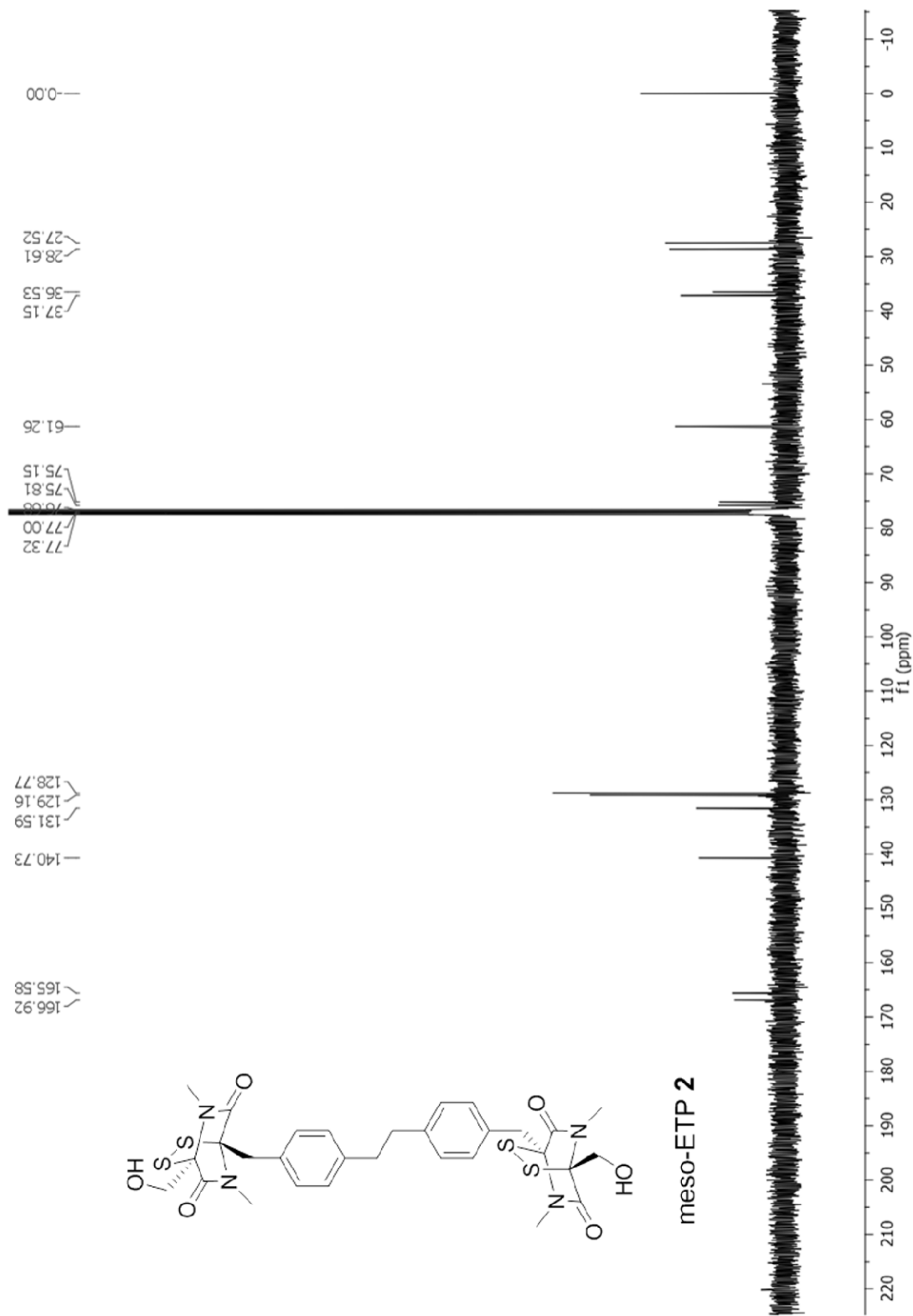


Figure S21. ^{13}C NMR spectrum of *meso*-ETP **2** (100 MHz, CDCl_3).

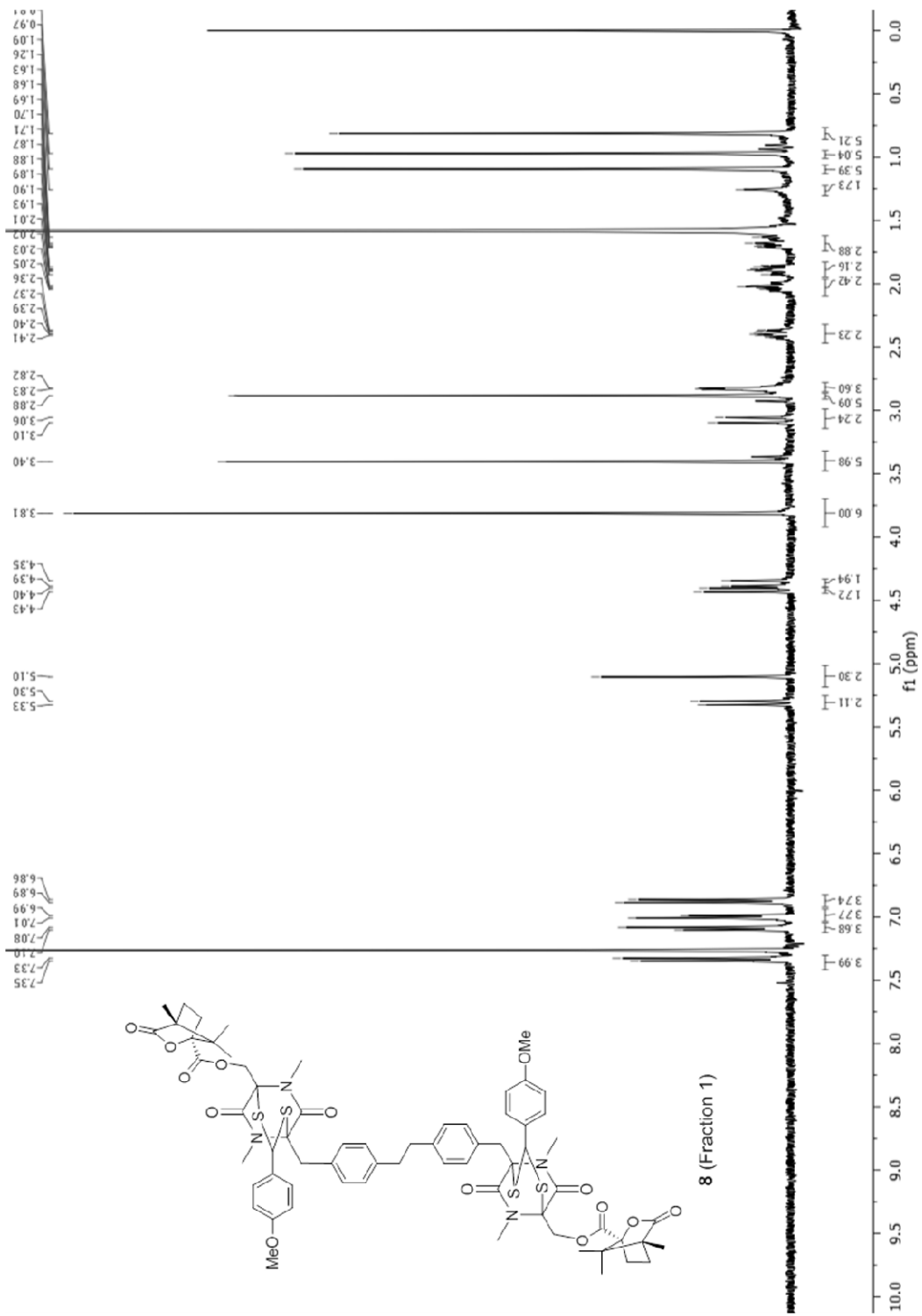


Figure S22. ^1H NMR spectrum of *dstl-8* (400 MHz, CDCl_3).

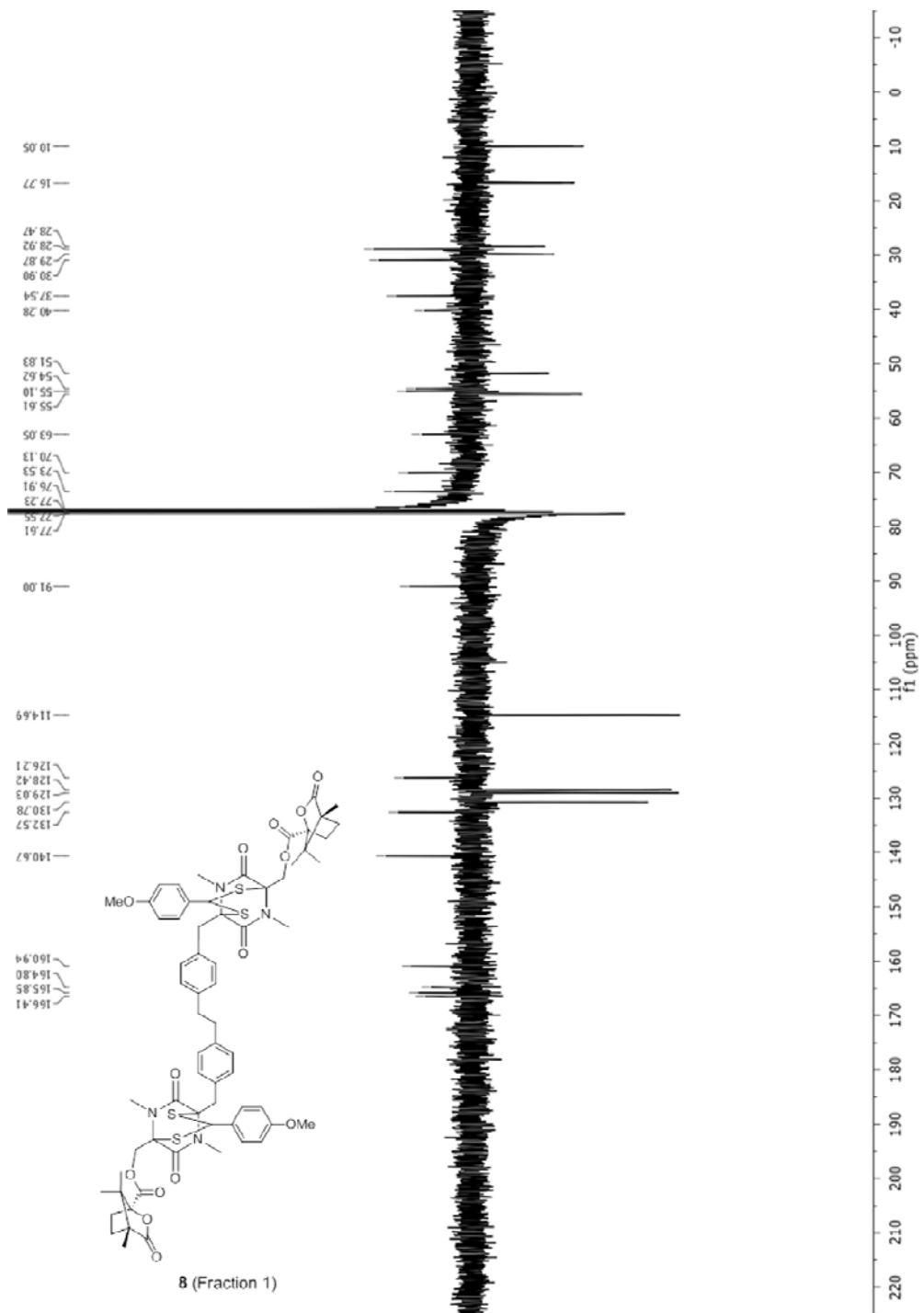


Figure S23. ^{13}C NMR APT spectrum of *dstI*-**8** (100 MHz, CDCl_3).

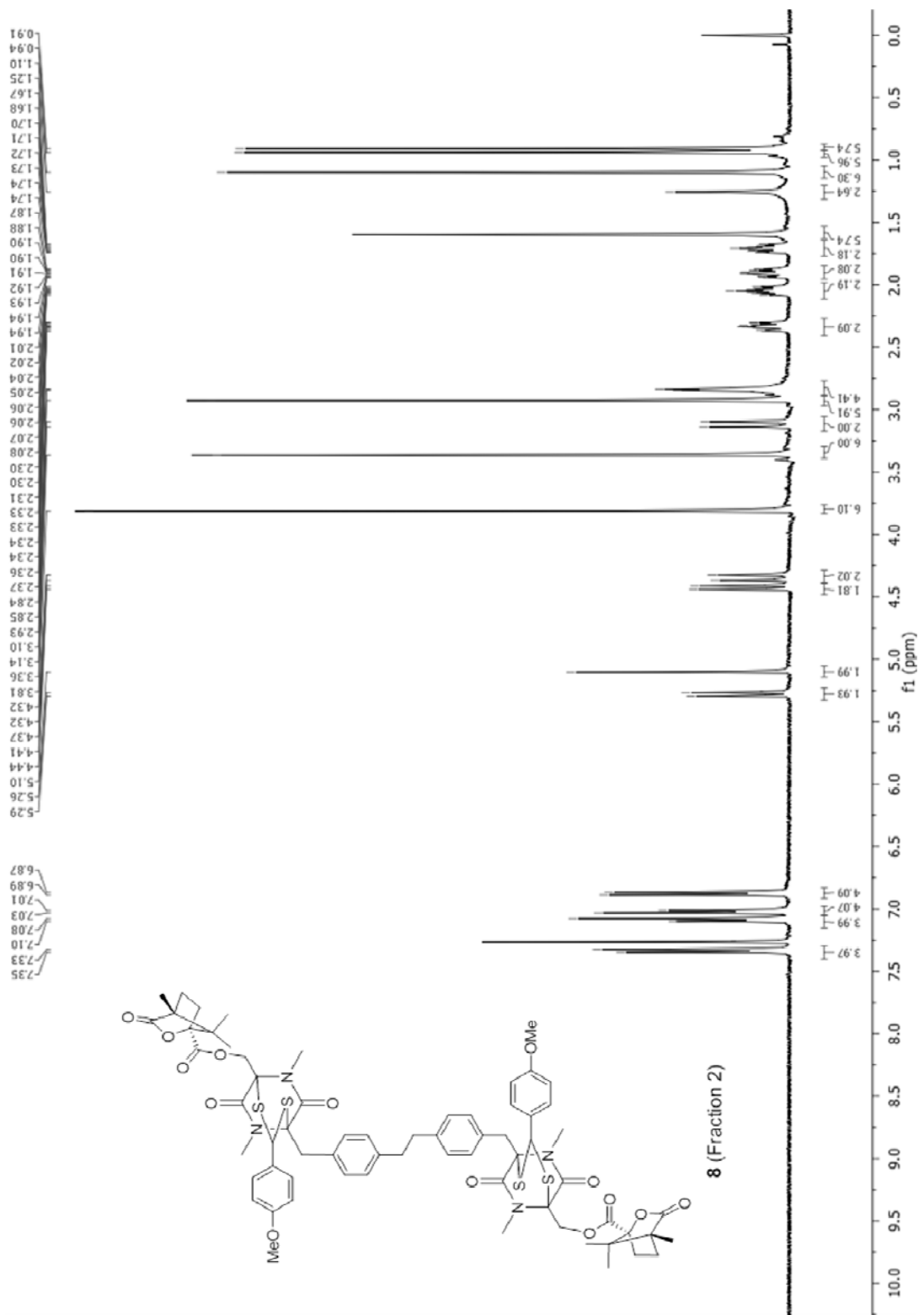


Figure S24. ^1H NMR spectrum of *dst2-8* (400 MHz, CDCl_3).

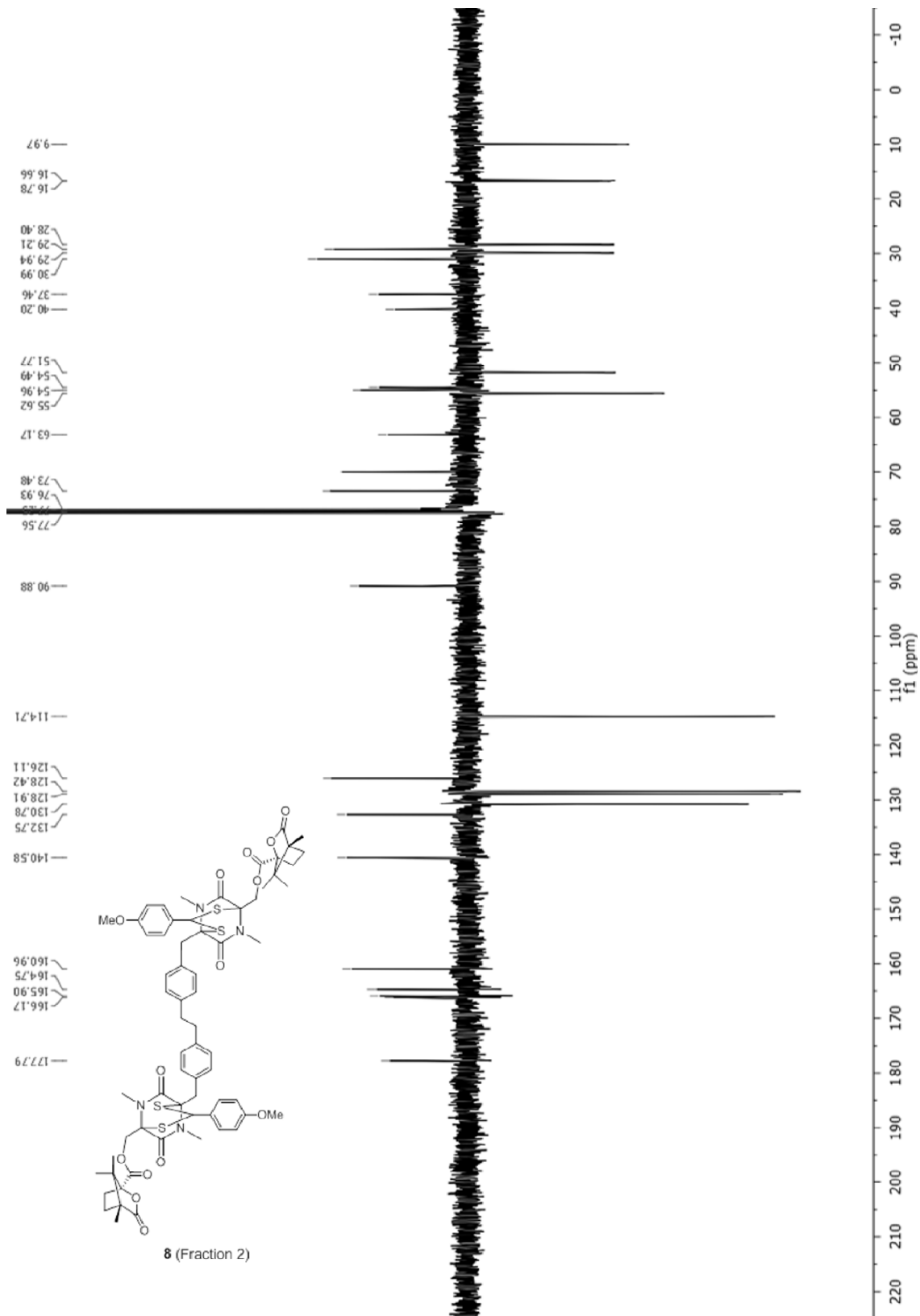


Figure S25. ^{13}C NMR APT spectrum of *dst2-8* (100 MHz, CDCl_3).